Controller Design for Precision Magnetic Bearings

by

Tetsuya Kubota

B.S., Mechanical Engineering (1986)

Tokyo Institute of Technology

M.Eng., Mechanical Engineering (1988)

Tokyo Institute of Technology

Submitted to the Department of Mechanical Engineering

in Partial Fulfillment of the Requirements for the degree of

Master of Science

at the

Massachusetts Institute of Technology

May, 1997

©Tetsuya Kubota 1997

Signature of Author _____

Department of Mechanical Engineering
May 9, 1997

Certified by _____

Dr. Kamal Youcef-Toumi
Associate Professor
Thesis Supervisor

Accepted by _____

Dr. Ain A. Sonin
Chairman, Department Committee on Graduate Students

Eng.

Controller Design for Precision Magnetic Bearings

by

Tetsuya Kubota

Submitted to the Department of Mechanical Engineering
on May 9, 1997 in partial fulfillment of the
requirements for the degree of Master of Science

ABSTRACT

For some uses of magnetic bearings such as precise positioning of a rotor, the ability
to control the rotor actively is essential. However, the consideration of performance
robustness is required for this application because of unknown parameters, unpre-
dictable disturbances, and the nonlinearity of magnetic force. This thesis focuses
on the achievable robustness of the system designed by linear theories and perfor-
mance comparison between the linear approach and adaptive approach. First, the
examples of the controller design for the magnetic bearing using the LQG design,
H_∞ design, LQG/LTR design, and μ-synthesis are presented to show how the linear
theories achieve stability and/or performance robustness. Second, the limitations of
linear controllers for the system with uncertainties are evaluated by using singular
value plots and structured singular value plots. Furthermore, it is revealed that when
the system reaches its limit, the gain of the controller becomes extremely high; there-
fore, it should be avoided. The effect of the order reduction of the controller is also
examined. Then, the robustness of the linear controller and adaptive controller using
local function estimation is compared by simulations. The results show the adaptive
controller can deal with wider range of uncertainties than the linear controller can,
but high frequency unmodeled dynamics impose limitations on adaptive gain.

Thesis Supervisor: Dr. Kamal Youcef-Toumi
Title: Associate Professor of Mechanical Engineering

Acknowledgement

First, I would like to thank my thesis adviser. His support and guidance have led me to the proper direction in this research. I also want to thank all the students I worked with at the mechatoronics reseach laboratory. Particulary, the advice from Jake and T.-J. much helped me at the early stage of the work. I am also thankful to Kawasaki Heavy Industries, which gave me the chance to study at MIT. Finally, I thank to my parents and wife. Without my wife's support, I could not have completed my thesis.

Contents

List of Figures

10

11

12

Chapter 1

Introduction

1.1 Motivation and Background

As a requirement of machines becomes faster and more precise, conventional design methods or machine elements may not be able to achieve the requirement. In this case, we must opt for an unconventional, yet practical approach to achive the requirement.

Even though magnetic bearings are not as widely-used as other conventional bearings, they have been used in several applications because of their distinctive features. No-contact nature may be the most attractive feature of magnetic bearings. Because there is no friction, magnetic bearings are used for high rotating speed machines such as fly-wheels and turbo-pumps. Also, because no lubrication is necessary, they are used for maintenance-free machines, high speed machines in high temperature environments, high speed machines in vacuum, and machines in clean rooms. For these applications, especially for industrial applications, many research and development works have been done, and magnetic bearings are widely in use.

There is another attractive feature in magnetic bearings. The fact that magnetic bearings are actively controlled provides some useful applications. One possible application is for machines that need high speed rotation and precise positioning of the rotor simultaneously. Precise machine-tool spindles and the joints of high-speed, high-precision robot manipulators may be achieved by magnetic bearings. Active control also makes force control and impedance control of moving parts possible. This feature is difficult to achieve by other conventional bearings such as ball bearings or

air bearings; therefore, using magnetic bearings largely enhances the machine's capability. However, due to the nonlinearity of magnetic force and nature of instability, the use of magnetic bearings for precise machines requires more effort on designing a control system than just making the rotor levitate for the bearing purpose. Unknown factors, such as unknown load, unmodeled dynamics, or unpredictable disturbances may cause the performance degradation of the system, and to precise machines, it is not acceptable. Nevertheless, the research in the area of precise control of magnetic bearings has not yet been well explored.

In the past decade, modern control theories have evolved to deal with the uncertainties in systems. This development is driven by the fact that in real systems, there are many unknown factors, and without considering these factors in the design process, the closed-loop system often fails to be stabilized, or the resulting performance becomes much poorer than expected. This fact can also be applied to the control of magnetic bearings. However, the recent development of robust control theories has enabled us to design a controller that achieves the desired performance even when uncertainties exist. Moreover, these theories are now readily available as computer aided design tools [1][2]. Nonami et al. applied μ-synthesis to the control design for a magnetic bearing and succeeded to robustly control the flexible-rotor magnetic bearing system [3]. Even though this proves that the linear robust control theory can be applicable to the real system with uncertainties, fixed gain linear controllers cannot always achieve the desired performance, and knowing the limitation of the controller designed by μ-synthesis is as important as the design procedure itself. Moreover, in precise magnetic bearings, the system is affected by nonlinearity because the operating point changes. However, the effect of the nonlinearity is not analyzed in [3].

Because of the strong nonlinearity, other approaches than linear controllers have been applied to magnetic bearings. For example, Shinha et al. applied sliding mode

control to the magnetic bearing even though the report does not include experimental results [4]. Yeh developed an adaptive control method using local function estimation and successfully controlled the rotor of the turbo-pump with magnetic bearings [5]. These results indicate that nonlinear approaches can deal with the strong nonlinearity of magnetic bearings and may be able to achieve performance robustness for precise control.

With these choices of control methods, we must analyze the advantages and disadvantages of these methods in order to design a proper controller. Generally, linear controllers are most widely used and can be applied easily. However, in some cases, other methods, such as adaptive controllers, far more exceed linear controllers in terms of achievable performance. Åström et al. discussed this issue in their literature [6]. However, it does not mention the limitation of robustness of linear controllers. With the advent of μ-synthesis now, we are able to judge the limitation of linear controllers applied to the system with uncertainties. One of the purposes of this thesis is to provide the information about the methodology and examples of the limitation of the magnetic bearing system designed by μ-synthesis along with the comparison with an adaptive method. This information helps control designers choose the proper control structure.

1.2   Scope and Contents of the Thesis

This thesis contains three schemes: linear control design examples, evaluation of limitations of linear controllers, and comparison of the linear approach and adaptive approach. By using design examples, it is shown how linear controllers are able to deal with the uncertainties that exist in the magnetic bearing system. The design methods used in this part are LQG, $H\infty$, LQG/LTR, and μ-synthesis, and in these

methods, only μ-synthesis can deal with performance robustness. Even though the design process of these theories is not trivial, commercially available CAD programs exist, and all four controllers are designed using these programs. The program codes to calculate the controllers are listed in the Appendix.

The limitation of linear controllers for the system with uncertainties are evaluated by singular value plots or structured singular value plots. In this part, the limitation by the bandwidth limit of the closed-loop system, limitation by the uncertainty of the rotor mass, and limitation by both the uncertain mass and bandwidth limit are evaluated. Also, as the adverse aspects of the robust linear controllers, high gain and high order of the designed controllers are discussed, and the effect of order reduction and prefilters is presented.

The effect of nonlinearity on the performance of the system with uncertainties is discussed by using nonlinear simulations. In this part, the adaptive control using local function estimation, by which the turbo-pump with magnetic bearings are controlled successfully, is briefly described to compare the linear approach and adaptive approach. Because of the strong nonlinearity of magnetic force, the system with the linear controllers may not be able to deal with the nonlinearity whereas with the adaptive approach, which estimates the nonlinear function as well as unknown disturbances, is not affected by the nonlinearity. Also, the effect of high frequency unmodeled dynamics is examined by simulations, and the reason why the adaptive gain chosen is not always able to be used in real sytems is presented.

This thesis is organized as follows. First, design examples using linear control theories are given in Chapter 2. The design procedures and comparison table for these methods are presented. In Chapter3, the limitations and disadvantages of the linear controllers for a robust design are evaluated. Chapter 4 contains the equivalent linear uncertainties of the nonlinearity, description of the adaptive control method

using local function estimation, and comparison between the adaptive approach and linear approach. Finally, concluding remarks are given in Chapter 5.

Chapter 2
Control of Magnetic Bearings with Linear Controllers

2.1 Introduction

In the design of a feedback controller, the structure of the controller is first sellected. There are two types of controller we can choose from: a linear controller and a nonlinear controller. Linear feedback controllers are simple. They involve only matrix calculation. There are no branch operations or special functions. Therefore, they are easy to install and debug. Thus, more reliable than nonlinear controllers. Also, the recent development of linear control design theories has made us able to deal with both stability robustness and performance robustness within the linear frame, and these theories are readily usable as a form of computer aided design software.

In this chapter, the controller design for the thrust magnetic bearing of a turbopump is demonstrated by using several linear control design methods. In addition, a discussion on how these methods achieve stability robustness and performance robustness is presented. In the end, summary of the existing linear design methods is presented in a comparison table. Performance robustness is necessary when we apply the magnetic bearing to a precise machine spindle and try to change the rotor position precisely because the characteristics of the system changes as the position changes. The advantages and disadvantages of linear controllers are discussed in the later chapters based on the design results presented in this chapter.

2.2 Model of the Magnetic Bearing

Figure 2.1 shows a cross section of the turbo-pump. This turbo-pump is designed and manufactured to use in the semiconductor industry for creating a vacuum environment. A simplified schematic diagram of the thrust magnetic bearing is shown in Figure 2.2. In ideal situations, the magnetic force is proportional to the square
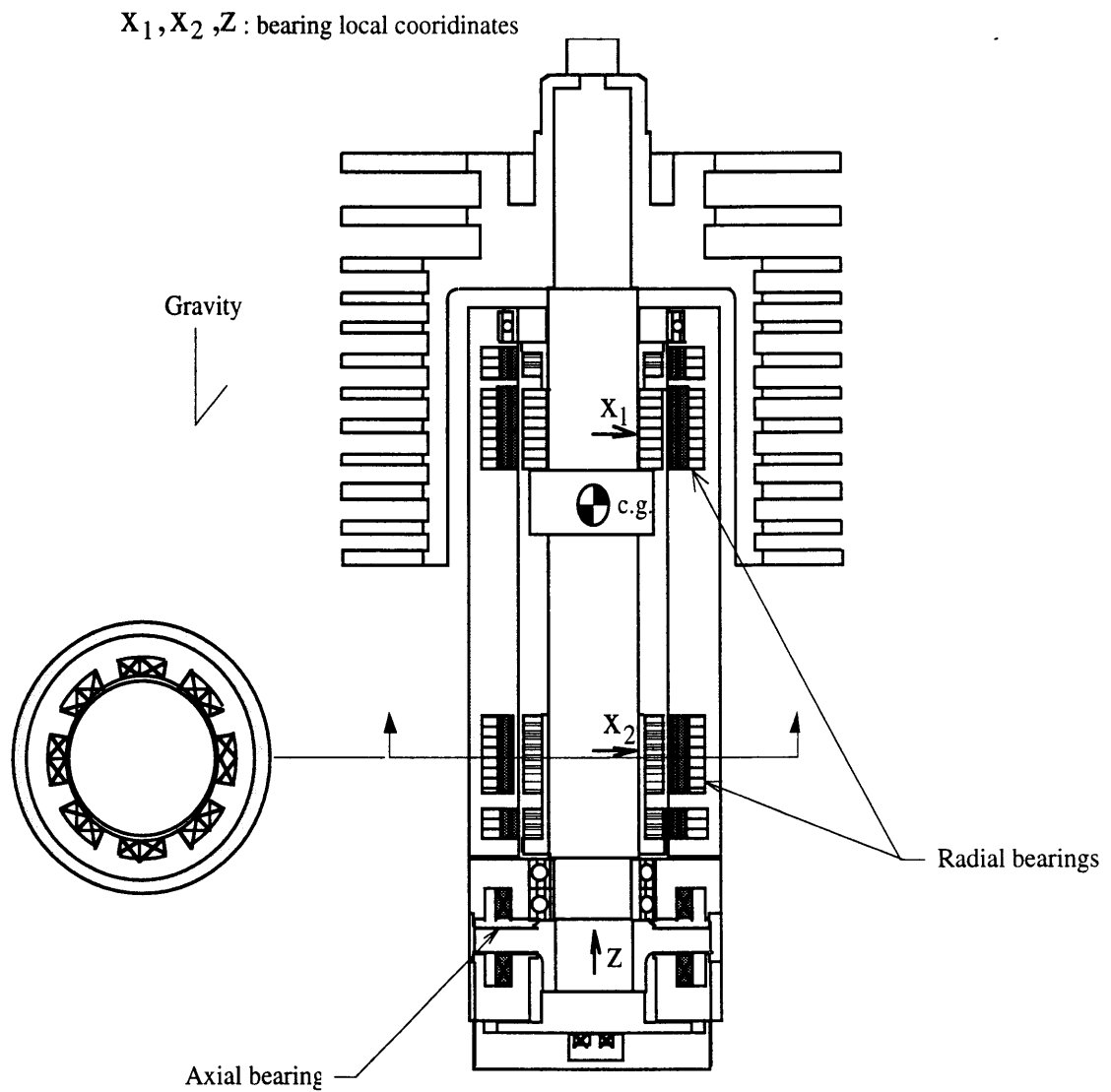
Figure 2.1: Cross section of the turbo-pump.
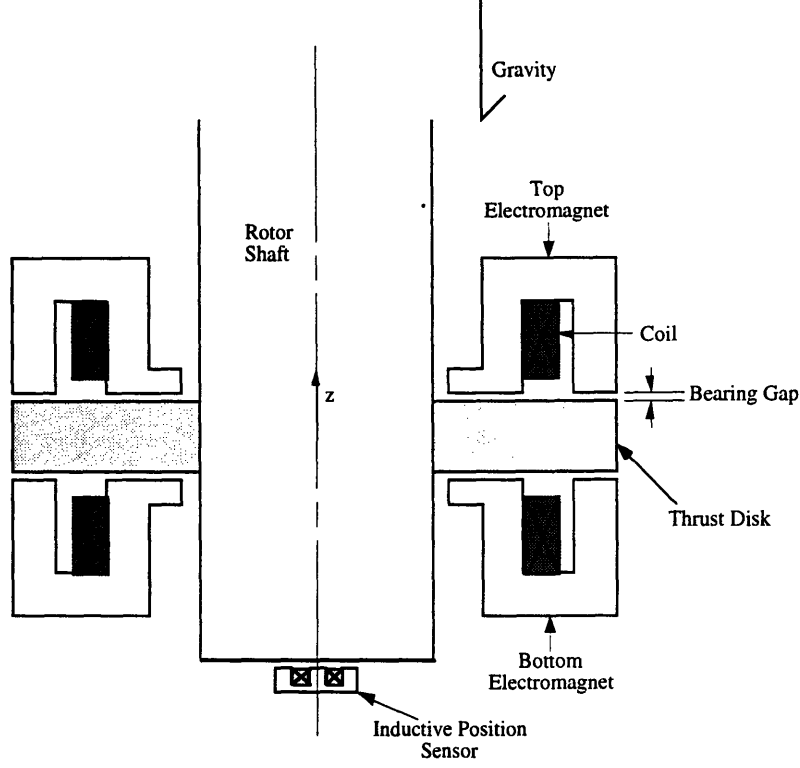
Figure 2.2: Schematic of the thrust bearing.

of the input current and inversely proportional to the square of the bearing air gap. Therefore, the equation that governs the magnetic bearing is

$$m\ddot{z} = \frac{k_0(i_0 + u_z)^2}{(z_0 - z)^2} - \frac{k_0(i_0 - u_z)^2}{(z_0 + z)^2} - mg \tag{2.1}$$

where z_0 is the nominal air gap, k_0 is the electromagnetic constant, m is the mass of the rotor, g is the gravity acceleration, i_0 is the bias current, and u_z is the control current [7]. The numerical values of the magnetic bearing are shown in Table 2.1.

At the equilibrium position, $u_z = 0$ and $z = 0$, Eq.(2.1) can be linearized and expressed as a state space form:

$$\dot{\mathbf{x}} = \mathbf{Ax} + \mathbf{Bu} \tag{2.2}$$

$$\mathbf{y} = \mathbf{Cx} \tag{2.3}$$

Parameters	Numerical Values
Nominal Air Gap z_0	400×10^{-6} m
Electromagnetic Constant k_0	4×10^{-6} Nm^2 /A^2
Mass m	2.0 kg
Bias Current i_0	0.5 A

Table 2.1: Numerical values of the thrust bearing.

where

$$\mathbf{x} = \begin{bmatrix} z \\ \dot{z} \end{bmatrix} \qquad (2.4)$$

$$\mathbf{A} = \begin{bmatrix} 0 & 1 \\ \frac{4k_0 i_0^2}{mz_0^3} & 0 \end{bmatrix} \qquad (2.5)$$

$$\mathbf{B} = \begin{bmatrix} 0 \\ \frac{4k_0 i_0}{mz_0^2} \end{bmatrix} \qquad (2.6)$$

$$\mathbf{C} = \begin{bmatrix} 1 & 0 \end{bmatrix} \qquad (2.7)$$

Gravity is neglected to make the analysis of the examples simple. With this linearized equation, (2.2), I design controllers that stabilize the magnetic bearing, and see how they achieve the stability robustness and performance robustness.

2.3 Design Examples

In this section, I proceed a linear quadratic Gaussian (LQG) design, H_∞ design, LQG loop transfer recovery (LQG/LTR) design, and μ-synthesis. These design methods are based on optimal control theories and considered to achieve high performance.

2.3.1 LQG Design

Figure 2.3 shows the structure of an LQG controller. An LQG design chooses the state feedback gain vector K such that the performance index

$$J = \int_0^\infty (\mathbf{x}^T \mathbf{Q} \mathbf{x} + \mathbf{u}^T \mathbf{R} \mathbf{u}) dt \tag{2.8}$$

where **x** is a state vector, **u** is a control vector, and **Q** and **R** are weighting matrices, becomes minimum, and chooses the filter gain **H** such that the variance of the state estimation error becomes minimum with the existence of disturbances whose intensity matrix is Ξ and noises whose intensity matrix is Θ [8]. The design aims to regulate
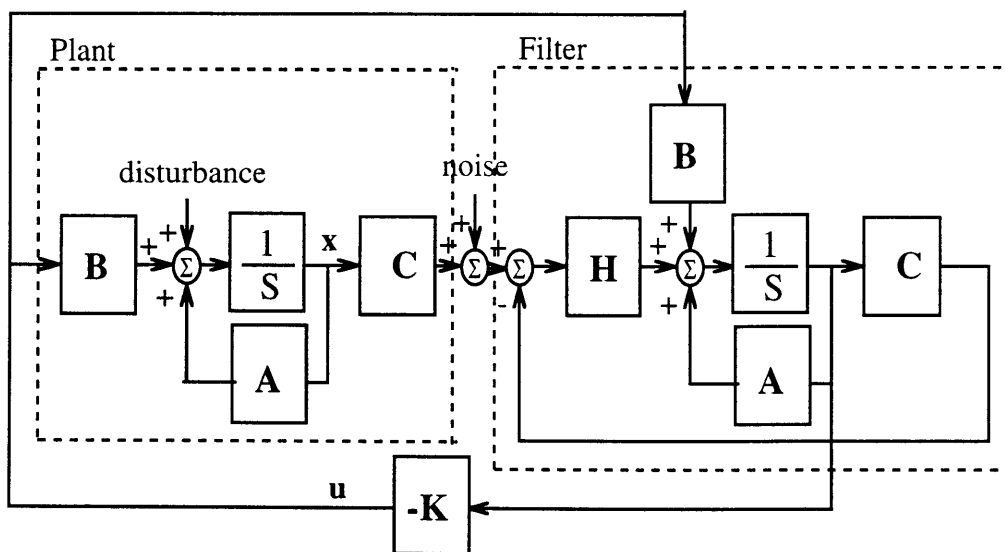
Figure 2.3: Structure of an LQG controller.

the output against a pulse disturbance that is 50 N and lasts 2 ms within 20 ms without overshoot. Ξ=1.0 N and $\Theta = 1.0 \times 10^{-15}$ m are assumed. The fact that we can separately design the filter gain **H** and state feedback gain **K** makes the design process simple (the separation principle). The weighting matrices **Q** and **R**

are decided as follows with a try and error process.

$$\mathbf{Q} = \begin{bmatrix} 1 & 0 \\ 0 & 1.0 \times 10^{-5} \end{bmatrix} \qquad (2.9)$$

$$\mathbf{R} = 3 \times 10^{-9} \qquad (2.10)$$

As a result, $\mathbf{K}$ and $\mathbf{H}$ are calculated as $\mathbf{K} = [1.995 \times 10^4 \ 69.98]$, $\mathbf{H} = [5.629 \times 10^3 \ 1.584 \times 10^7]^T$. The simulation result when the pulse disturbance is applied is shown in Figure 2.4. The output is settled within 20 ms without overshoot.
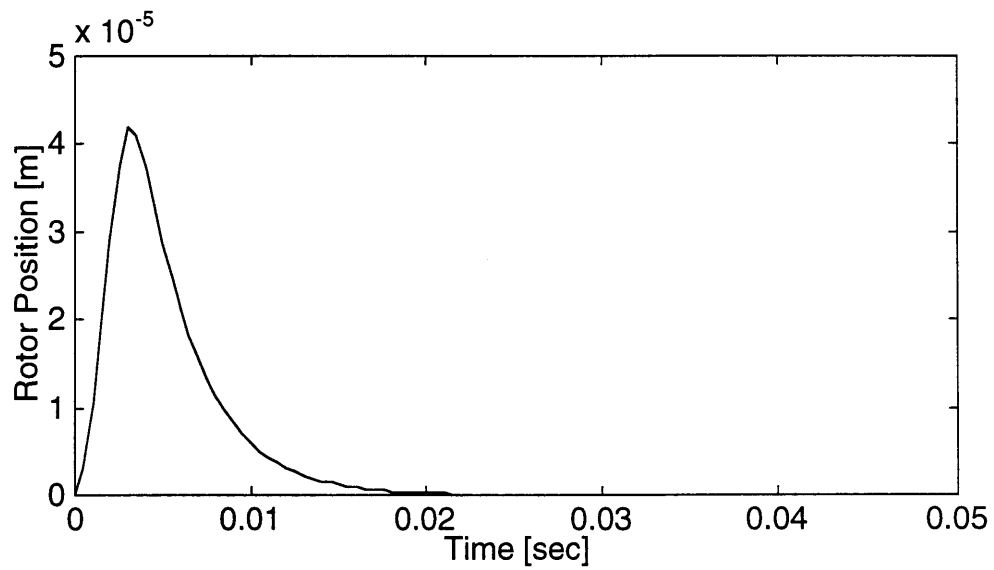
Figure 2.4: Time response of the LQG designed system.

2.3.2 H_∞ Design

One of the critical issues about designing a controller for a real mechanical system is stability robustness with the existence of high frequency uncertainties. These uncertainties include elasticity of the structure and sensor dynamics. In order to maintain the stability of the system, we have to limit the bandwidth of the closed-loop system

24

if unmodeled high frequency dynamics exist. Since the LQG design developed in the previous section does not limit the bandwidth to a specific frequency, I need to an alternative design method needs to be considered if we have to limit the bandwidth to maintain the stability.

For example, suppose the position sensor of the magnetic bearing has dynamics described as

$$G_s(s) = \frac{4000^2}{s^2 + 560s + 4000^2} \qquad (2.11)$$

The magnitude plot of the sensor dynamics is shown in Figure 2.5. Then, the real transfer function of the magnetic bearing becomes different from the ideal transfer function as described in Figure 2.6 in a frequency domain. If we design a controller without considering these dynamics, the closed loop system may become unstable. Figure 2.7 shows the time response when the same disturbance of Figure 2.4 is applied but the sensor dynamics exist. As can be seen from Figure 2.7, the closed-loop system becomes unstable because there is no stability margin in this system.

The so-called H_∞ design is a design method that can minimize the maximum value of a principle gain throughout the frequency domain [8]. With a certain frequency weighting function, an H_∞ design method can achieve an optimal nominal performance while limiting the bandwidth. Figure 2.8 shows the concept of an H_∞ mixed sensitivity design described in a block diagram. While limiting the high frequency gain of the closed-loop transfer function by the weighting function $\mathbf{W_2(s)}$, the design procedure maximize the performance by shaping the sensitivity function to the sensitivity weighting function $\mathbf{W_1(s)}$. The theory can also judge the existence of the controller that achieves the desired sensitivity function. If the controller does not exist, the specification must be changed to realize the controller.

In order to achieve the same performance as achieved in Section 2.3.1, the weight-
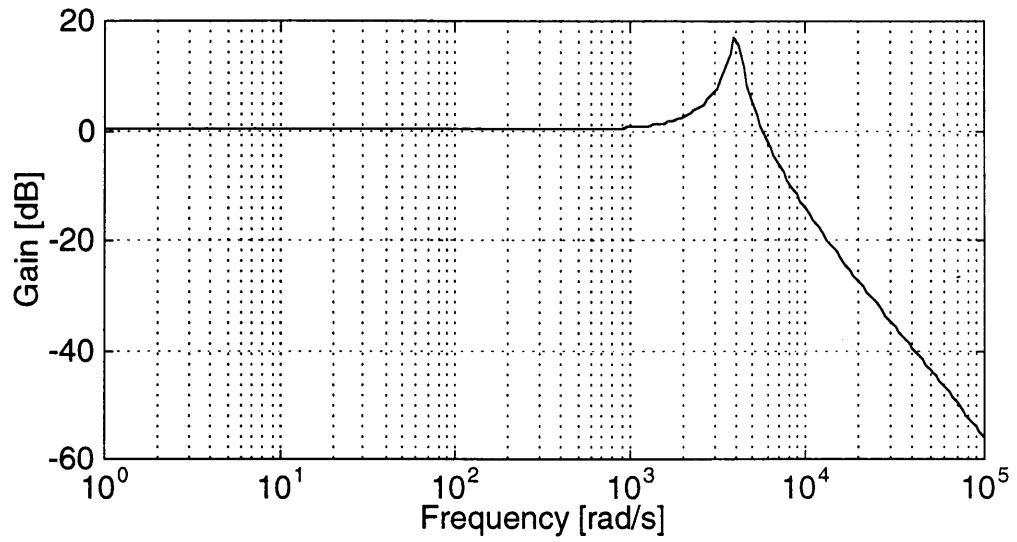
Figure 2.5: Frequency response of the position sensor.
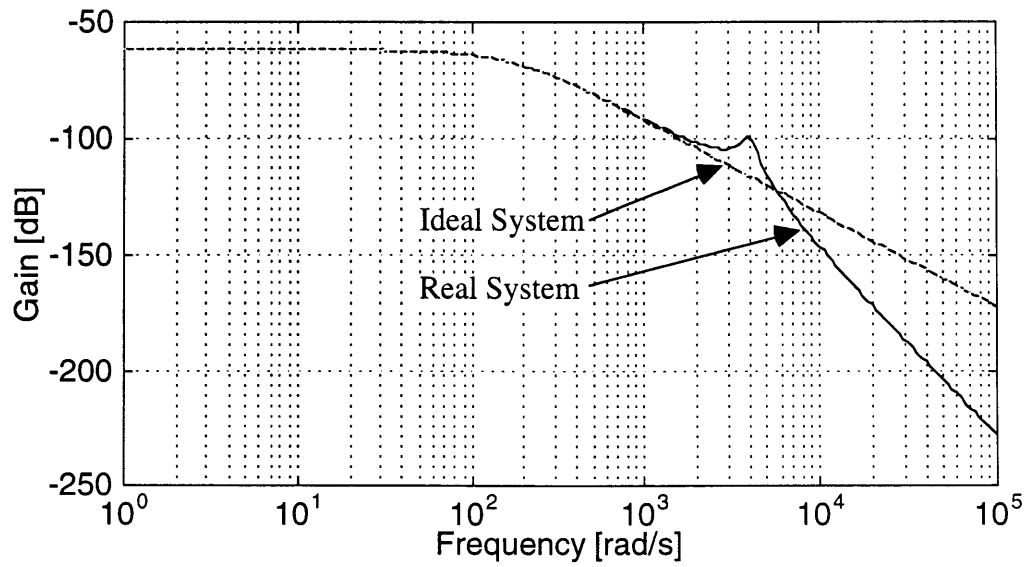
Figure 2.6: Frequency response of the real system.
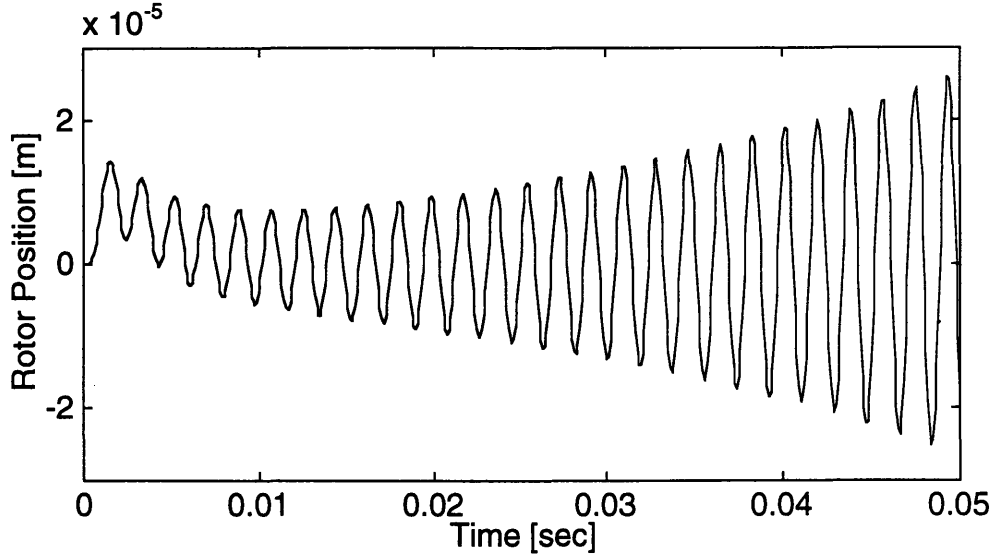
Figure 2.7: Time response of the LQG designed system.

ing function $W_1(s)$ is chosen as shown in Figure 2.9. The designed controller must

achieve the smaller sensitivity function than the curve shown in Figure 2.9 in the low

frequency region. However, because of the relation between the settling time t_s and a

dominant pole p_d, $t_s \approx -4/p_d$, the frequencies over 200 rad/s of the sensitivity func-

tion do not count to achieve the settling time of 20 ms. Therefore, we must choose

the weighting function as simple as possible while it covers the frequency area under

200 rad/s because the order of $W_1(s)$ is added to the order of the controller designed

by the H_∞ design method. The dotted line in Figure 2.9 is the inverse of the selected

weighting function:

$$W_1(s) = \frac{9 \times 40000}{s^2 + 400s + 40000} \tag{2.12}$$

One way of describing uncertainties is to use a multiplicative error $\Delta(s)$ from the

nominal plant. Figure 2.10 shows the block diagram of a multiplicative uncertainty.

If we can asses that the sensor dynamics in Figure 2.5 is the worst deviation from

27
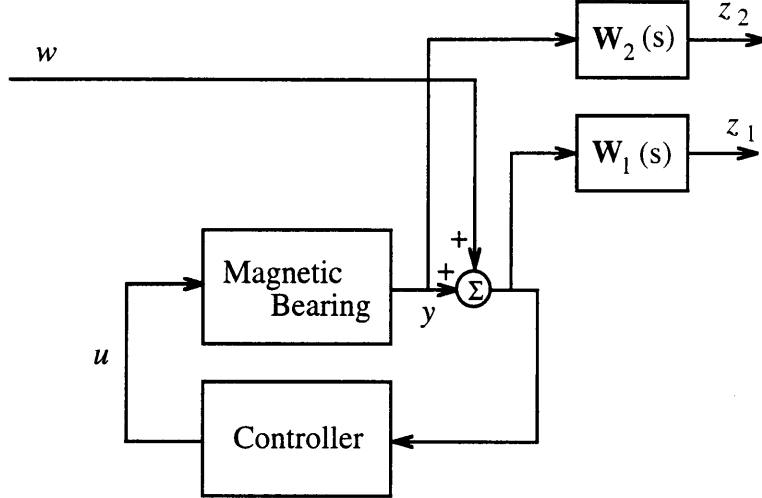
Figure 2.8: Mixed sensitivity H_∞ design.

the nominal plant, we can consider $\mathbf{\Delta(s)}$, the solid line in Figure 2.10, as $\mathbf{G_s(s) - I}$, where $\mathbf{G_s(s)}$ is a transfer function of the sensor and $\mathbf{I}$ is a unit matrix. Then, we can choose the weighting function for the closed-loop transfer function to cover $\Delta(s)$ in the high frequency region as the dotted line in Figure 2.11:

$$W_2(s) = \frac{s^2}{1400^2} \tag{2.13}$$

Again, since the order of $\mathbf{W_2(s)}$ is added to the order of the controller, we should not choose a high order transfer function for $\mathbf{W_2(s)}$. In addition, $\mathbf{W_2(s)}$ can be improper, but the relative order of the combination of $\mathbf{W_2(s)}$ and the plant cannot be negative.

Once we choose the weighting functions, we can calculate the controller by using the commercially available MATLAB m-files. What the program does is to find the controller that achieves the following inequality:

$$\left\| \begin{array}{c} W_1(s)S(s) \\ W_2(s)T(s) \end{array} \right\|_\infty < 1 \tag{2.14}$$

If the controller that achieves Eq.(2.14) does not exit, we have to revise the specifica-
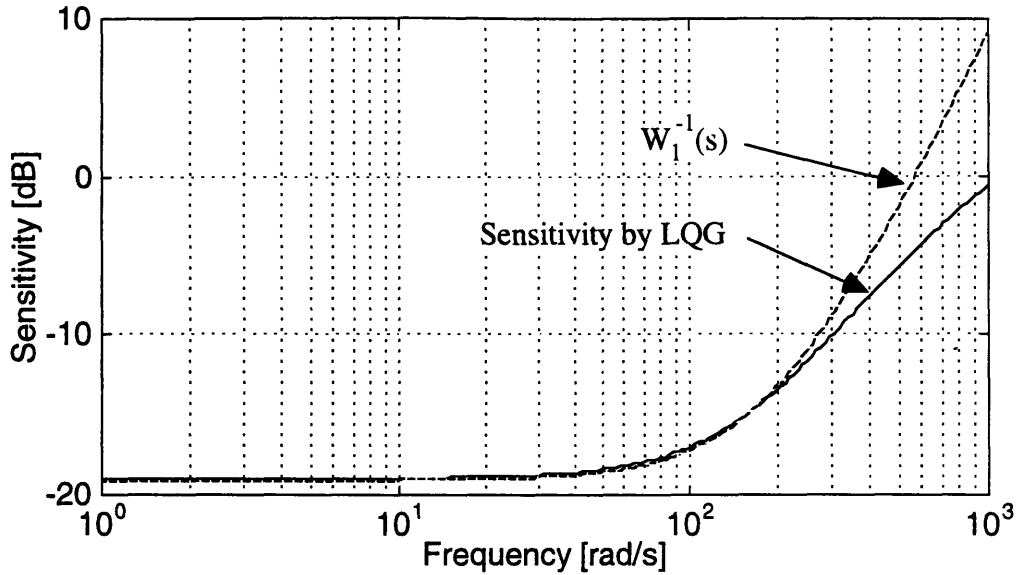
Figure 2.9: Desired sensitivity function.
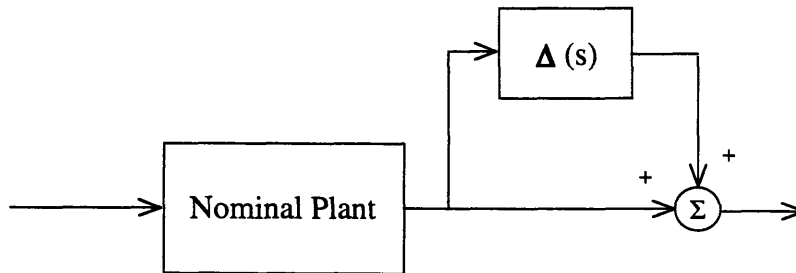
Figure 2.10: Multiplicative uncertainty.

tion. In fact, the controller that satisfies the specification, Eq.(2.12) and Eq.(2.13), simultaneously does not exist. Therefore, the performance specification needs to be revised in terms of $W_1(s)$, not $W_2(s)$, because stability must be maintained. This revision can be either to make the gain lower, to make the dominant pole slower, or both. The procedure to find a controller by making the gain of $W_1(s)$ lower is called "gamma iteration," and it is also commercially available as a MATLAB m-file. Figure 2.12 shows a sensitivity function bode plot of the designed closed system. The dotted

29
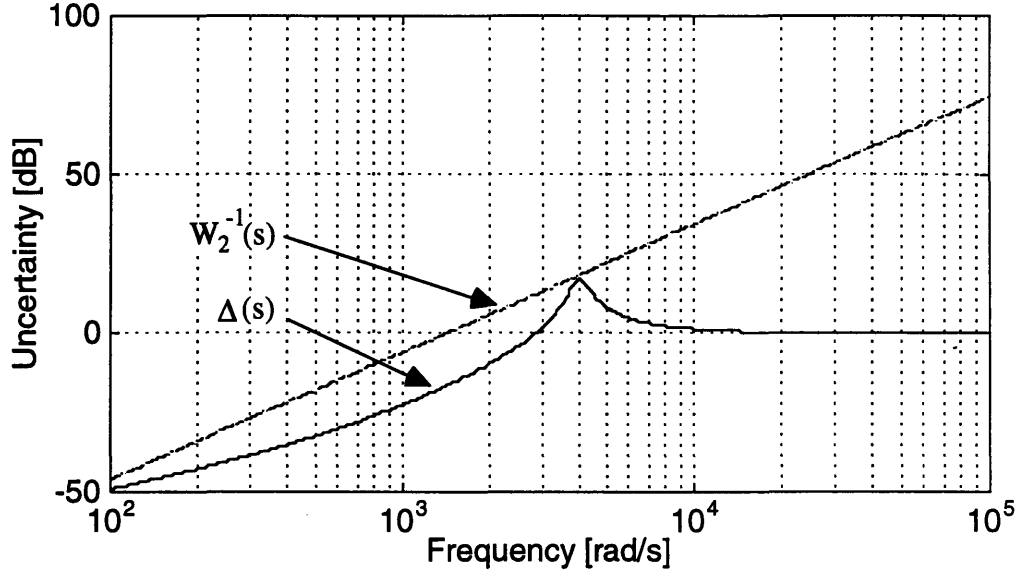
Figure 2.11: Necessary robustness bound.

line is the revised weighting function used for the design. Instead of using $W_1(s)$ of Eq.(2.12), the following $W_1(s)$, whose gain is lowered to make the controller exist, is used.

$$W_1(s) = \frac{6.1 \times 40000}{s^2 + 400s + 40000} \tag{2.15}$$

The closed-loop transfer function of the designed system is shown in Figure 2.13, and the inverse of the weighting function $W_2(s)$ is shown in Figure 2.13 as a dotted line. The closed-loop transfer function is lower than $W_2(s)$ throughout all frequencies. The response of the rotor when the same disturbance as Figure 2.4 is applied to the system is shown in Figure 2.14. In this simulation, the sensor dynamics are not included in the plant. Even though it achieves almost the same settling time as Figure 2.4, the performance is not as good as the system designed by the LQG method. However, as can be seen in Figure 2.15, even when the sensor dynamics exist, the closed-loop system maintains stability.

30
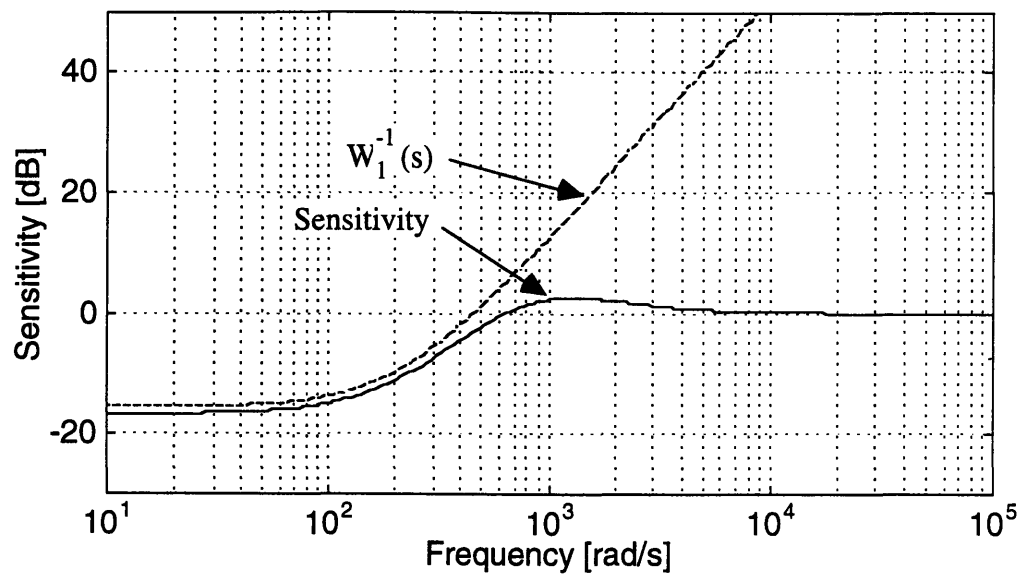
Figure 2.12: Sensitivity function of the H_∞ designed system.
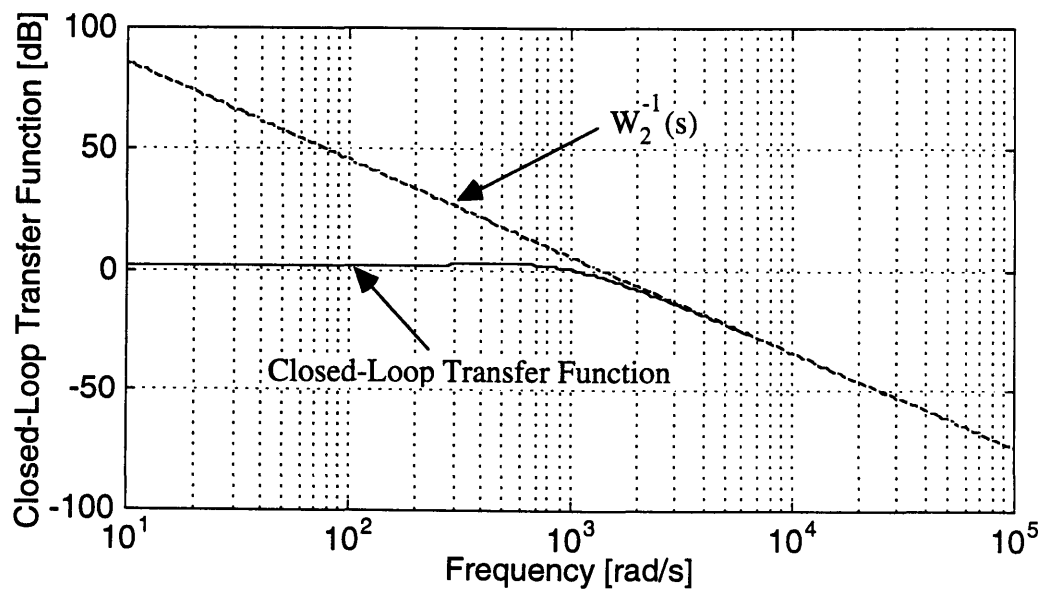
Figure 2.13: Closed-loop transfer function of the H_∞ designed system.

31
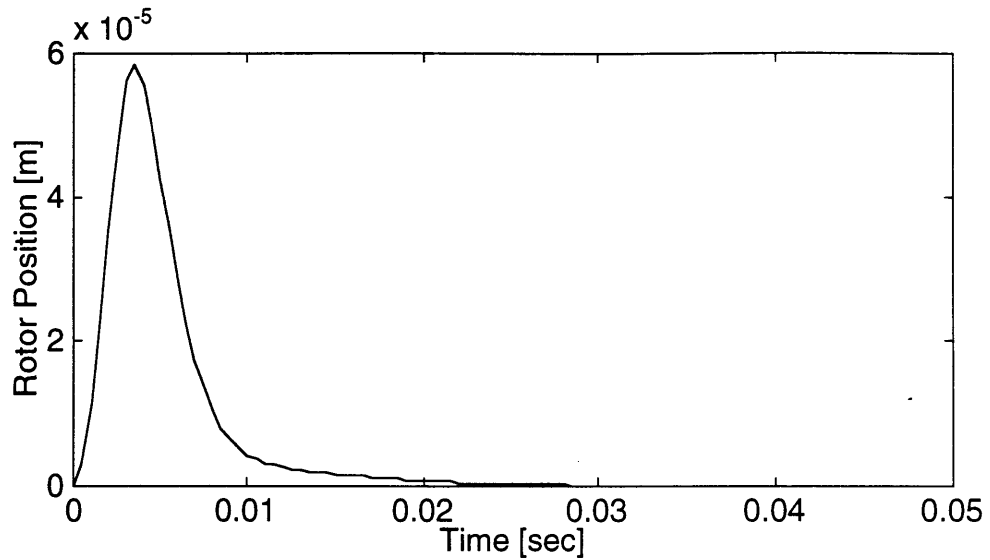
Figure 2.14: Time response of the H_∞ designed system.
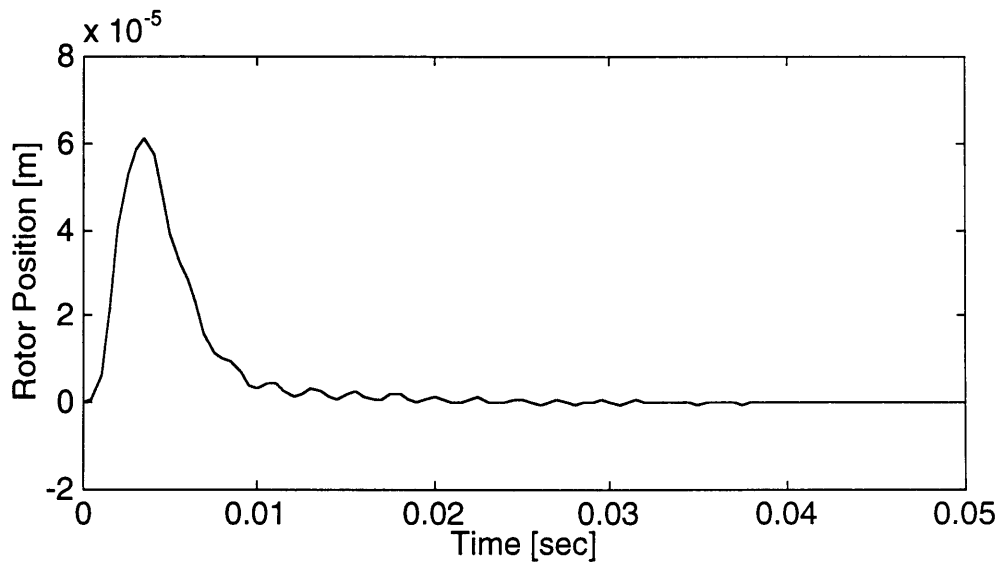
Figure 2.15: Time response of the H_∞ designed system with the sensor dynamics.

2.3.3 LQG/LTR Design

An LQG/LTR design is the other approach to achieve stability robustness. The LTR method recovers the closed loop system to the filter loop. Therefore, we first design

the filter loop that has the characteristics the closed-loop system is supposed to have, and next, approximate the system by the solution of the cheap control LQR problem [8].

The structure of the controller is the same as that in Figure 2.3. First, the filter gain $\mathbf{H}$ is chosen to have the desired characteristics. By tuning the gain of the filter to make the gain of the closed-loop transfer function smaller than $\mathbf{\Delta}^{-1}(\mathbf{s})$ and make the sensitivity function close to the one in Figure 2.12, $\mathbf{H} = [4.66 \times 10^2 \; 1.09 \times 10^5]^T$. is chosen. The sensitivity function and the closed-loop transfer function of the filter loop are shown in Figure 2.16 and Figure 2.17. Figure 2.18 and Figure 2.19 are the bode plots of the sensitivity function and closed-loop transfer function of the recovered closed-loop system. Both functions are almost the same as those of the filter's. As a result, we obtain a time response that is similar to but slightly slower than the response in Figure 2.12 (Figure 2.20). The disturbance applied to the system is the same disturbance mentioned in Section 2.3.1, which is the pulse whose amplitude is 50 N and that lasts 2 ms. The stability robustness is also satisfied because the bandwidth of the closed-loop system is properly limited, and as Figure 2.21 shows, even when the sensor dynamics exist, the closed-loop system is stable (However, it shows oscilations because the system is almost on the stable limit).

The problem of the LQR/LTR design is that it is not easy to find the filter gain that realizes the desired filter loop. Moreover, it is difficult to estimate the limitation of the performance we can achieve with the LQG/LTR design procedure. In this example, the limitation of achievable performance was known from the result in the previous section. However, in general case, we might waste a time to select a filter gain by pursuing the impossible performance.

33
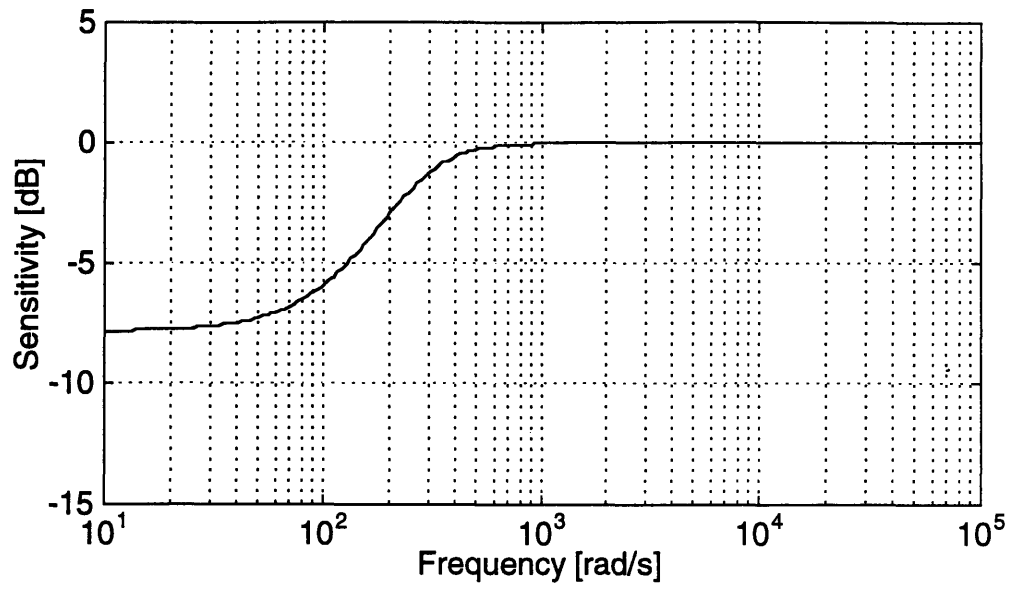
Figure 2.16: Sensitivity function of the filter loop.
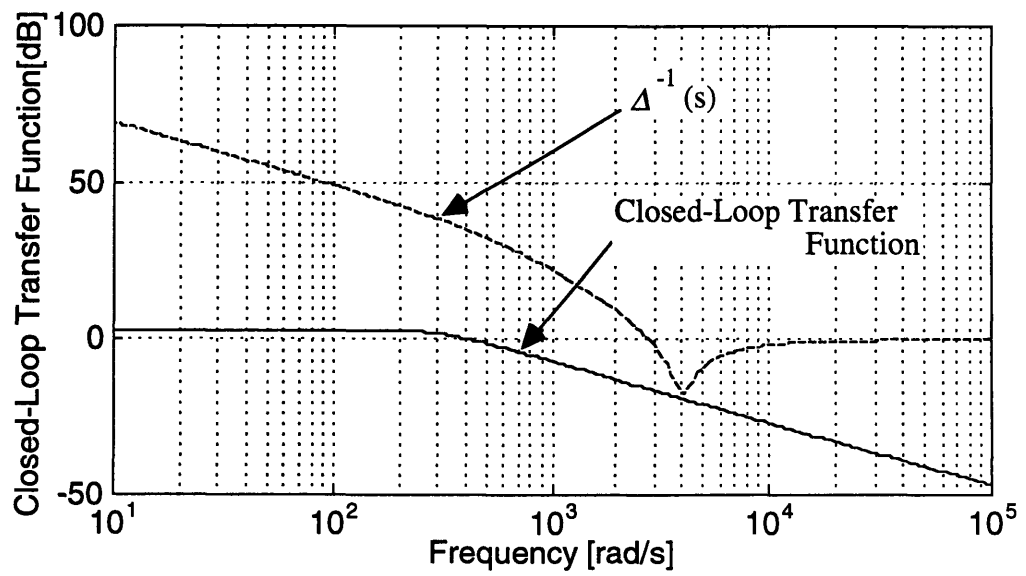
Figure 2.17: Closed-loop transfer function of the filter loop.
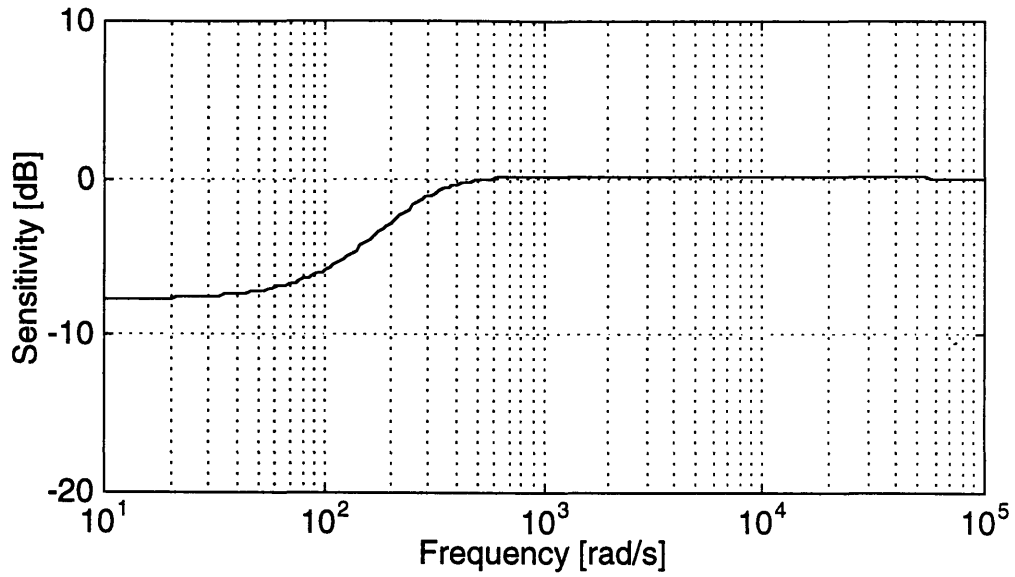
Figure 2.18: Sensitivity function of the LQG/LTR designed system.
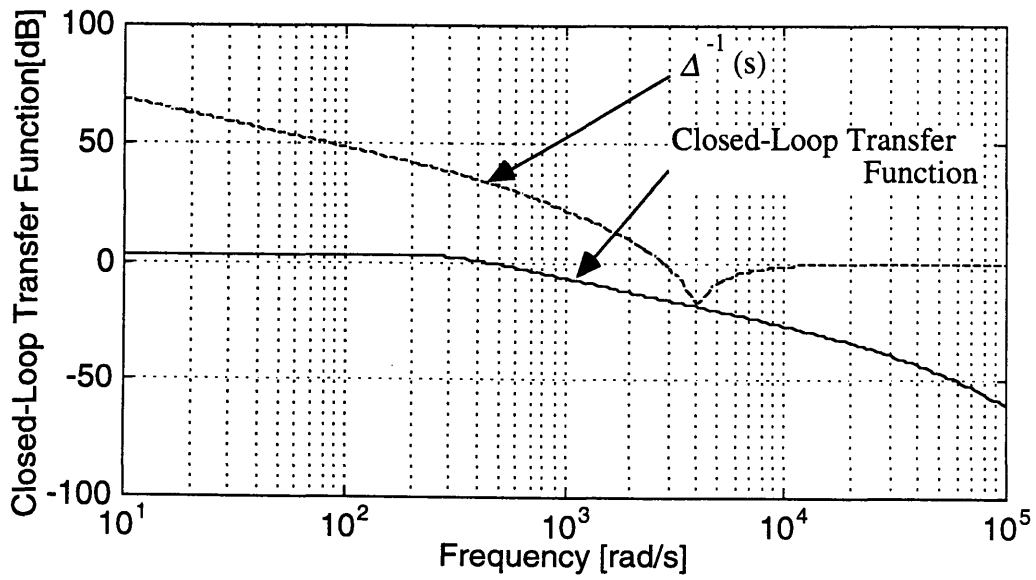
Figure 2.19: Closed-loop transfer function of the LQG/LTR designed system.

35
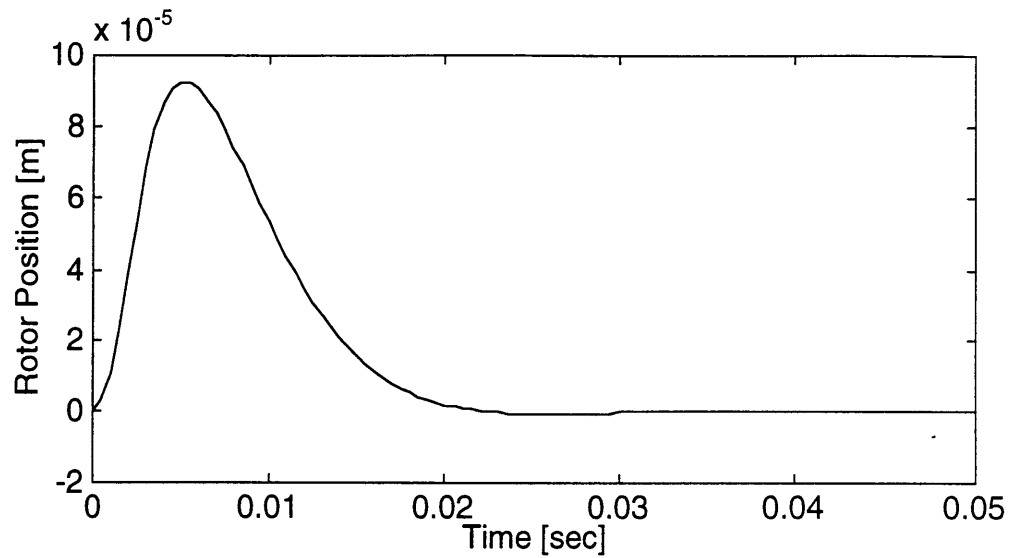
Figure 2.20: Time response of the LQG/LTR designed system.
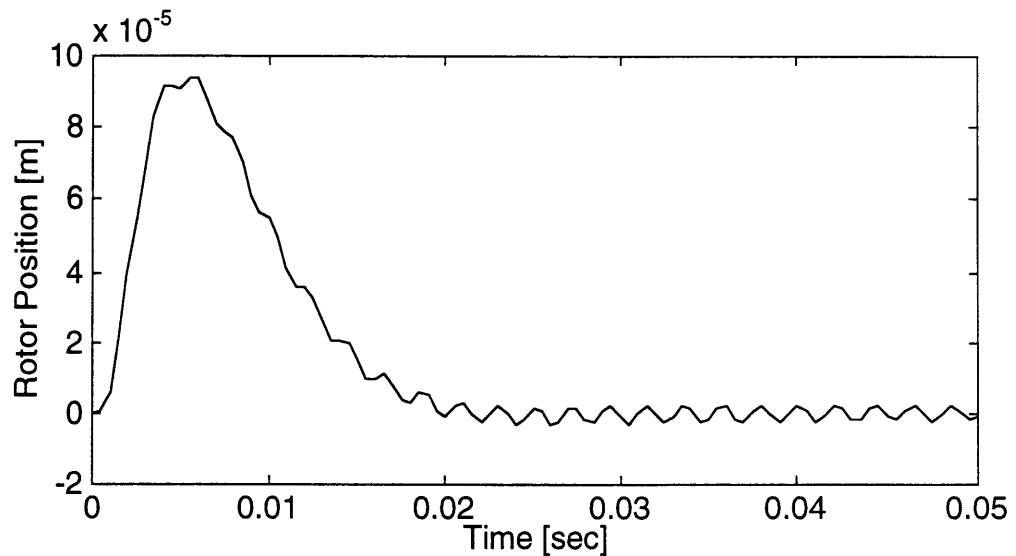
Figure 2.21: Time response of the LQG/LTR designed system with the sensor dynamics.

2.3.4 μ-Synthesis

The H_∞ design and LQG/LTR design can achieve only stability robustness. μ-Synthesis has the potential of solving the overall robust control problem including

performance robustness. Dyle et al showed performance robustness is expressed in the form of fictitious uncertainties and the small gain theorem [9]. Therefore, the robust control problem can be considered to solve a problem described in Figure 2.22 as a generalized form, and using structure singular values as judging values, we can design a controller that achieves performance robustness as well as stability robustness [1].
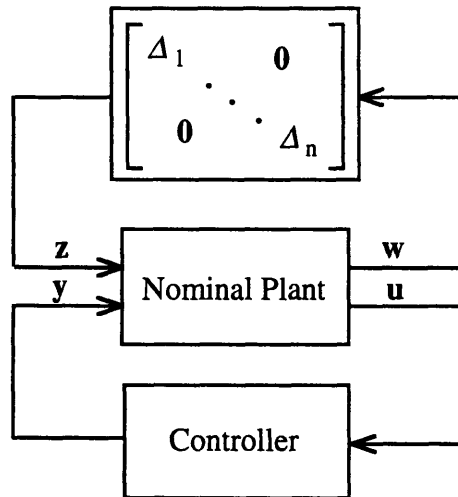
Figure 2.22: Generalized robust control design problem.

In order to demonstrate performance robustness, suppose the case that the mass of the rotor is unknown, but the maximum mass does not exceed 4.5 kg and minimum mass does not become less than 3.0 kg. I try to achieve a sensitivity function lower than the bound described below in Eq.(2.16) no matter how much the mass is within the range from 3.0 kg to 4.5 kg.

$$W_1(s) = \frac{10 \times 200}{s + 200} \tag{2.16}$$

This uncertainty is expressed as a form in Figure 2.23 [1]. By choosing $\mathbf{B_2}$, $\mathbf{C_2}$,

and $\mathbf{D_2}$ in Figure 2.23 as

$$\mathbf{B_2} = \begin{bmatrix} 0 \\ \frac{4k_0 i_0^2}{z_0^3} \end{bmatrix} \tag{2.17}$$

$$\mathbf{C_2} = \begin{bmatrix} 1 & 0 \end{bmatrix} \tag{2.18}$$

$$\mathbf{D_2} = \frac{z_0}{i_0} \tag{2.19}$$

Then, the system matrices $\mathbf{A}$ and $\mathbf{B}$ can be written as

$$\mathbf{A} = \begin{bmatrix} 0 & 1 \\ \frac{4k_0 i_0^2}{z_0^3}(\frac{1}{m_n} + \Delta_2) & 0 \end{bmatrix} \tag{2.20}$$

$$\mathbf{B} = \begin{bmatrix} 0 \\ \frac{4k_0 i_0^2}{z_0^3}(\frac{1}{m_n} + \Delta_2) \end{bmatrix} \tag{2.21}$$

where m_n is the nominal value of the mass of the rotor. Then, the corresponding
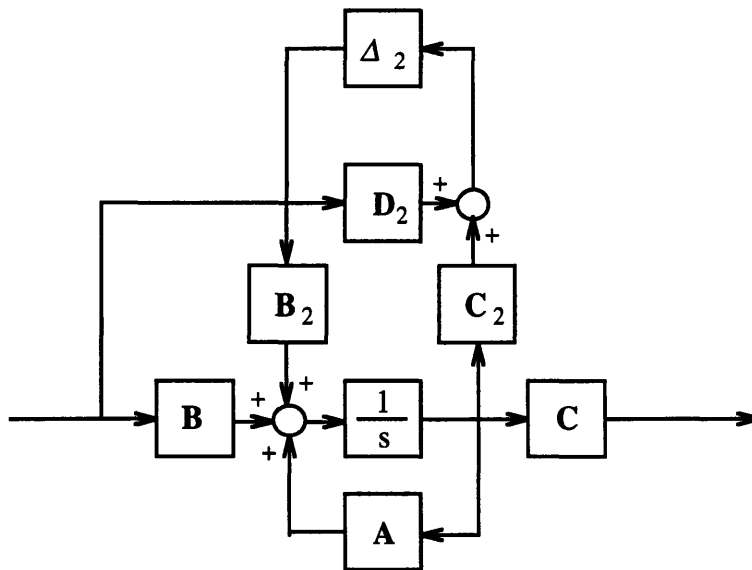
Figure 2.23: Parametric uncertainty of the system.

nominal mass m_n and Δ_2 to $m = 3.0 \sim 4.5$ kg become the values in Table 2.2.

Figure 2.24 shows the block diagram for this robust performance problem. Once we can describe the problem as this canonical form. we can use the computer aided

	Numerical Values

Nominal Mass	m_n	3.6 kg
Uncertainty	Δ_2	5.556×10^{-2}

Table 2.2: Nominal mass and uncertainty.
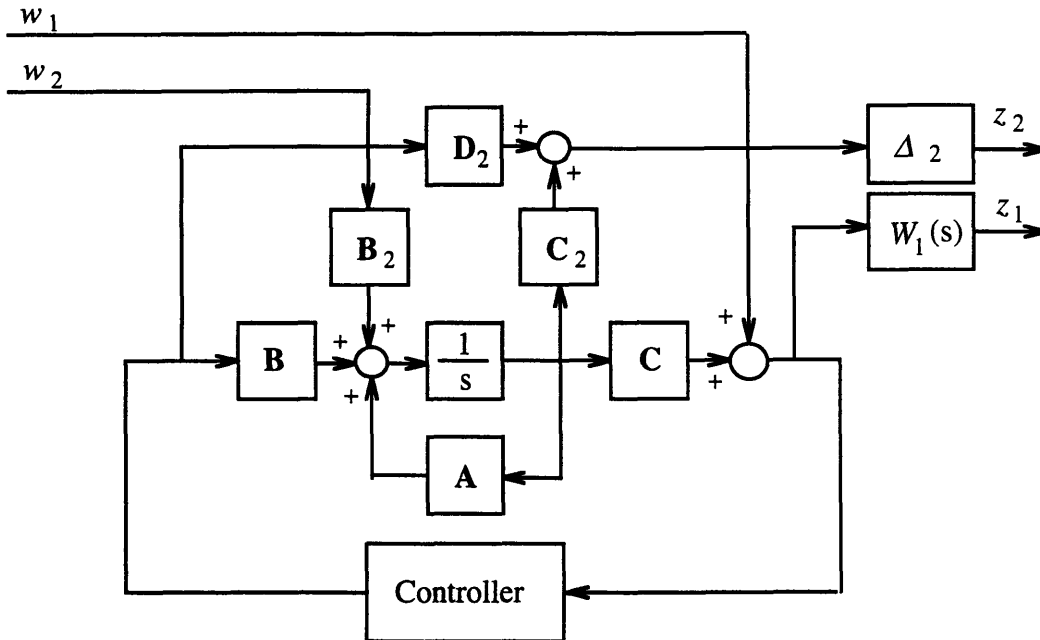
Figure 2.24: Block diagram of the μ-synthesis structure.

design tool to design the controller. μ-Synthesis consists of the iteration of an H_∞ optimal design and curve fitting (D-scale fitting). The design completes when the structured singular values become less than one throughout the all frequencies [1]. Figure 2.25 shows the structured singular value plot before the D-scale fitting has not been done. With the D-scale fitting, I try to minimize the maximum structured singular value and make it less than one. D-scale must be approximated with finite systems. The order of the approximated system should be as low as possible because
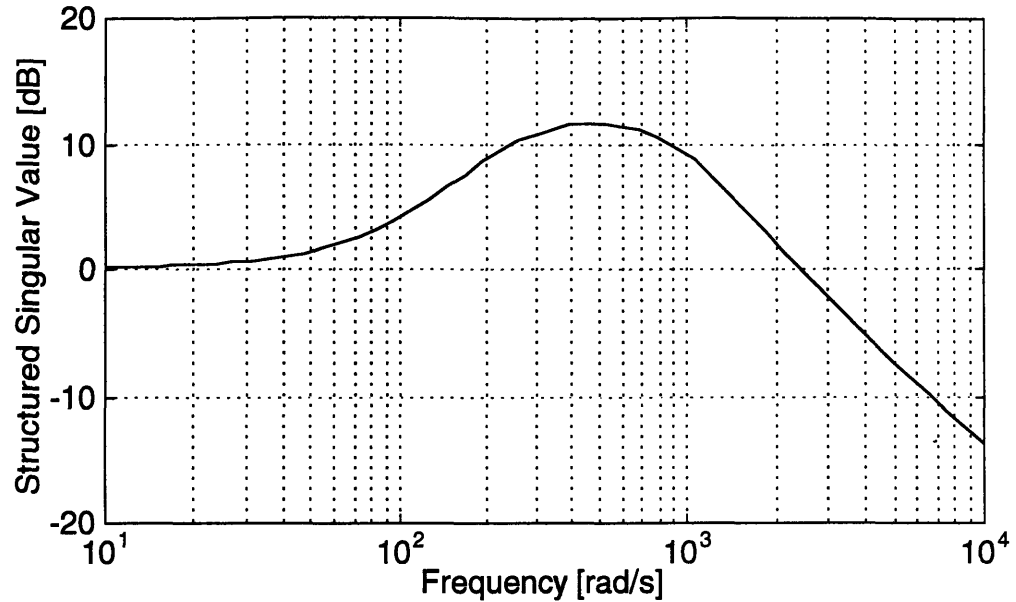
Figure 2.25: Structured singular values before D-scale fitting.

the order of the controller becomes huge if we choose a high-order approximation. In this case, a 5th order system is appropriate to approximate the D-scale derived in the process of calculating the structured singular values (Figure 2.26 and Figure 2.27). This D-scale fitting leads the maximum structured singular value of the closed-loop system less than one. How the maximum structured singular value is lowered is shown in Figure 2.28. As seen in Figure 2.28, the structured singular values in the frequency domain become flat (all pass) with the iteration of the H_∞ optimization and D-scale optimization.

In general case, structured singular values cannot be directly obtained. Only if the number of the blocks, Δ_i, is less than or equal to three, the structured singular value can be evaluated. Otherwise, we can only evaluate performance robustness by the upper bounds of structured singular values. Yet, the research indicates that even if the number of Δ_i is more than three, the difference between the upper bound obtained by D-scale fitting and the structured singular value is usually less than 5 %

40
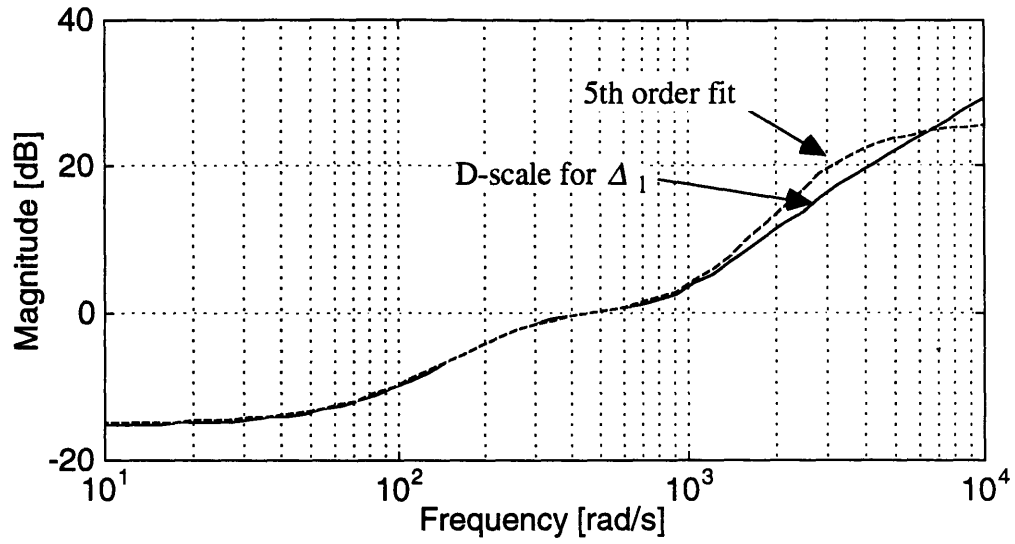
Figure 2.26: D-scales and the fitted 5th order curves for Δ_1.
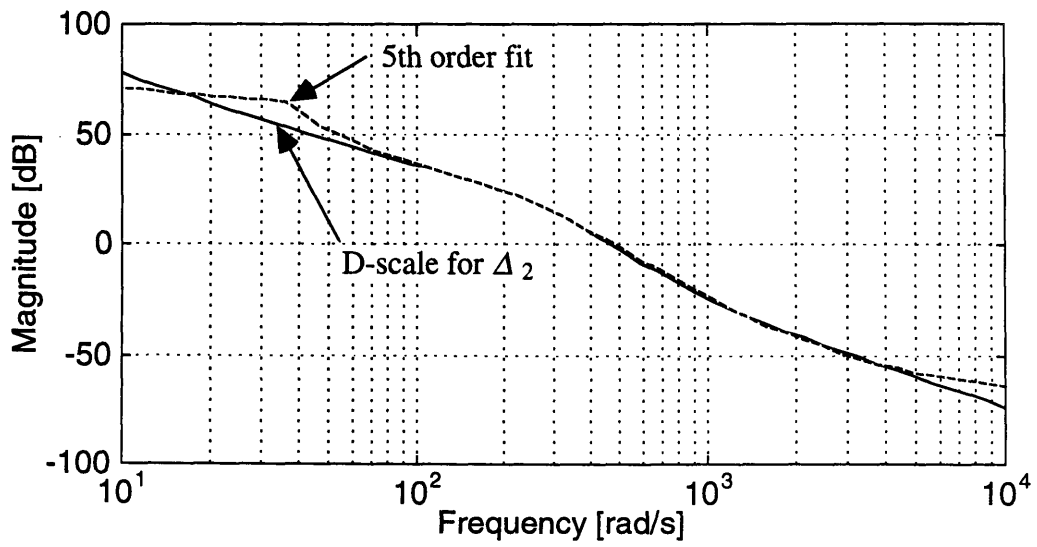
Figure 2.27: D-scales and the fitted 5th order curves for Δ_2.
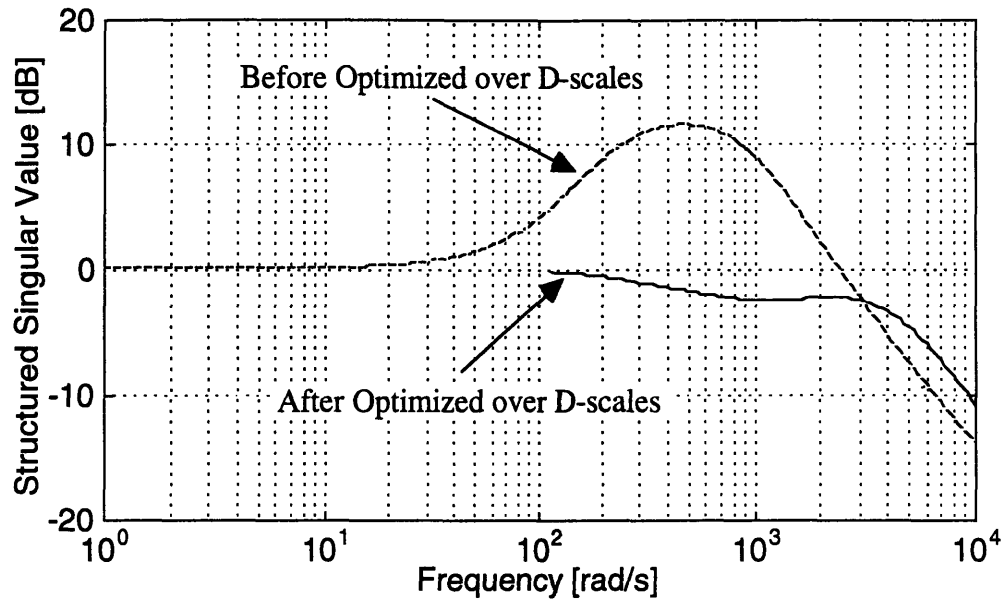
Figure 2.28: Structured singular values after the D-scale fitting.

[8]. In this case, the number of Δ_i is two; therefore, the result of the μ-synthesis is not conservative. Figure 2.29 is the magnitude plot of the sensitivity functions with three different rotor masses. The μ-synthesis makes all the sensitivity functions less than the sensitivity bound set as a specification.

2.4 Summary

In this chapter, several controller design methods based on the linear theories were demonstrated. Many of the existing design methods are based on linear theories, and we can choose one of them to achieve the specific purpose such as to minimize the quadratic function of the time response or to guarantee the response time even when uncertainties exist in the system.

In the case of magnetic bearings, stability robustness is essential because of their unstable nature. Moreover, when we use the magnetic bearing for precise position-
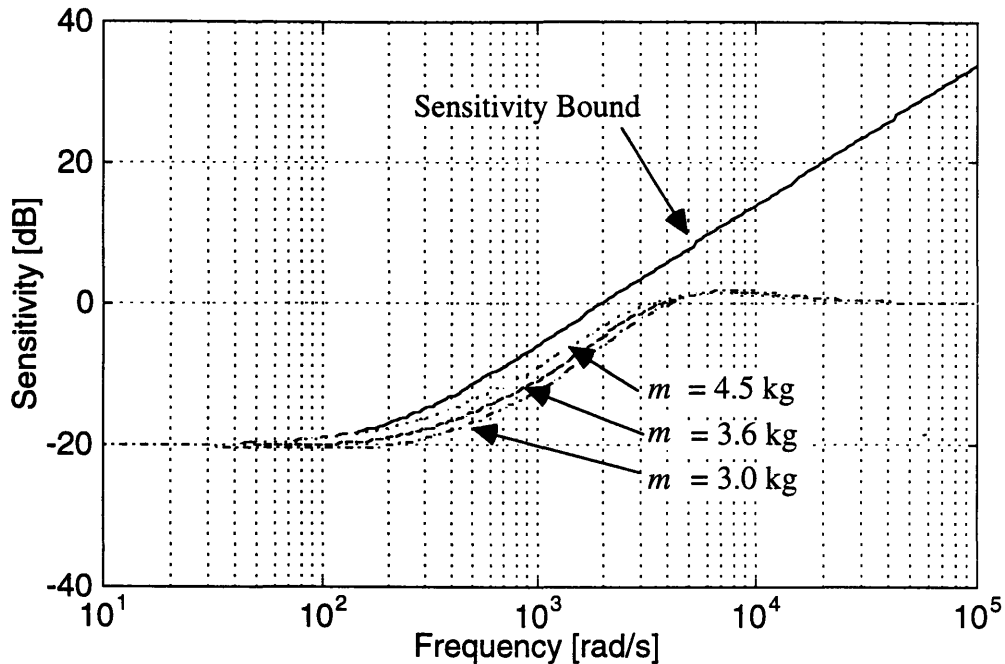
Figure 2.29: Sensitivity function with the various rotor masses.

ing, performance robustness is required as well as the stability robustness. For this purpose, μ-synthesis is suitable to achieve uniformed responses when uncertainties exist. This robust performance issue is the result of relatively recent researches; thus, there still is an immaturity in the process of design. However, in this chapter, it was demonstrated that the designed system is guaranteed the performance robustness even though conservativeness may exist in some cases.

Table 2.3 shows the comparison among the most often-used linear design methods. As design specifications become complicated, more sophisticated calculations are required. However, most of the design sequences in Table 2.3 are programmed in MATLAB m-files as listed and commercially available. Therefore, all we have to do is to formulate the problems as a canonical form that can fit the computer aided design. The Matlab programs that are used to design the controllers in this chapter are attached in Appendix.

	Features	Guarantees	Disadvantages	MATLAB Commands
Pole Placement	• Uses pure gain controller • Places the closed loop poles	• Stability	• Need full-state feedback • Cannot specify the trade-off	• acker (SISO) (Control System Toolbox) • place (MIMO) (Control System Toolbox)
Eigenstructure Assignment	• Uses pure gain controller • Assignes the closed loop poles and eigenvectors	• Stability	• Need full-state feedback • Cannot specify the trade-off	
LQR	• Uses a quadratic performance index • Uses pure gain controller	• Stability margin (gain ∞, phase 60°)	• Need full-state feedback • Need accurate model • Possibly many iterations	• lqr (Control System Toolbox)
LQG	• Uses a quadratic performance index • Uses available noise information in plant and measurement	• Stability	• Need accurate model • No stability margin guaranteed • Possibly many iterations	• lqr & lqe (Control System Toolbox) • lqg (Robust Control Toolbox)
LQG/LTR	• Recovers the target filter loop	• Robust stability	• High gain controller • Minimum phase plant only	• ltru (Robust Control Toolbox)
H∞	• Specifies the performance and robust stability by H∞ norms • Exact loop shaping	• Robust stability	• Restrictions exist in the form of an augmented plant	• hinf (Robust Control Toolbox) • hinfsyn (μ-Analysis and Synthesis Toolbox)
μ-Synthesis	• Uses structured singular values • Has potential to solve the overall robust control problem	• Robust stability • Robust performance	• Problem is nonconvex • Controller size is huge	• musyn (Robust Controll Toolbox) • dkit (μ-Analysis and Synthesis Toolbox)

Chapter 3
Limitations of Linear Controllers

3.1 Introduction

In Chapter 2, it was shown that it is possible to design a controller that satisfy the specification with μ-synthesis even when uncertainties exist. This performance robustness is especially necessary for the precision magnetic bearings for machining center spindles or the joints of robot manipulators because pay load changes as the machining tool is changed or the configuration of the manipulator changes. We can implement uncertainties in the design specification, and μ-synthesis guarantees the uniformed responses within the specified uncertain range. However, if uncertainties are large, linear controllers may not be able to satisfy the specification. The existence of the linear controller that satisfies the specification when uncertainties exist is of interest because if we cannot achieve the specification with linear controllers, we must consider an alternative method. The H_{∞} design method can judge the existence of the controller that satisfies the specification. Since μ-synthesis is a combination of the H_{∞} optimal design and D-scale fitting, it has the potential to judge the limitations of linear controllers for overall robustness problems.

In this chapter, it is first shown how the limitation of the linear controllers is determined by the H_{∞} design method. Then, the effect of the range of the uncertainty, which is used in Chapter 2 as a design example is examined. In addition, we try to reveal the limitations by using the structured singular value plot. Finally, the possible adverse aspects are listed and how to avoid these disadvantages is discussed.

3.2 Achievable Performance with Limited Bandwidth

The H_∞ optimal design method is known to shape the closed-loop transfer function (or sensitivity function) exactly the same shape we plan to be as a shape of the weighting functions. In addition, it gives us the information about the existence of the controller that satisfies the specification given as a shape of weighting functions within the linear frame. For example, consider the case to design a controller for the magnetic bearing that has the parameters shown in Table 2.1. Suppose the sensitivity bound (performance specification) $W_1(s)$ is given as

$$W_1(s) = \frac{10 \times 200}{s + 200} \tag{3.1}$$

and the bandwidth of the closed-loop system and the roll-off at the high frequencies are defined as

$$W_2(s) = \frac{s^2}{\omega_c^2} \tag{3.2}$$

The performance bound is set to achieve the settling time of about 1 ms and reasonably-small steady state error. The parameter ω_c is decided by the unmodeled dynamics that exist in the high frequency region as shown in Chapter 2. The stability must be maintained; therefore, the closed-loop transfer function of the designed system must have lower gain than $W_2^{-1}(s)$ in Eq.(3.2). Thus, the design is proceeded to make the H_∞-norm of the closed-loop system

$$J = \left\| \begin{array}{c} \gamma W_1(s)S(s) \\ W_2(s)T(s) \end{array} \right\|_\infty \tag{3.3}$$

less than one, where S(s) is the sensitivity function and T(s) is the closed-loop transfer function. If γ exists such that $\gamma > 1$ and $J < 1$, the controller that satisfies the specification exists. However, if it does not exist, we have to revise the specification.

The so-called γ-iteration automatically changes the γ and evaluates the maximum γ that leads $J < 1$. The maximum singular values of the transfer function from $\mathbf{w}$ to $\mathbf{z}$

$$T_{wz}(s) = \begin{bmatrix} W_1(s)S(s) \\ W_2(s)T(s) \end{bmatrix} \tag{3.4}$$

of the system designed by γ-iteration are plotted in Figure 3.1 with several ω_c. From this figure, we can observe that the limitation of a linear controller that satisfies the performance specification, Eq.(3.1), is somewhere between $\omega_c = 3000$ rad/s and $\omega_c = 4000$ rad/s. In this calculation, the tolerance of γ is set to 0.001. The reason why the maximum singular values of T_{wz} at the high frequencies rolls off is that the optimization is not perfectly done. If a tighter tolerance is chosen, the maximum singular values of T_{wz} become flat for all frequencies. However, that is not necessary because the tolerance of 0.001 covers all the necessary frequencies.
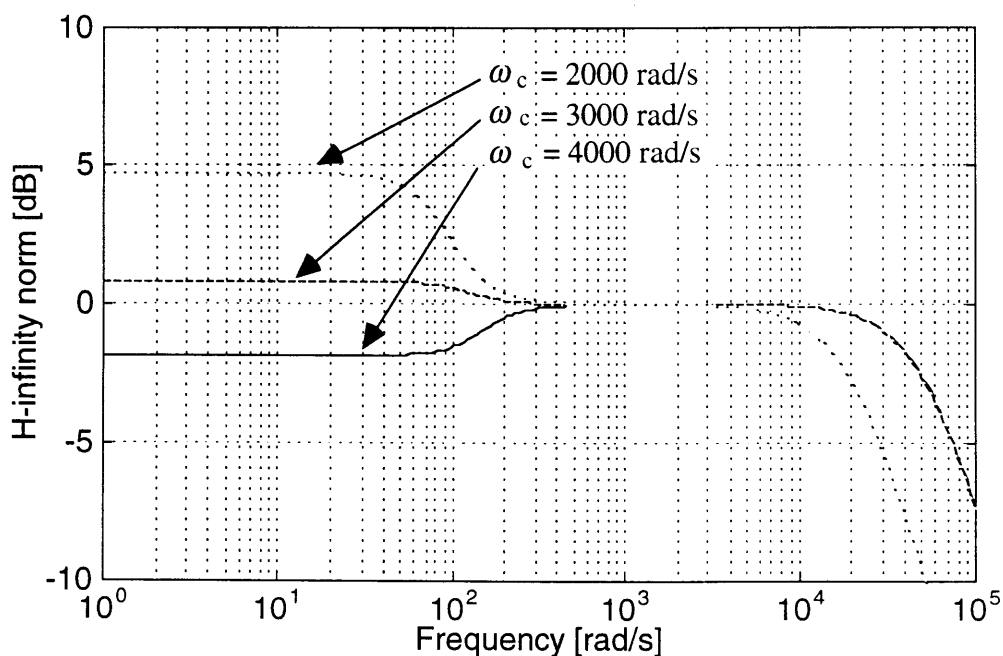
Figure 3.1: Maximum singular values of $T_{wz}(s)$.

This limitation forces us to revise the performance specification. Figure 3.2 shows the achievable performances with several bandwidth limits ω_c, and the corresponding closed-loop transfer functions are shown in Figure 3.3.

This feature, to judge the existence of the controller, of the H_∞ design method is powerful because it reveals the limitation of linear controllers with bandwidth limit.

3.3 Limitation with Parameter Uncertainties

In Chapter 2, I showed that we can judge performance robustness by structured singular values. Even though there still is a room to improve, μ-synthesis gives us an insight of the limitation of linear controllers when we try to achieve performance robustness. Consider the case given in Section 2.3.4. A controller that satisfies the performance specification even when the mass of the rotor changes at the range of 3.0 to 4.5 kg was designed. Here, how wide range the linear controller can tolerate is of interest because if there are no linear controllers that can achieve the performance robustness, we have to consider other approaches.

Figure 3.4 shows the structured singular value plot of the closed-loop system designed by μ-synthesis with various uncertainties. As can be seen from the figure, we can design the controller that satisfies the performance bound, Eq.(3.1), even if the mass of the rotor is unknown but within the range of 3.0 to 4.5 kg. Figure 3.5 shows 10-μm step responses of the closed-loop system with the cases of $m = 3.0$ kg, $m = 3.6$ kg (nominal mass), and $m = 4.5$ kg. Even though the mass increases 50 %, the shapes of the responses are uniformed, and the settling time keeps 1 ms for all three cases. However, if the upper bound of the uncertainty exceeds 4.5 kg, the maximum structured singular value becomes more than one. That means the designed system does not satisfy the specification for the specified uncertainty range.
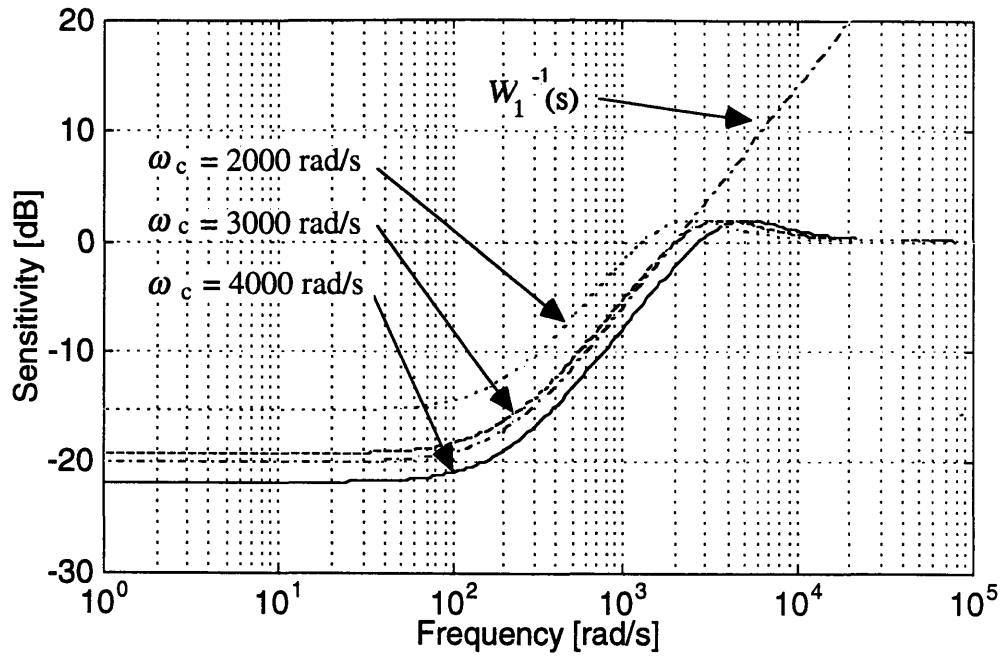
Figure 3.2: Achievable sensitivity functions with various ω_c.
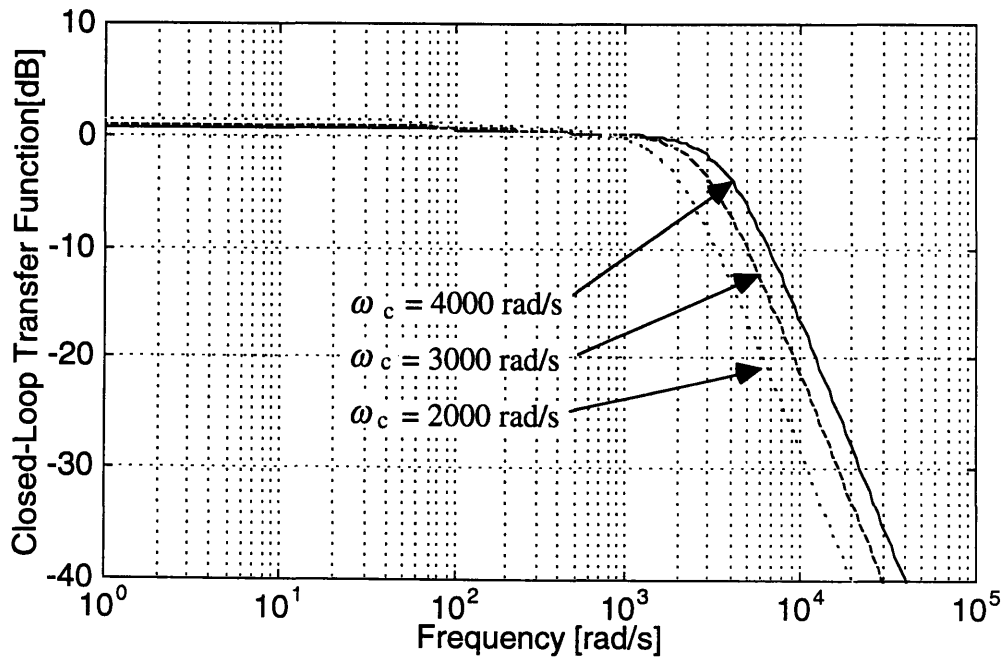
Figure 3.3: Closed-loop transfer function of the systems.

49
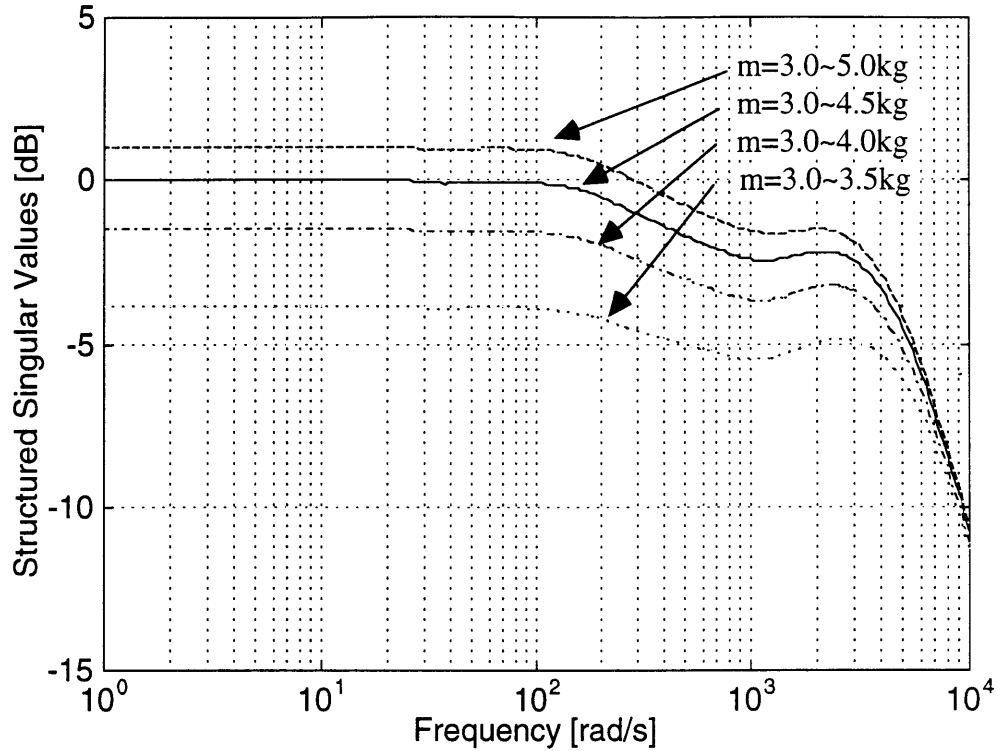
Figure 3.4: Structured singular values with various uncertainty ranges.

Therefore, if the uncertainty range of the mass is 3 to 5 kg, the resultant sensitivity function by μ-synthesis does not become less than $W_1^{-1}(s)$ for all frequencies (Figure 3.6). As a result, in the 10-μm step response, the shape of the response can have overshoot, or the settling time can take more than 1 ms (Figure 3.7).

When looking into Figure 3.4, we observe that the structured singular values are not flat for all the frequencies. That means the design is not perfectly optimized in terms of lowering the maximum structured singular value. The limitation of linear controllers is precisely estimated when we can obtain an all-pass structured singular values. However, it requires more precise (higher order) approximation for D-scale fitting and smaller tolerance for H_∞ optimization in the μ-synthesis process. In this case, a 5th-order approximation for D-scale fitting and a tolerance of 0.01 for
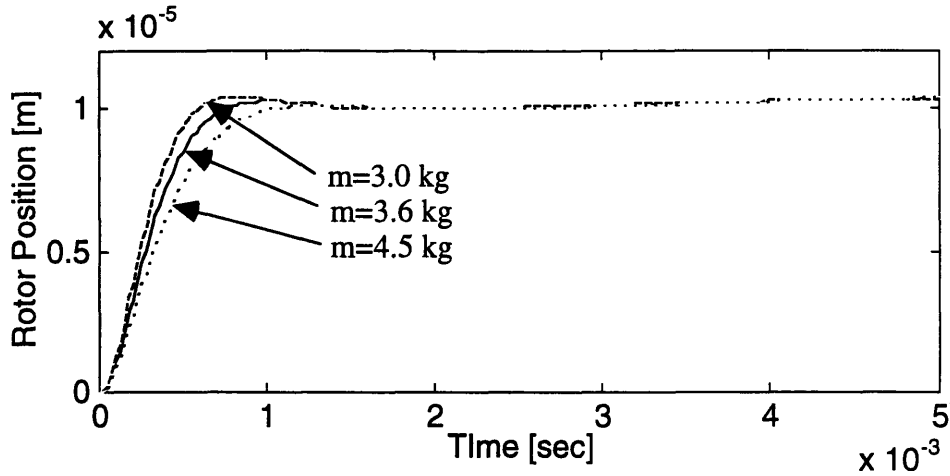
Figure 3.5: Step responses of the system designed for $m = 3.0 \sim 4.5$ kg with various m.

γ-iteration are used, and limitations are reasonably estimated.

3.4 Adverse Aspects of Large Uncertainties

It is easily imagined that the robust controller designed by μ-synthesis achieves the performance robustness by making the loop gain high. High gain is inevitable within the linear frame to make the system robust. However, high gain causes three adverse effects: high control input, noise magnification, and instability due to unmodeled dynamics. High control input may cause actuator saturation.

It is also imagined that the larger uncertainties the plant has, the higher gain the controller has. Figure 3.8 shows the gain plot of the controller designed by three μ-synthesis cases: $m_\Delta = 0.5$ kg, $m_\Delta = 1.0$ kg, and $m_\Delta = 1.5$ kg for

$$m = 3.0 + m_\Delta \quad \text{(kg)} \tag{3.5}$$

As expected, the gain becomes higher when the uncertainty becomes larger. It is also said that the increase of the gain is not proportional to the increase of the uncertainty;

51
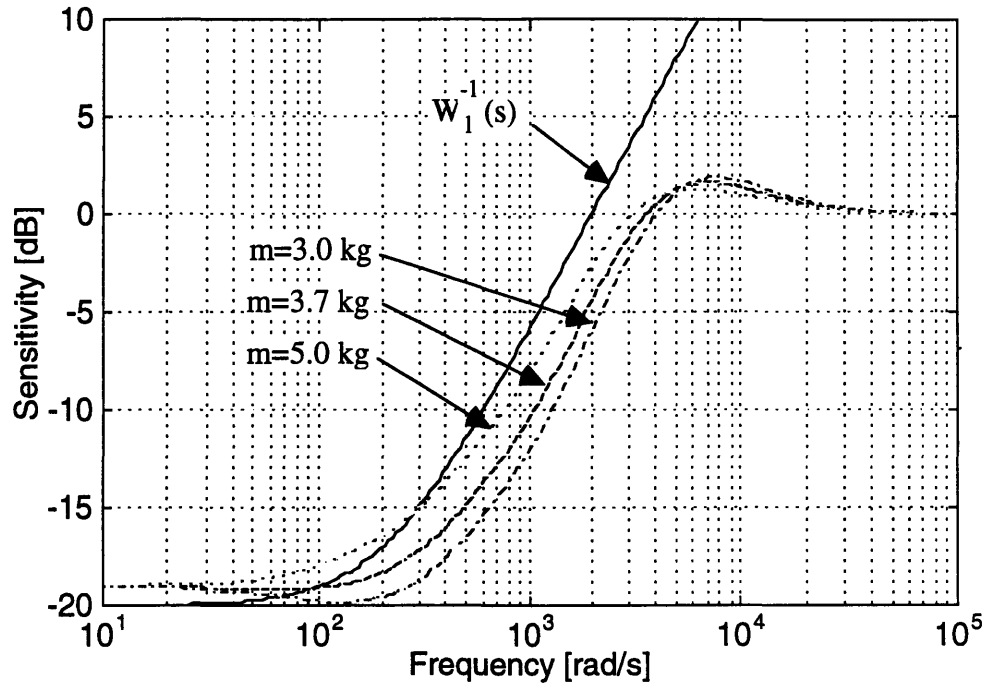
Figure 3.6: Sensitivity functions designed for $m = 3.0 \sim 5.0$ kg with various m.
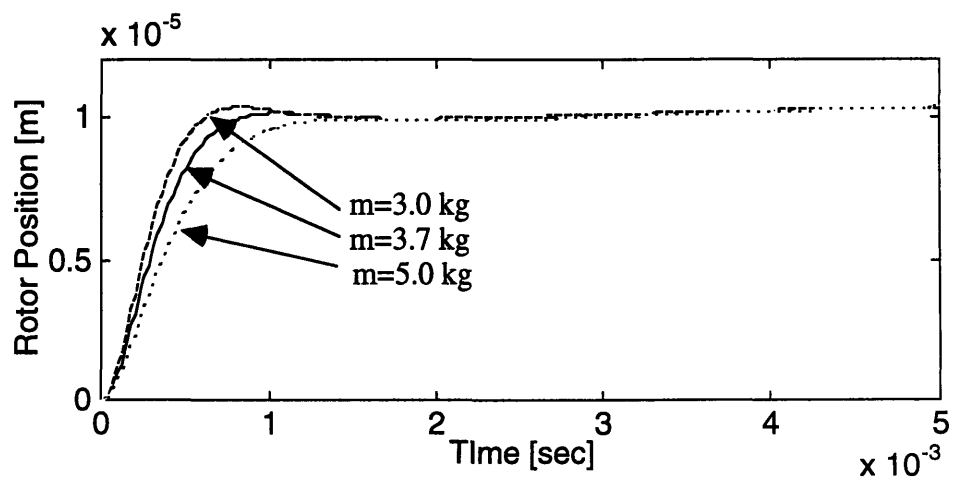
Figure 3.7: Step responses of the system designed for $m = 3.0 \sim 5.0$ kg with various m.

the gain plots of the controller designed for $m_\Delta = 0.5$ kg and $m_\Delta = 1.0$ kg are almost the same shape whereas the gain of the controller designed for $m_\Delta = 1.5$ kg is more than 20 dB higher than the other two cases in high frequencies. This fact is more
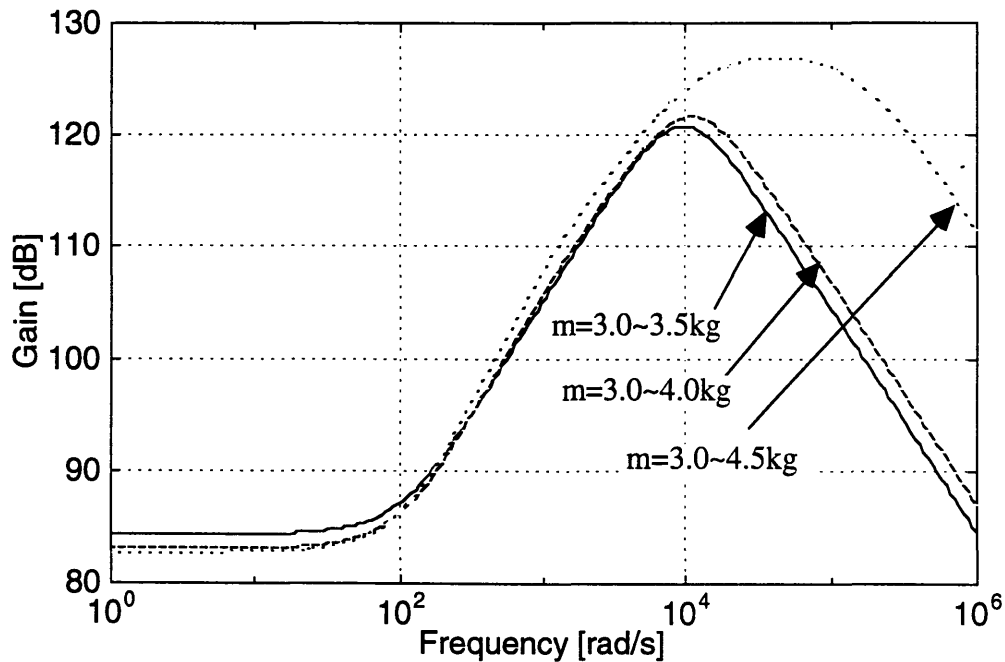
Figure 3.8: Gain plot of the controller designed by μ-synthesis.

clearly shown in Figure 3.9 that shows how high the maximum gain (H_∞ norm of the controller) becomes when m_Δ increases. As it was mentioned in the previous section, if the uncertainty of the mass exceeds 4.5 kg (m_Δ becomes more than 1.5 kg), the controller that satisfies the specification does not exist. However, even though the controller exists at $m_\Delta < 1.5$ kg, the gain of the controller becomes significantly higher when m_Δ becomes close to the limitation, especially in the high frequency region.

The effect of this high gain can be seen in the control input of step responses. Figure 3.10, 3.11, and 3.12 respectively show the 10-μm step responses of the system
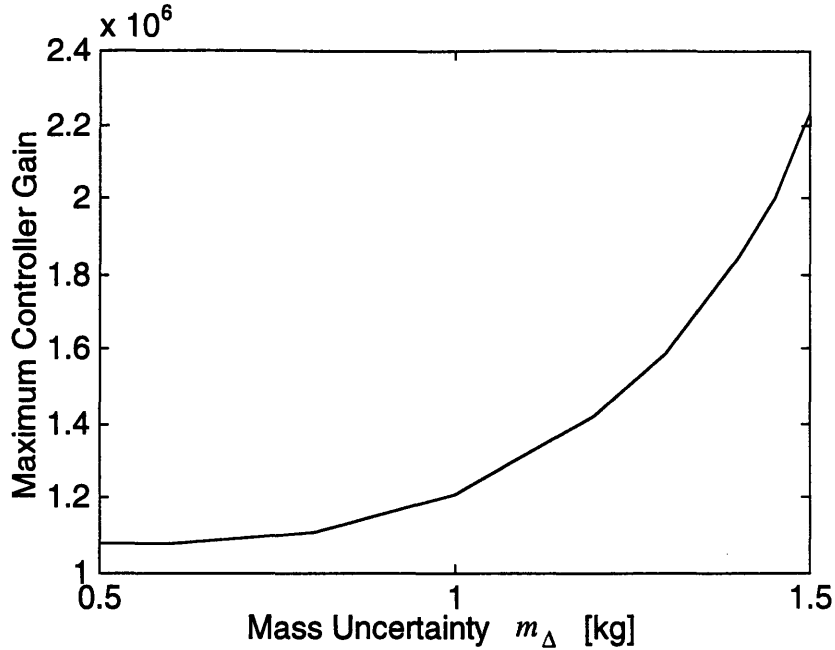
Figure 3.9: Increase of the maximum controller gain with the increase of the mass uncertainty.

designed for $m = 3.0 \sim 3.5$ kg, $m = 3.0 \sim 4.0$ kg, and $m = 3.0 \sim 4.5$ kg. The systems designed for $m = 3.0 \sim 3.5$ kg and $m = 3.0 \sim 4.0$ kg show the slow responses at $m = 4.5$ kg. However, the control input in both cases does not exceed 10 A whereas in the system designed for $m = 3.0 \sim 4.5$ kg, the control input almost reaches 20 A.

The reason why the gain is high when the uncertainties become close to the limitation is that in the optimization process, μ-synthesis tries to make the gain highest to make the system insensitive for the parameter change as long as it does not violate the stability robustness. If the uncertainties are not close to the limitation, the system satisfies the specification far before the gain becomes as high as possible. Therefore, we should avoid to design the system that is close to the limitation if we try to use linear controllers in order to avoid the adverse effects that high gain controllers cause.
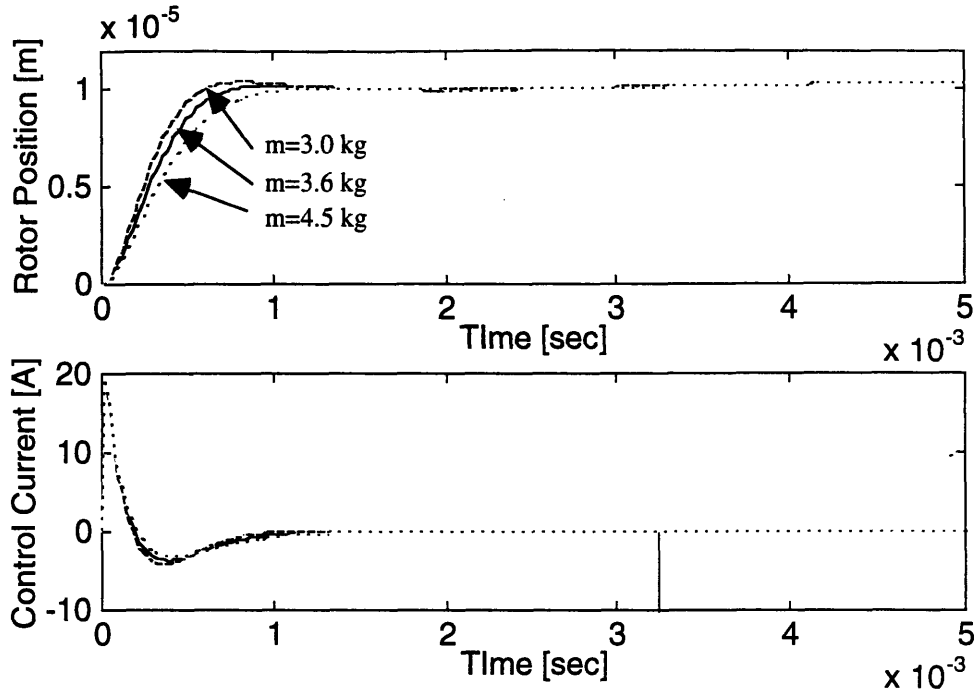
Figure 3.10: Step response and the control input of the system designed for $m = 3.0 \sim 4.5$ kg.
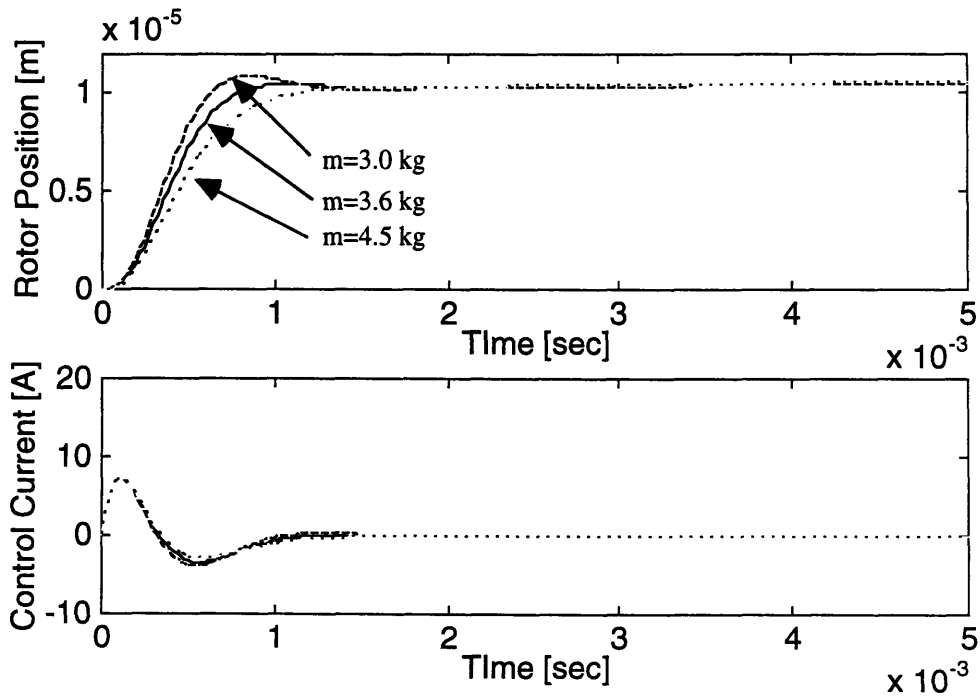
Figure 3.11: Step response and the control input of the system designed for $m = 3.0 \sim 4.0$ kg.
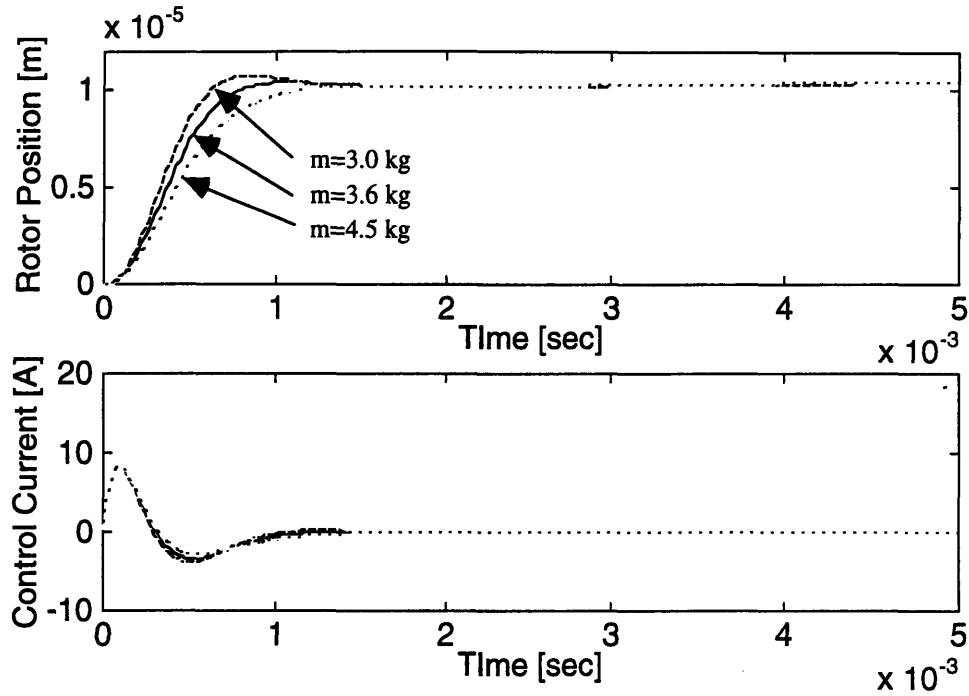
Figure 3.12: Step response and the control input of the system designed for $m = 3.0 \sim 3.5$ kg.

3.5 Limitation with Parameter Uncertainties and Bandwidth Limitation

In Chapter 2, it was shown in an example that if a plant has unmodeled dynamics in the high frequency region, a closed-loop system may become unstable; thus, the bandwidth of the system must be limited. This is also applied to the system discussed in the previous section. Moreover, this consideration is important for the system that is designed by μ-synthesis because the controller designed by μ-synthesis tends to be a high-gain controller and to have high bandwidth. To limit the bandwidth of the closed-loop system, I set the bound of the closed-loop transfer function as.

$$W_3(s) = \frac{s^2}{\omega_c^2} \tag{3.6}$$

56

This is the same bound used for the H_∞ design in Section 3.1. Then, the corresponding block diagram is described in Figure 3.13. In this case, the controller guarantees not only the robust stability for the uncertainty of the mass of the rotor, but also the robust stability for the high-frequency unmodeled dynamics.

Figure 3.13: Concept of μ-synthesis with bandwidth limit.

Figure 3.14 shows the structured singular values of the system designed by μ-synthesis for targeting $m = 3.0 \sim 4.5$ kg with three ω_c: 10000 rad/s, 20000 rad/s, and 30000 rad/s. As can be seen, the maximum structured singular value becomes less than one only when ω_c is greater than 20000 rad/s. As a result, when $\omega_c = 20000$ rad/s, the sensitivity function and the closed-loop transfer function simultaneously become less than the desired bounds for all the frequencies for all the masses between 3.0 kg and 4.5 kg (Figure 3.15 and 3.16). However, when $\omega_c = 10000$ rad/s, the sensitivity function becomes higher than $W_1^{-1}(s)$ in low frequencies whereas the closed-loop transfer function still is lower than $W_3^{-1}(s)$ for all the frequencies (Figure

Figure 3.14: Structured singular values of the system designed for $m = 3.0 \sim 4.5$ kg and various ω_c.

3.17 and 3.18). Therefore, as can be seen in Figure 3.19, the step response designed to achieve $\omega_c = 10000$ rad/s fails to settle within 1 ms, but the control input becomes smaller because the bandwidth is limited.

Figure 3.20 and 3.21 respectively show the structured singular values of the system designed for $m = 3.0 \sim 4.0$ kg and $m = 3.0 \sim 3.5$ kg with several ω_c. As the range of the uncertainty becomes wider, we have to take higher ω_c. To achieve the performance robustness for $m = 3.0 \sim 4.0$ kg, $\omega_c \approx 10000$ rad/s is required whereas for $m = 3.0 \sim 3.5$ kg, $\omega_c \approx 7000$ is the necessary bandwidth to achieve the performance robustness.

This result indicates that we have to compromise the performance to maintain stability if unknown factors in the plant are significant. Also, we instinctively under-
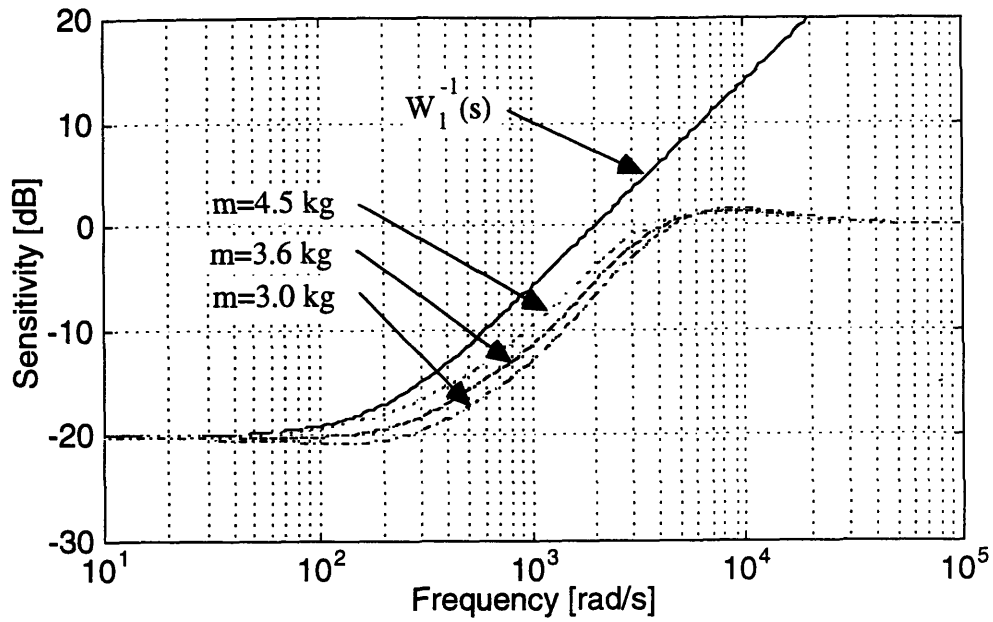
Figure 3.15: Sensitivity functions of the system designed for $\omega_c = 20000$ rad/s.
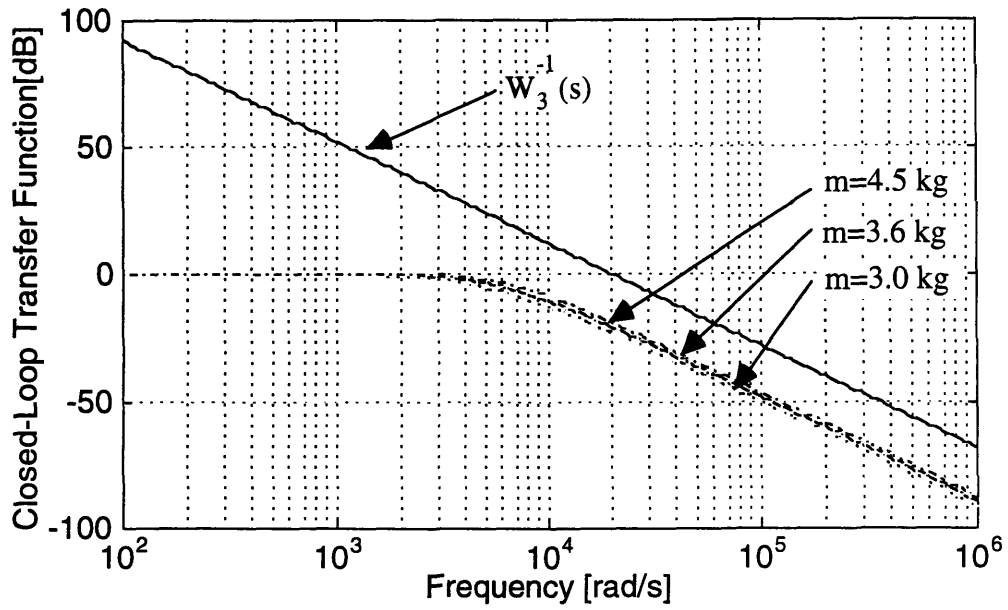
Figure 3.16: Closed-loop transfer functions of the system designed for $\omega_c = 20000$ rad/s.
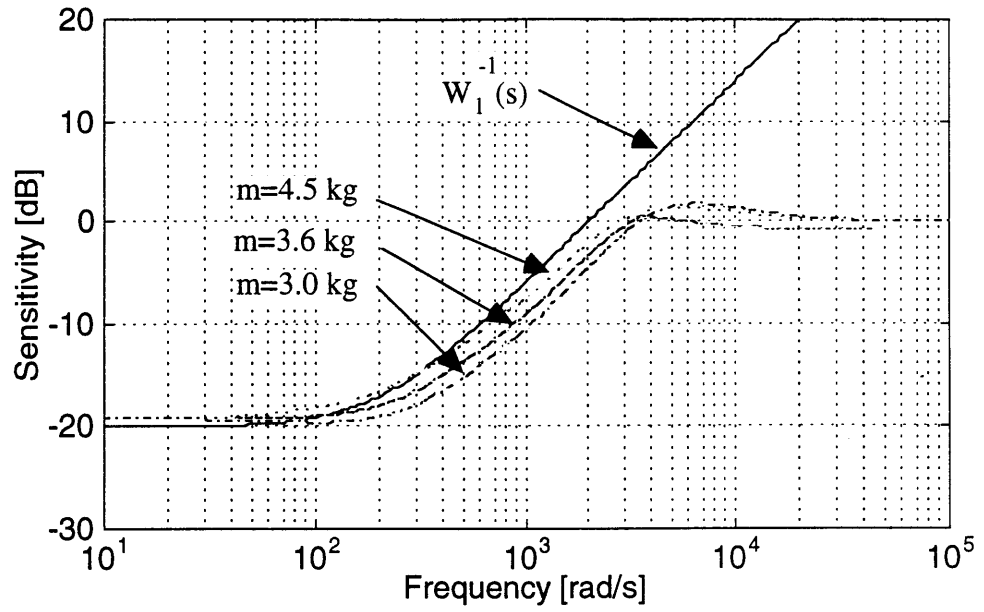
Figure 3.17: Sensitivity functions of the system designed for $\omega_c = 10000$ rad/s.
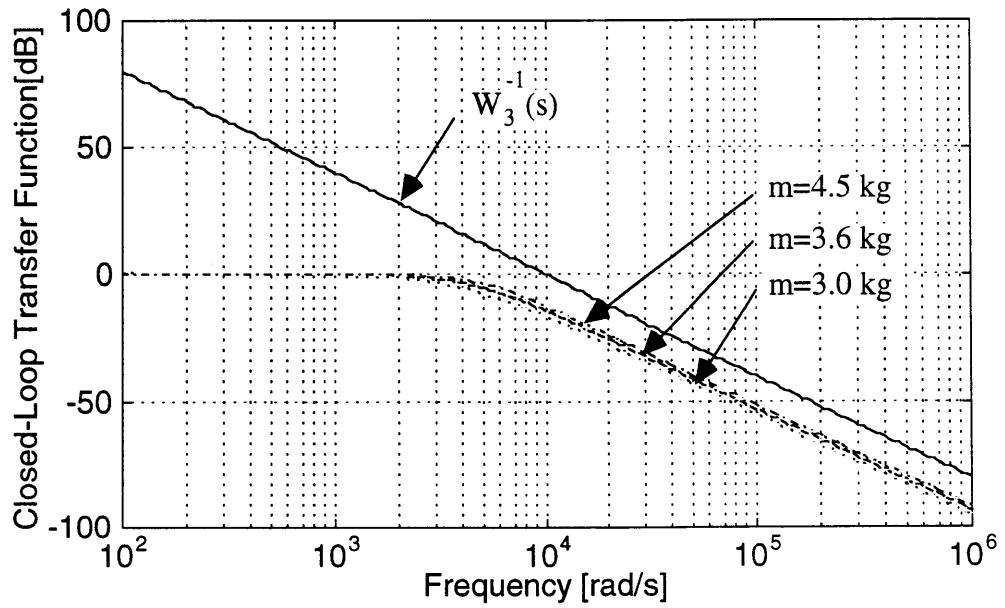
Figure 3.18: Closed-loop transfer functions of the system designed for $\omega_c = 10000$ rad/s.
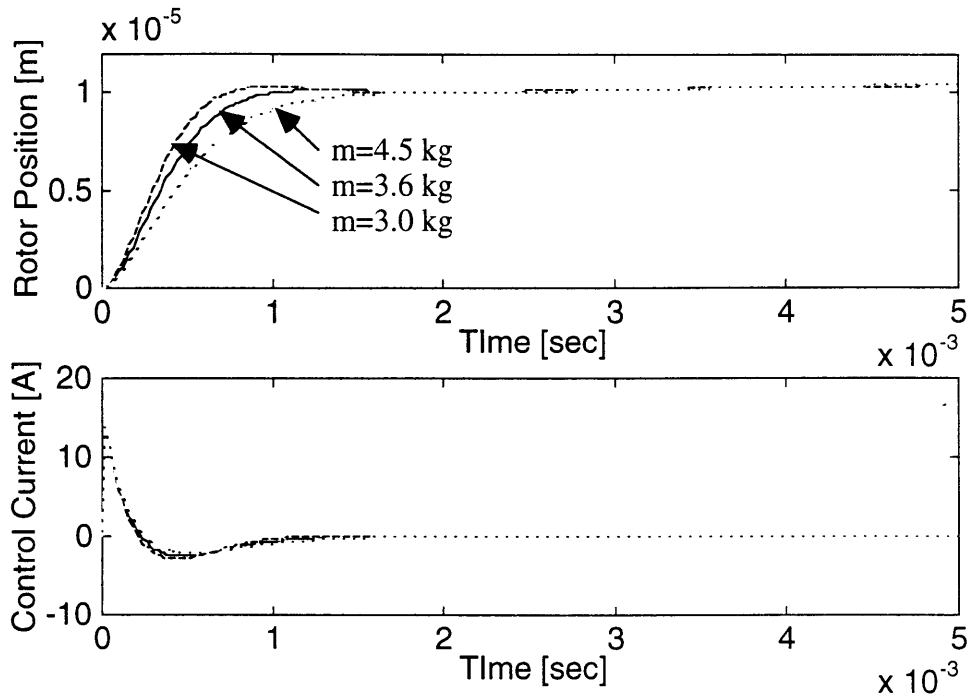
Figure 3.19: Step responses and the control inputs of the system designed for $\omega_c = 10000$ rad/s.

stood that a high-gain controller leads performance robustness, but with the advent of μ-synthesis, it becomes possible to quantitatively know how the high-gain controller achieves the performance robustness and the limitation of linear controllers.

As it was mentioned in Section 3.3, the optimization to obtain all-pass structured singular values must be compromised to a certain point where the optimization process requires reasonable computation. This compromise affects the results shown in Figure 3.14, 3.20, and 3.21. In the high frequency region, the structured singular values become less than the values in the low and middle frequency region. As a result, the closed-loop transfer function does not perfectly fit $W_3^{-1}(s)$ (Figure 3.16). That means that ω_c can be less than 20000 rad/s to achieve the required performance robustness for $m = 3.0 \sim 4.5$ kg. In the calculation, I used a tolerance of 0.001
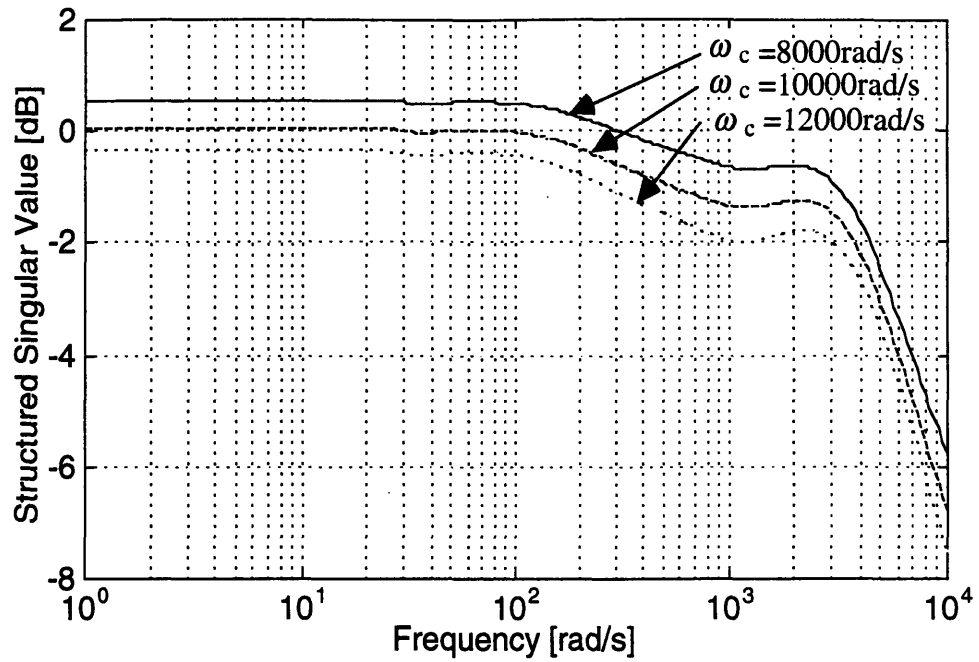
Figure 3.20: Structured singular values of the system designed for $m = 3.0 \sim 4.0$ kg and various ω_c.
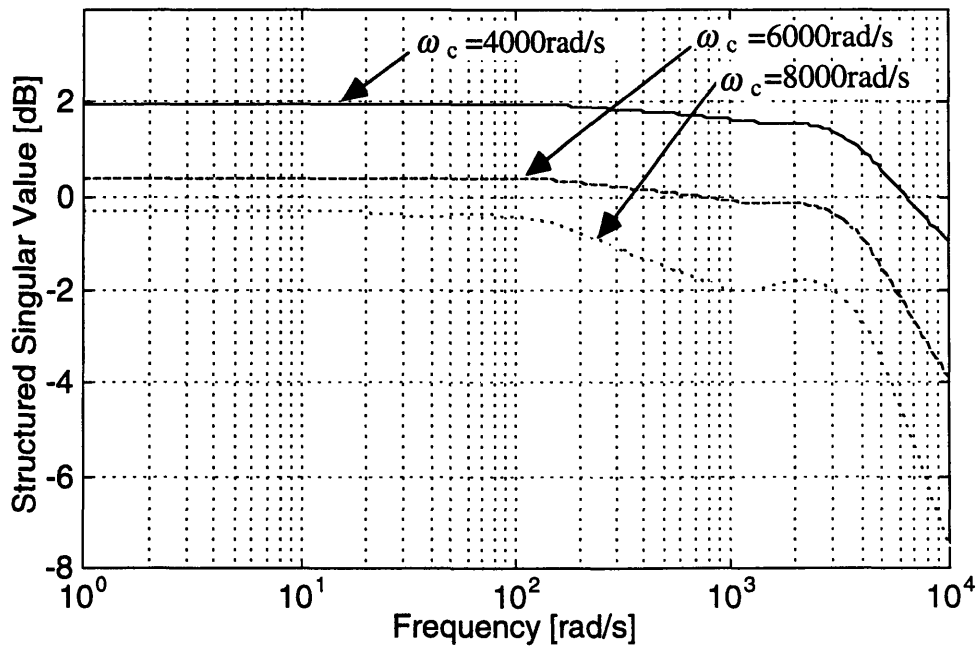
Figure 3.21: Structured singular values of the system designed for $m = 3.0 \sim 3.5$ kg and various ω_c.

for γ-iteration and 5th-order approximation for D-scale fitting. With the 5th-order approximation, the order of the controller becomes 33rd. This order is large enough for the 2nd-order plant. Curve fitting with orders ranging from 6 to 9 were tried, but that did not change the frequency shape of the structured singular values. One more D-scale fitting and H_∞ optimization may further optimize the system, but it makes the order of the controller much larger. Usually, the order of a controller designed by μ-synthesis becomes huge, and order reduction is required to make the controller practical. However, as it will be shown in the next section, an order- reduction method does not always significantly work. Therefore, the results shown in this section are not perfectly optimized; thus, they are not the ultimate limitations. Nevertheless, they are the practical limitations for the real system.

3.6 Order Reduction of the Designed Controller

Though the order of the controller designed by μ-synthesis depends on the order of the weighting functions and the order of the functions used for D-scale fitting, it tends to become huge. For example, the controller designed in Section 3.3 has a 23rd order. The controller designed in Section 3.5 has 33rd order. Considering the order of the plant (second), the order of those controllers is huge. Usually, order-reduced controllers are used for the implementation to real systems. Eliminating insignificant orders from the balanced-realized controller is commonly used and is reportedly able to reduce the order of the controller significantly without changing the characteristics of the system.

Figure 3.22 is the plot of the diagonal of gramian of the balanced realization of the controller designed in Section 3.3. As can be seen in the figure, there are no significantly small elements in the diagonal of the Gramian. As a result, eliminating a

63

small portion changes the characteristics of the closed-loop system. Yet, the first and the second smallest orders can be eliminated from the controller without violating the specification. Figure 3.23 shows the magnitude plot of the reduced controller and the
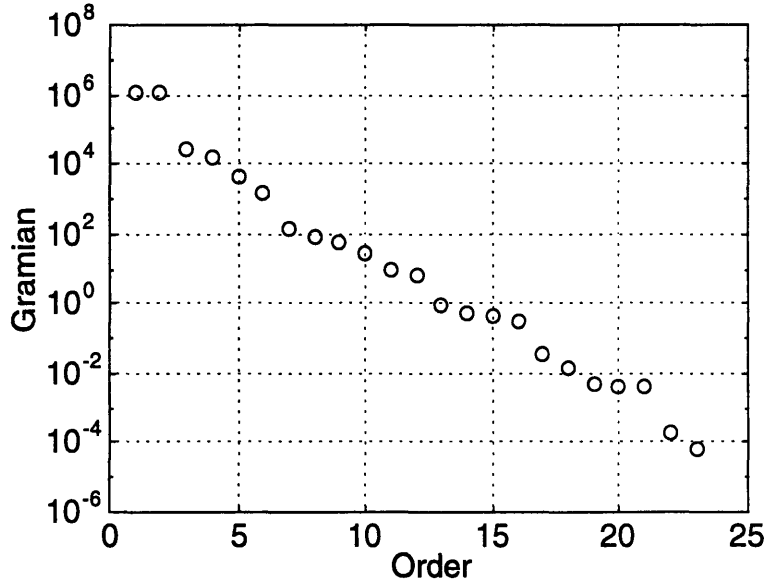
Figure 3.22: Diagonal of the gramian of the balanced-realized controller.

original controller. In the low frequency region, both controllers have the same gain, but in the high frequencies, the gain of reduced controller becomes higher than the original controller. It occurs because high-frequency poles are eliminated. However, the system with the reduced controller keeps the maximum structured singular value less than one as shown in Figure 3.24. Therefore, the sensitivity function is kept less than $W_1^{-1}(s)$ within the range of $m = 3.0 \sim 4.5$ kg with the reduced 21st-order controller (Figure 3.25). The controller designed with the consideration of bandwidth in Section 3.5 has higher order than the controller designed in Section 3.3 because the new weighting function $W_3(s)$ is added. There are also no significant small elements in the diagonal of the gramian; the order of the controller cannot be significantly reduced. Only 3 orders can be reduced without losing the robustness.

64
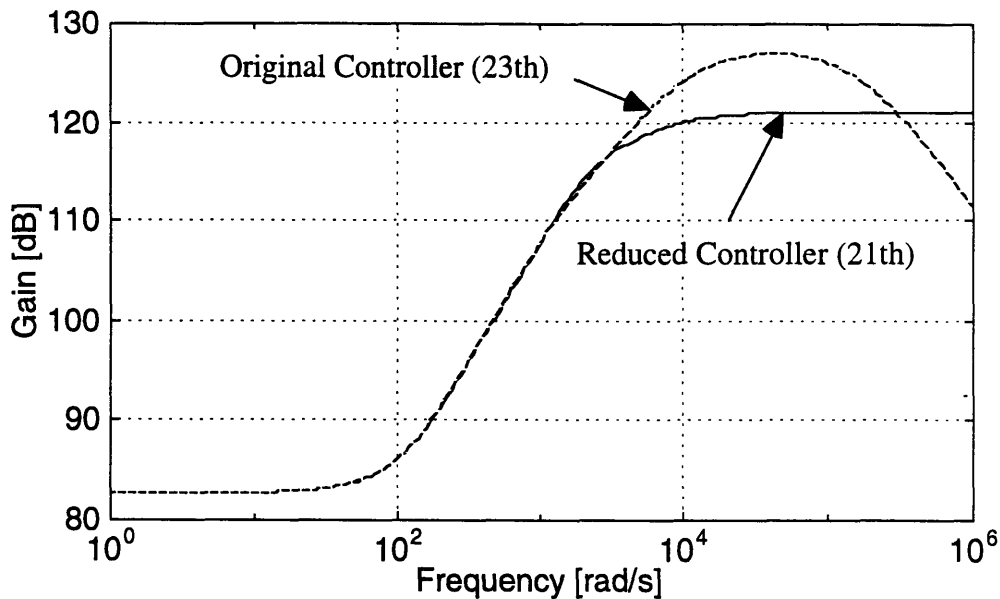
Figure 3.23: Gain plot of the reduced controller and original controller.

Figure 3.26 shows the magnitude plot of the reduced controller, and Figure 3.27 shows the structured singular value plot of the system with the reduced 30th order controller. Even reducing three orders changes the shape of the structured singular value plot, and no more reduction is possible to keep the robustness.

3.7 Using Prefilters to Reduce Control Input

In Section 3.4, it was shown that when the range of uncertainties becomes close to the limitation, the gain of the controller becomes high, and it causes large control input for step responses. This disadvantage of the high-gain feedback controller can be averted by using prefilters. For example, in the case of the controller designed to achieve the performance robustness for $m = 3.0 \sim 4.5$ kg in Section 3.3, the maximum control input for the 10-μm step response becomes almost 20 A (Figure 3.10). This high control input is mainly due to the high gain of the controller at the

65
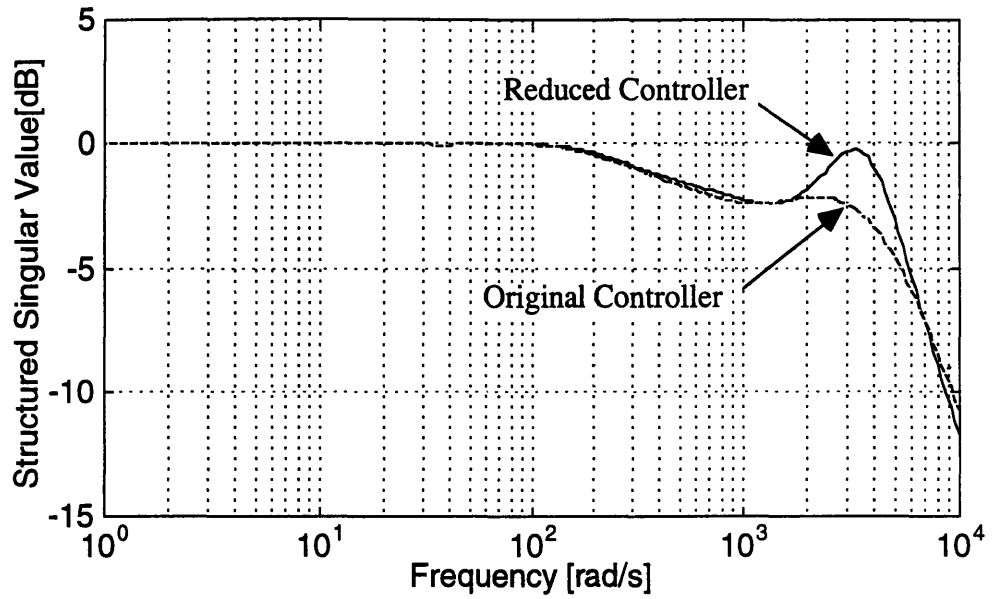
Figure 3.24: Structured singular value plot of the system with the reduced and original controller.
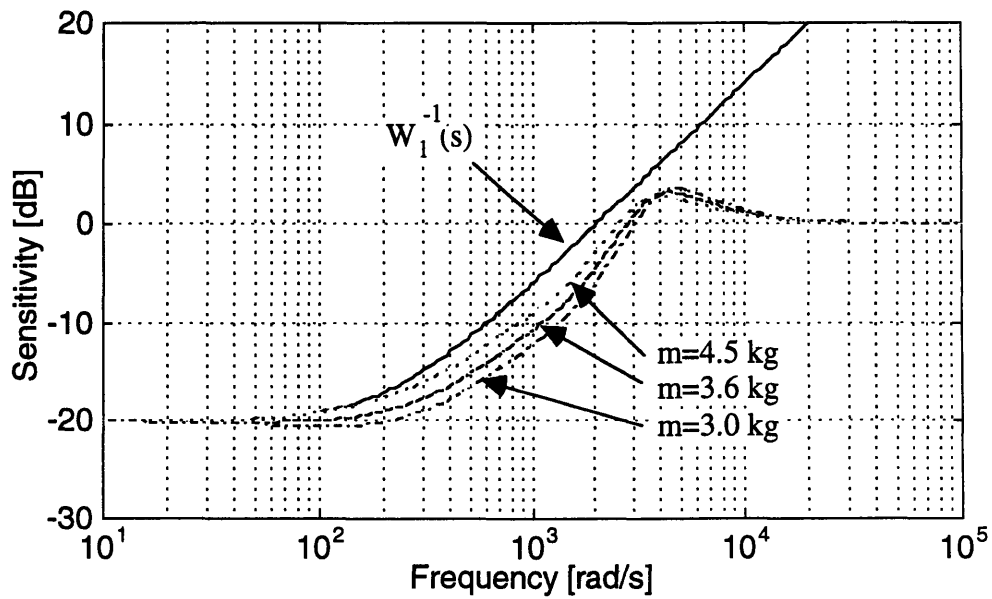
Figure 3.25: Sensitivity functions of the system with the reduced controller.
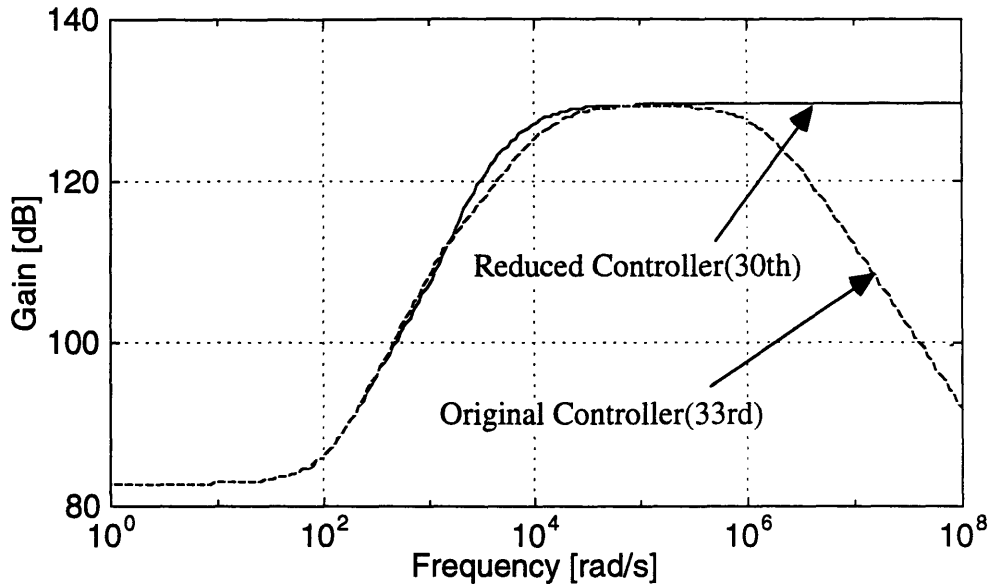
Figure 3.26: Gain plot of the reduced controller and original controller.
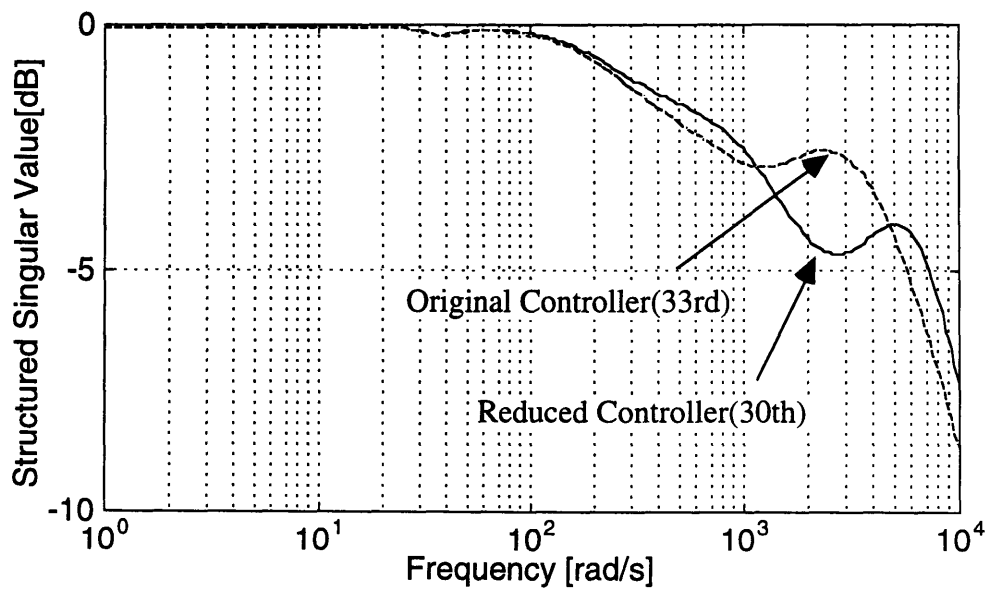
Figure 3.27: Structured singular value plot of the system with the reduced and original controller.
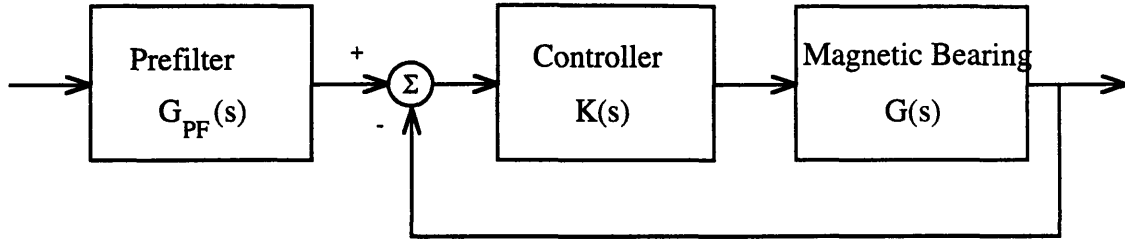
Figure 3.28: Concept of a prefilter.

high frequencies, zeros in the μ-synthesis controller, and the fact that a step input contains high frequencies. Therefore, if we use a filtered step input as shown in Figure 3.28, it reduces the control input.

Figure 3.29 is an example of the filtered step response. The used filter is

$$G_{PF}(s) = \frac{\omega_{PF}^2}{s^2 + 2\zeta_{PF}\omega_{PF} + \omega_{PF}^2} \tag{3.7}$$

where $\omega_{PF} = 20000$ rad/s and $\zeta_{PF} = 1.0$. The resulting time responses and control inputs are shown in Figure 3.30. The maximum control input becomes about 8 A. Though the rising time increases, the settling time changes only a little. Therefore, with the use of proper prefilters, we can avoid the high controller input caused by μ-synthesis.

3.8 Summary

The H_∞ design theory reveals the existence of the controller that can achieve the required specifications. If the maximum singular values are less than one for all the frequencies, the desired closed-loop system is achieved. In the same manner, the structured singular values give us an insight where the limitation of linear controllers is. In this chapter, the relation between the range of uncertainties and the limitation of the linear controllers were evaluated. The achievable performance is limited when
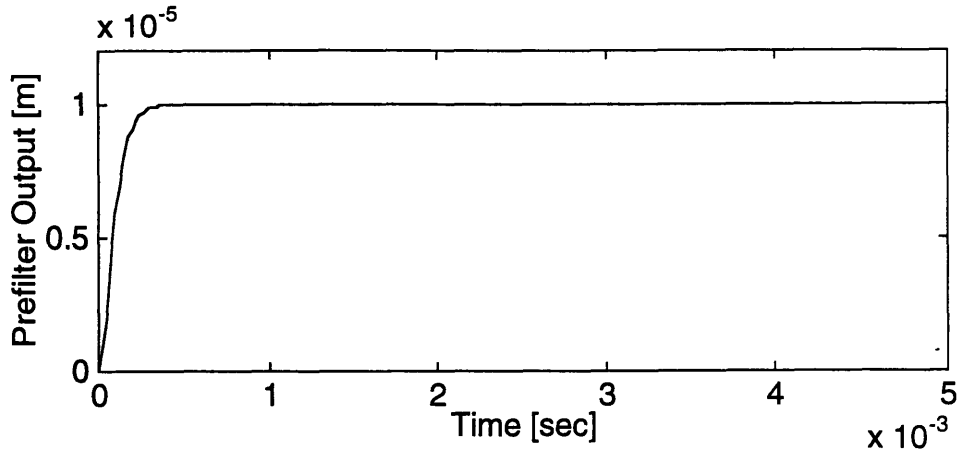
Figure 3.29: Prefiltred step input.
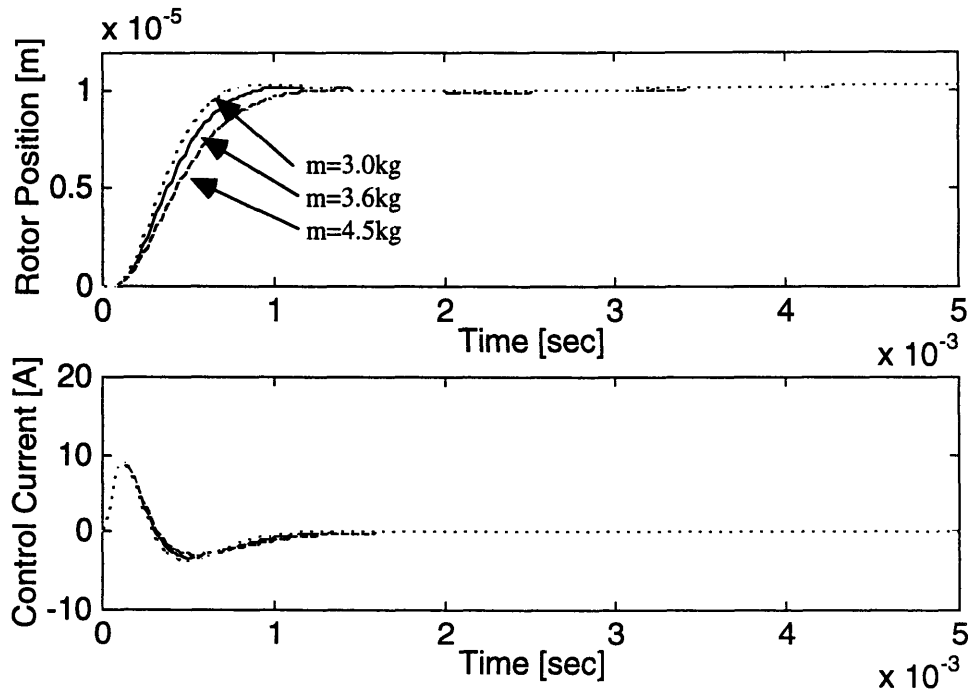
Figure 3.30: Step responses and the control inputs of the system with the prefilter.

the range of uncertainties is wide and it is successfully evaluated by the structured singular value plot. In addition, it is revealed that if the range of the uncertainties is close to the limitation, the gain of the controller increases sharply. Therefore, to design a robust controller that is close to the limitation should be avoided. Also, if the range of uncertainties is wider, the achievable bandwidth limit becomes higher; thus, system's stability robustness becomes poor. An order reduction of the designed controller and prefilter to reduce the control input are also discussed. These results help the designers of controllers to choose the specifications as well as the structure of the controller.

Chapter 4
Control of Magnetic Bearings with an Adaptive Approach

4.1 Introduction

In the preceding chapters, how μ-synthesis achieves performance robustness and the limitation of the controller designed by μ-synthesis with an uncertain rotor mass are discussed. In the real system, the other factors, such as the nonlinearity of magnetic force, gyroscopic effect, and gravity, may play an important role to characterize the performance of the system. For example, Yeh demonstrated that the poles of the magnetic bearing migrate drastically as the rotation of the rotor accelerates or decelerates [5]. Considering these factors within the linear frame may not be a good idea. As it was pointed out in the previous chapter, if the range of uncertainties is wide, the undesired aspects such as high gain or high order of the controller may be needed. Moreover, the controller that achieves the desired characteristics may not exist. Especially, if the bounds of uncertainties are unclear because of linear approximation of nonlinearities or combined uncertainties, the designed system may become conservative and sometimes fail to achieve the desired performance with linear controllers.

If the purpose of the magnetic bearing is just to levitate the rotor to eliminate friction, performance robustness is not necessarily a critical issue. However, in case of precision magnetic bearings, this limitation especially affects the achievable performance because the change of characteristics is significant in the positioning system.

Adaptive control is another possible approach to the system with uncertainties,

and the case to successfully control the system with unknown dynamics is reported [5]. In this chapter, an adaptive control method using local function estimation for the precise positioning will utilized. In addition, the feasibility of the method for this application by using the magnetic bearing in the turbo-pump model as well as the comparison with the controller designed by μ-synthesis will be evaluated to determine the advantages of this relatively fast adaptation scheme.

4.2 Nonlinear Model of the Real Magnetic Bearing

In order to demonstrate the feasibility of the controllers, simulations will be conducted with the nonlinear model that is close to the real system. The linearized model gives us the insight of the system, e.g. where the poles are, and makes us able to design the linear controller. However, magnetic bearings have strong nonlinearity and we cannot ignore this nonlinearity if the operating point changes.

In the real system described in section 2.2, one coil current in each of the opposite pairs is turned off if the corresponding control current becomes too excessive in order to reduce the power consumption. This scheme is done by the electronic circuit implemented in the controller and represented as

$$
\begin{array}{lll}
i_{zu} = i_0 + 0.5u_z, & i_{z\ell} = i_0 - 0.5u_z & \text{if } |u_z| \leq 2i_0 \\
i_{zu} = i_0 + 0.5u_z, & i_{z\ell} = 0 & \text{if } |u_z| > 2i_0 \\
i_{zu} = 0, & i_{z\ell} = i_0 - 0.5u_z & \text{if } |u_z| < -2i_0
\end{array}
\tag{4.1}
$$

where i_{zu} is the upper coil current, i_{zl} is the lower coil current.

Figure 4.1 shows the nonlinear relation among the control current, rotor position, and magnetic force in the operating range. The range is limited to ± 200 μm and ± 3 A by the physical limitation. The figure indicates that around the origin, where the system is linearized and the controllers are designed according to this linearization in the preceding chapters, there is a flat part. However, when the operating point

deviates from the origin, the slope of the surface significantly changes. This characteristic of the magnetic bearing affects the performance of the system even when the position is fixed at $z = 0$. For example, if the magnetic bearing is used in the gravity environment, where it is usually used, and if the magnetic bearing tilts, the operating point in Figure 4.1 changes; thus, the characteristics of the system change. In case that the magnetic bearing is used for precision positioning, the rotor position frequently changes, and again, the characteristics change.
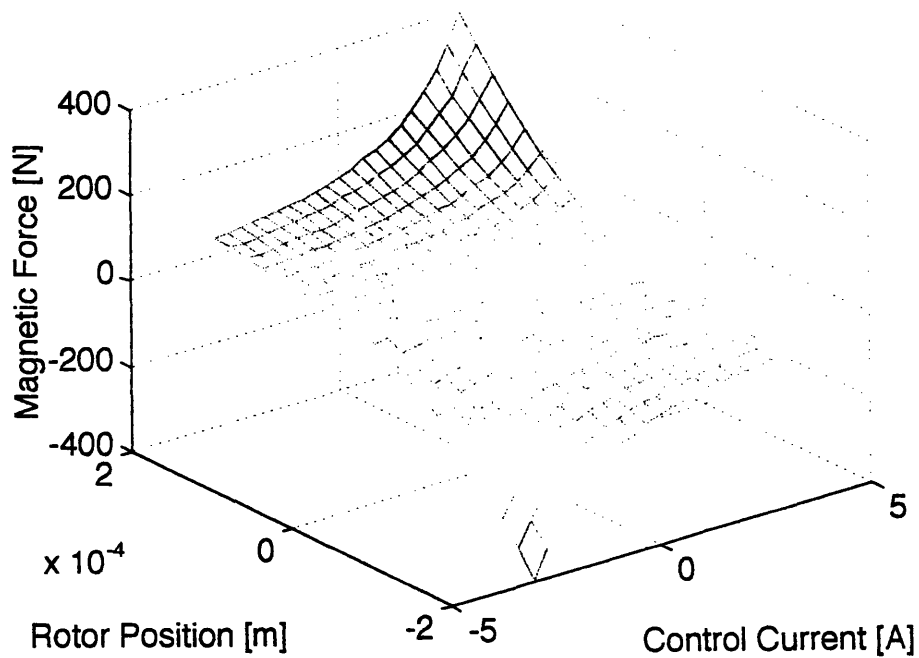
Figure 4.1: 3-D plot of the magnetic force.

4.3 Equivalent Uncertainties of the Nonlinearity

Several methods are proposed to estimate the bounds of uncertainties as an equivalent linear system of a nonlinear system [1]. However, it is impossible to evalutate an exactly-equivalent uncertainty that corresponds to the nonlinearity. What we can do is to decide a relatively large uncertainty that covers the nonlinear function. In this section, an attempt is made to calculate the equivalent linear uncertainties of the nonlinearity as a mass uncertainty by just comparing the matrix $\mathbf{A}$s in Eq.(2.2 at several points in the surface in Figure 4.1. Then, we can compare the result with the limitation evaluated in Chapter 3.

The linearized equation at the point of $z = z_{OP}$ and $u_z = u_{OP}$ is

$$
m\ddot{z} = \begin{cases}
\left[\frac{2k_0(i_0+0.5u_{OP})^2}{(z_0-z_{OP})^3} + \frac{2k_0(i_0-0.5u_{OP})^2}{(z_0+z_{OP})^3} \right] z + \left[\frac{k_0(i_0+0.5u_{OP})}{(z_0-z_{OP})^2} + \frac{k_0(i_0-0.5u_{OP})}{(z_0+z_{OP})^2)} \right] u_z \\
\qquad\qquad\qquad\qquad\qquad\qquad\qquad\qquad\qquad \text{if } |u_{OP}| \leq 2i_0 \\
\frac{2k_0(i_0+0.5u_{OP})^2}{(z_0-z_{OP})^3} z + \frac{k_0(i_0+0.5u_{OP})}{(z_0-z_{OP})^2} u_z \qquad\qquad \text{if } u_{OP} > 2i_0 \\
\frac{2k_0(i_0-0.5u_{OP})^2}{(z_0+z_{OP})^3} z + \frac{k_0(i_0-0.5u_{OP})}{(z_0+z_{OP})^2} u_z \qquad\qquad \text{if } u_{OP} < -2i_0
\end{cases}
\tag{4.2}
$$

The change of the operating point changes the system matrices $\mathbf{A}$ and $\mathbf{B}$ in Eq.(2.2). Here, the change of the matrix $\mathbf{A}$ is calculated and evaluate the equivalent m_Δ in Eq.(3.5). The matrices $\mathbf{A}$s correspond to the maximum mass and minimum mass are respectively as follows.

$$
\mathbf{A} = \begin{bmatrix} 0 & 1 \\ \frac{4k_0 i_0^2}{z_0^3}(\frac{1}{m_n} - \Delta_2) & 0 \end{bmatrix}
\tag{4.3}
$$

$$
\mathbf{A} = \begin{bmatrix} 0 & 1 \\ \frac{4k_0 i_0^2}{z_0^3}(\frac{1}{m_n} + \Delta_2) & 0 \end{bmatrix}
\tag{4.4}
$$

Because of the nonlinearity, the (2,1)-element changes as the operating point changes. Therefore, by comparing the maximum value and minimum value of (2,1)-element of changing $\mathbf{A}$ with the values in Eq.(4.3) and Eq.(4.4), we can evaluate the equivalent Δ_2; thus, the equivalent m_Δ can be calculated.

Table 4.1 shows the calculated m_Δ with various operating ranges. Considering the limitation calculated in section 3.3 and 3.4, the range in Figure 4.1 is too large to achieve the performance bound of Eq.(2.16) with robustness.

Operating Range	Equivalent m_Δ
z = 0~100 μm u = 0 A	1.4 kg
z = 0~150 μm u = 0 A	3.8 kg
z = 0~200 μm u = 0 A	9.5 kg
z = 0 μm u = 0~1 A	3.0 kg
z = 0 μm u = 0~2 A	10.5 kg
z = 0 μm u = 0~3 A	10.5 kg

Table 4.1: Equivalent m_{Delta} at the points in the operating range.

The results in this section indicate that if the system has strong nonlinearity, linear controllers may not be able to deal with the change of characteristics, which occurs when an operating point moves widely, no matter how large the gain of the controller becomes.

4.4 Adaptive Control Using Local Function Estimation

To overcome the nonlinearity of magnetic force and unknown factors in the system, the adaptive control method using local function estimation is proposed and reportedly control the magnetic bearing successfully [5]. This method approximates an

unknown function just around the operating point as the coefficients of the Taylor's expansion of the unknown function instead of estimating the function globally. By updating the approximation constantly, this method enables the controller to make a fast adaptation. In this section, this adaptive control approach is briefly described to later contrast it with the linear robust approach that was described in the preceding chapters.

Consider a plant and a reference model described by

$$\dot{\mathbf{x}} = \mathbf{Ax} + \mathbf{f(x)} + \mathbf{Bu} \quad \text{(Plant)} \tag{4.5}$$

$$\dot{\mathbf{x}}_m = \mathbf{A}_m\mathbf{x}_m + \mathbf{B}_m\mathbf{r} \quad \text{(ReferenceModel)} \tag{4.6}$$

where $\mathbf{f(x)}$ is an uncertain, nonlinear function, $\mathbf{x}_m$ is a state vector of the reference model, $\mathbf{r}$ is a command input, and $\mathbf{A}_m$ and $\mathbf{B}_m$ are the system matrices that create the desired response. The objective is to estimate the unknown function $\mathbf{f(x)}$ online and force $\mathbf{x}(t)$ to follow the reference trajectory $\mathbf{x}_m(t)$. To achieve this objective, the control law is given by

$$\mathbf{u} = \mathbf{Kx} + \Delta\mathbf{r} - \mathbf{u}_{ad} \tag{4.7}$$

where $\mathbf{Kx}$ is a full-state feedback component, $\Delta\mathbf{r}$ is a feedforward term based on the reference input $\mathbf{r}$, and $\mathbf{u}_{ad}$ is an adaptive compensating control signal. Figure 4.2 shows the concept of this adaptation. First, we define an n-dimensional moving sphere $\Phi(t)$ that has the radius of ρ and whose center is $x_m(t)$. Once the state trajectory is out of the sphere, the controller starts estimating the unknown function $\mathbf{f(x)}$. The function is estimated by using the approximation of the first several terms of the Taylor's expansion series. For example, if we use the first two terms, the unknown function $\mathbf{f(x)}$ can be approximated as

$$\mathbf{f(x)} \approx \mathbf{B} \sum_{k=0}^{1} \mathbf{C}_k(\mathbf{x}_i)\mathbf{w}_k(\mathbf{x}, \mathbf{x}_i) \tag{4.8}$$

76
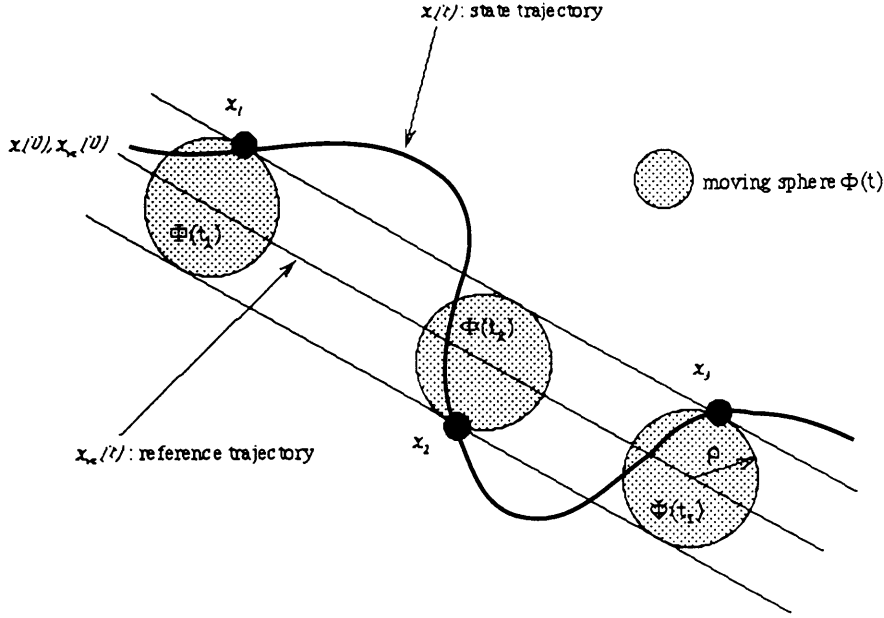
Figure 4.2: Adaptive control scheme using local function estimation.

where $\mathbf{x}_i$ is $\mathbf{x}$ when the state trajectory becomes out of the sphere in FIgure 4.2, $\mathbf{BC}_k(\mathbf{x}_i)$'s are the coefficients of Taylor's expansion, $\mathbf{w}_0(\mathbf{x},\mathbf{x}_i) = [1 \cdots 1]^T$, and $\mathbf{w}_1(\mathbf{x},\mathbf{x}_i) = \mathbf{x} - \mathbf{x}_i$. Therefore, the adaptive compensating control signal $\mathbf{u}_{ad}$ can be calculated as

$$\mathbf{u}_{ad} = \sum_{k=0}^{1} \hat{\mathbf{C}}_k(\mathbf{x}_i)\mathbf{w}_k(\mathbf{x},\mathbf{x}_i) \tag{4.9}$$

The coefficients, $\hat{\mathbf{C}}_k(\mathbf{x}_i)$'s, are estimated by integrating the following adaptation law

$$\dot{\hat{\mathbf{C}}}_k(\mathbf{x}_i) = \begin{cases} \gamma \mathbf{B}^T \mathbf{P} \mathbf{e} \mathbf{w}_k^T(\mathbf{x},\mathbf{x}_i) & \text{if } \|\mathbf{e}\| \geq \rho \\ 0 & \text{othewise} \end{cases} \tag{4.10}$$

where $\mathbf{e}$ is a trajectory error vector defined as $\mathbf{e} = \mathbf{x}_m - \mathbf{x}$, γ is an adaptation gain, and $\mathbf{P}$ is the solution of a Lyapunov function

$$\mathbf{A}_m^T \mathbf{P} + \mathbf{P} \mathbf{A}_m = -\mathbf{I} \tag{4.11}$$

The design guidelines in choosing the adaptation gain are discussed in [5].

In the case of magnetic bearings, the nonlinearity is the function of both $\mathbf{x}$ and $\mathbf{u}$. However, $\mathbf{u}$ can be separated from the function by using least square mapping. Also, to reduce the noise sensitivity, a hysteresis loop is generally used. In this case, the adaptation is triggered at $\|\mathbf{e}\| \geq \rho + \sigma$ and is turned off at $\|\mathbf{e}\| < \rho - \sigma$. Table 4.2 shows the control parameters used in the later sections for the simulations. The state feedback gain $\mathbf{K}$ is decided to make the closed-loop system have repeated two poles, -600 rad/s, at $z = 0$ and $u_z = 0$.

Parameters	Numerical Values
Adaptation Gain γ	2×10^9
Sphere Radius ρ	$1.0 \ \mu m$
Hysteresis Width σ	$0.5 \ \mu m$
State Feedback Gain $\mathbf{K}$	$[1.71 \times 10^4 \ \ 52.8]$

Table 4.2: Parameters of the adaptive controller using local function estimation.

4.5 Reference Model and Equivalent μ-Synthesis Design

For the application of adaptive control to the magnetic bearing, we choose a second-order reference model

$$\dot{\mathbf{x}}_m = \mathbf{A}_m \mathbf{x}_m + \mathbf{B}_m r \tag{4.12}$$

where

$$\mathbf{x}_m = \begin{bmatrix} z_m \\ \dot{z}_m \end{bmatrix} \tag{4.13}$$

$$\mathbf{A} = \begin{bmatrix} 0 & 1 \\ -\omega_n^2 & -2\zeta\omega_n \end{bmatrix} \tag{4.14}$$

78

$$\mathbf{B} = \begin{bmatrix} 0 \\ \omega_n^2 \end{bmatrix} \tag{4.15}$$

for the desired trajectory. The case that $\omega_n = 600$ rad/s and $\zeta = 1$ are chosen and that the effect of adaptive control using local function estimation to the real magnetic bearing is experimentally proven is reported. Here, a linear controller that achieves the equivalent response is designed and its performance is compared with that of the system with the adaptive controller.

The sensitivity function of the system described in Eq.(4.12) with $\omega_n = 600$ rad/s and $\zeta = 1$ is shown in Figure 4.3. To achieve this sensitivity with the controller designed by μ-synthesis, the performance bound is set to

$$W_1(s) = \frac{18 \times 17}{s + 17} \tag{4.16}$$

By using the bandwidth-limit formula in Section 3.5, the range of the uncertainty of
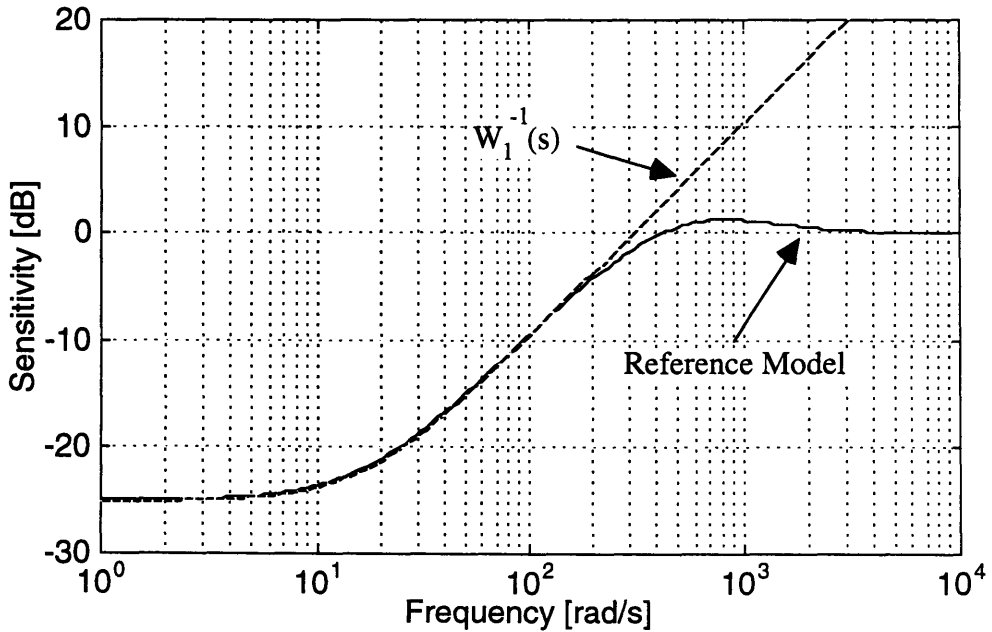
Figure 4.3: Sensitivity function of the reference model and performance bound.

the rotor mass can be from 2.2 kg to 4.5 kg with $\omega_c = 2000$ rad/s. The structured

singular value plot of the closed loop system and sensitivity functions with $m = 2.2$, $m = 3.0$, and $m = 4.5$ kg are respectively shown in Figure 4.4 and 4.5. As a result, the step response of the closed loop system becomes similar to that of the reference model with a proper prefilter. Figure 4.6 and Figure 4.7 respectively show the 10-μm step responses of the reference model and the closed-loop system controlled by the linear controller designed by μ-synthesis. The prefilter used is

$$G_{PF}(s) = \frac{1000^2}{s^2 + 2000s + 1000^2} \qquad (4.17)$$

Even though the responses vary as the mass of the rotor changes, the performance in both the 2.2-kg and 4.5-kg cases is close to that of the reference model.

4.6   Nonlinear Effect on the System with the Linear Controller and Adaptive Controller

In Section 4.2, the nonlinearity of magnetic force is examined as a form of equivalent linear uncertainties. Though only the system matrix **A** at the several points in the operating region are compared, the result suggests that if the rotor position or control current changes in the operating range, linear controllers designed by μ-synthesis cannot deal with the equivalent uncertainties that nonlinearity has. In this case, alternative approaches such as adaptive control may achieve better performance. Therefore, how much the performance of the system controlled by linear controllers deteriorates as compared with the adaptive approach is of interest. In this section, the response of the system controlled by the linear controller or adaptive controller are simulated with the nonlinear model.
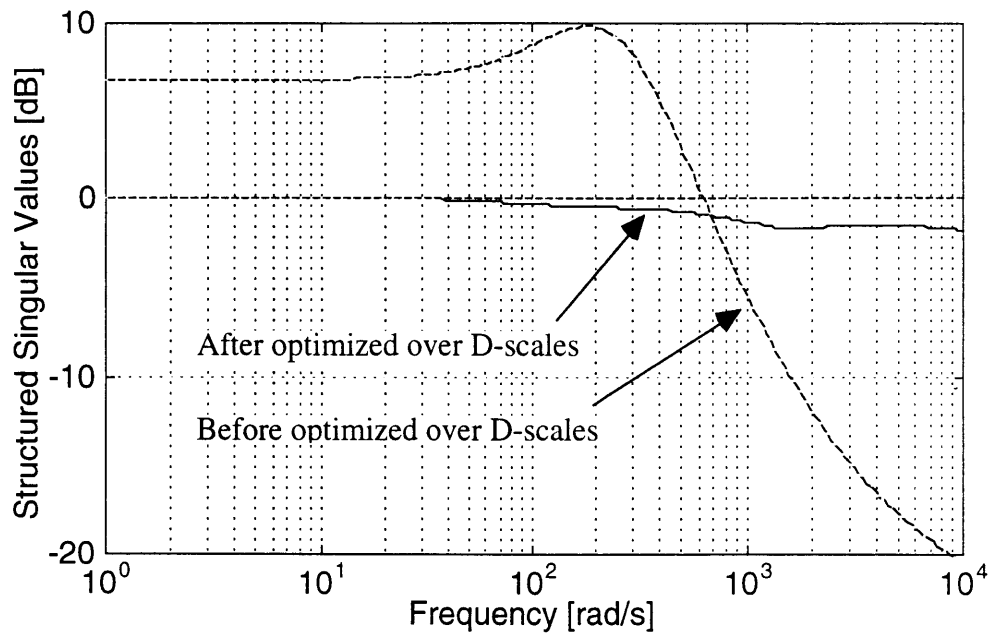
Figure 4.4: Structured singular value plot of the designed system.
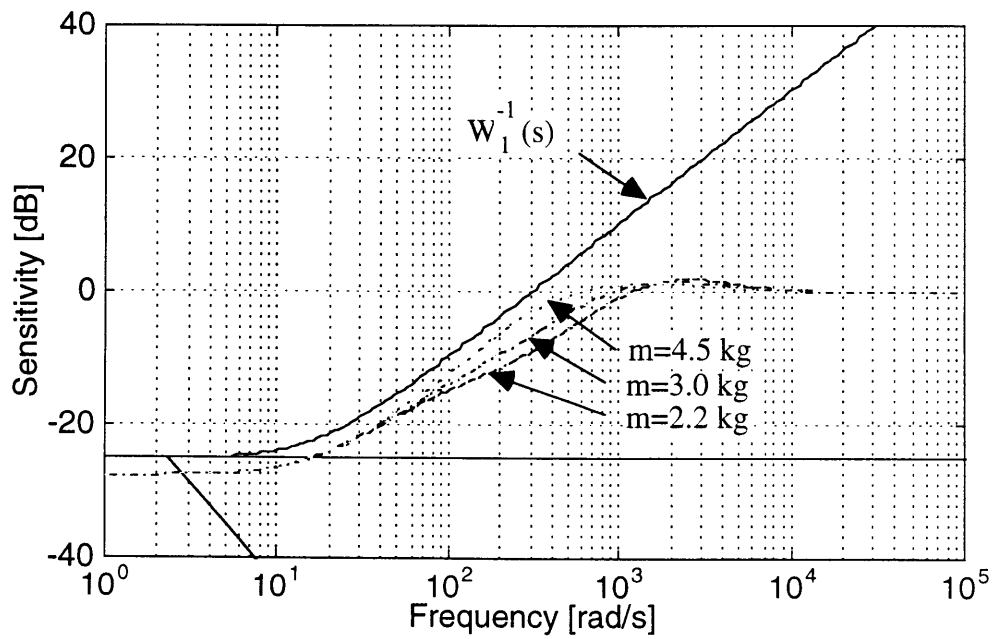
Figure 4.5: Sensitivity function of the designed system with $m = 2.2$, 3.0, and 4.5 kg.
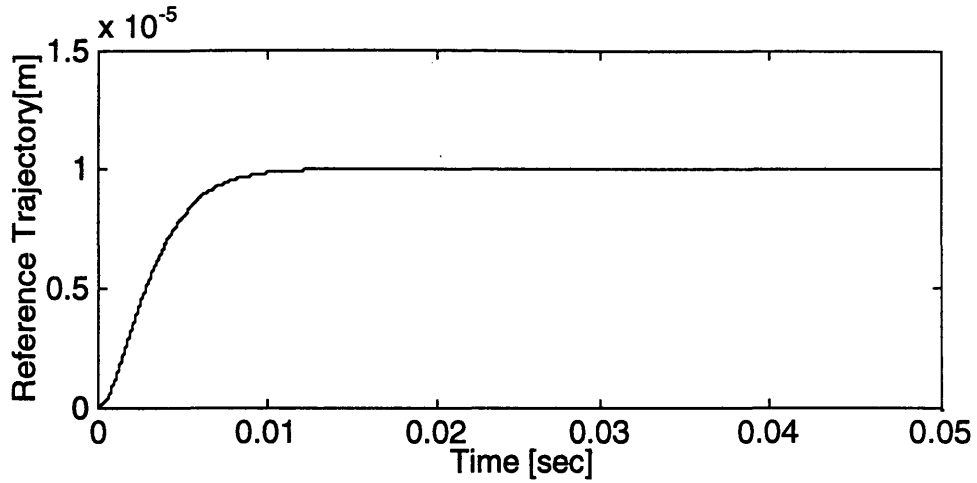
Figure 4.6: A 10-μm step response of the reference model.
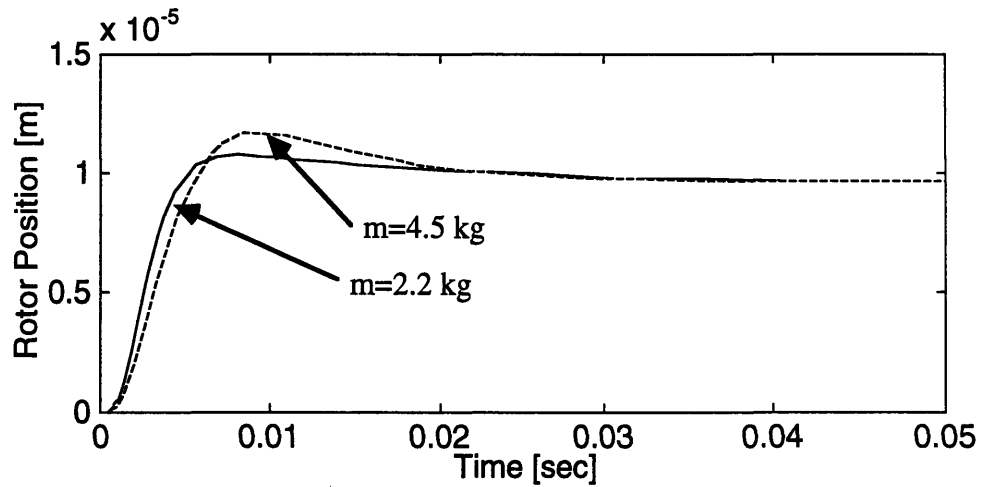
Figure 4.7: Step responses of the system with a μ-synthesis controller.

4.6.1 Effect of Large Displacement

As can be seen in Figure 4.1, the characteristics of the magnetic bearing change if the rotor moves within the operating range. This change affects the performance of the system. Figure 4.8 and 4.9 respectively show the 100-μm and 200-μm step responses of the system designed by μ-synthesis with the cases of $m = 2.2$ kg and $m = 4.5$

kg. As the step becomes larger, the overshoot becomes larger and the settling time becomes longer. The response deteriorates more for the larger step because the design is done by using the plant linearized at $z = 0$. Including nonlinearity as a form of linear uncertainties may be possible. However, as it was mentioned in Section 4.3, considering nonlinearity as linear uncertainties requires large uncertainties, and in this case, the controller that achieves the required performance does not exist because the range of $m = 2.2 \sim 4.5$ kg is already the maximum range that the linear controller can achieve.

Using the adaptive control with local function estimation, large deviation from the nominal plant does not affect the performance as much as the system controlled by the linear controller. The deviation from the nominal plant is locally estimated and eliminated by subtracting the deviation. Therefore, the characteristics of the controlled system at the trajectory are almost the same as those of the nominal plant as long as the adaptation is properly working. Figure 4.10 and 4.11 are the 100-μm and 200-μm step responses of the system controlled by the adaptive controller. The shape of the response is not affected by the height of the step as well as the mass of the rotor. The tracking errors are converged within the range of $\rho + \sigma$ (1.5 μm).

4.6.2 Effect of Gravity

Control input also affects the characteristics of the system. The characteristics of the system significantly change when the control input widely changes even when the position of the rotor remains the same. If a magnetic bearing is used in a gravity environment and if the direction or magnitude of the gravity changes, the control current must be changed to keep the rotor position. However, this change may cause performance deterioration. The bias current i_G to balance the gravity mg at $z = 0$ is
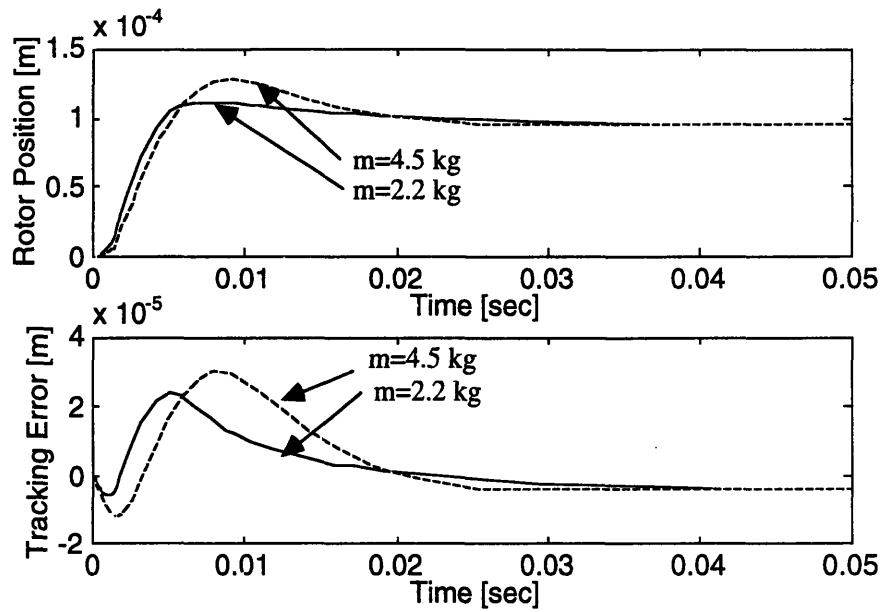
Figure 4.8: 100-μm step responses of the system with the linear controller with $m = 2.2$ and 4.5 kg.
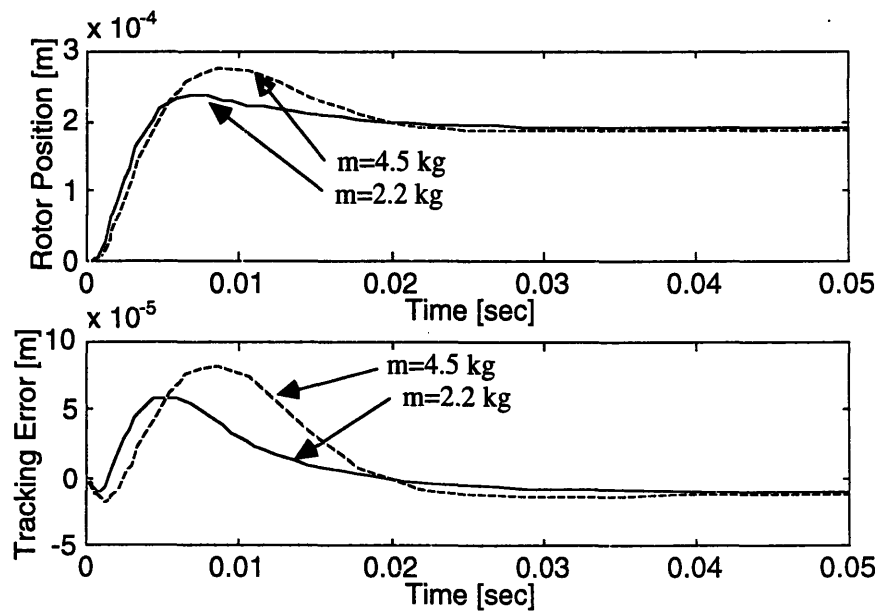
Figure 4.9: 200-μm step responses of the system with the linear controller with $m = 2.2$ and 4.5 kg.
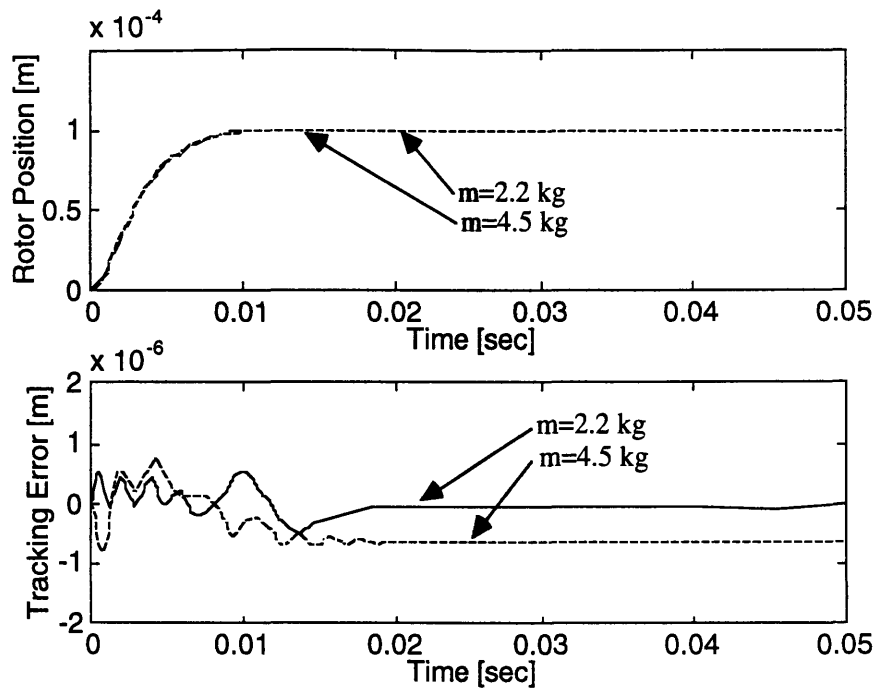
Figure 4.10: 100-μm step responses of the system with the adaptive controller with $m = 2.2$ and 4.5 kg.
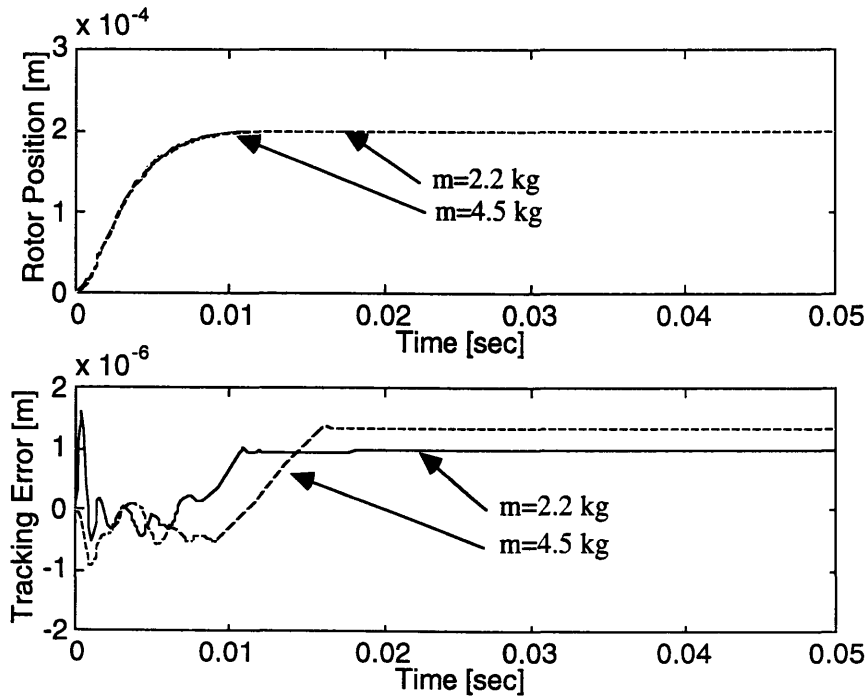
Figure 4.11: 200-μm step responses of the system with the adaptive controller with $m = 2.2$ and 4.5 kg.

calculated by

$$i_G = \frac{z_0^2 mg}{2k_0 i_0} \qquad (4.18)$$

Figure 4.12 shows a 10-μm step responses when the gravity acceleration $g = 4.9$ m/s^2 (half of the general earth's gravity) exists. The bias current calculated by Eq.(4.18) is applied to balance the gravity. The responses are slightly slower and have larger overshoot than those without the gravity. Figure 4.13 is the case when $g = 9.8$ m/s^2. In this case, the settling time when $m = 4.5$ kg is much longer than that without the gravity. This result shows that if we design a controller for a precision magnetic bearing used in a gravity environment that may change, we must take this change into consideration if we use a linear controller. However, as I showed in Section 4.3, the equivalent uncertainty is large, and the controller that satisfies the specification may not exist.

With the adaptive controller, the gravity is estimated as part of the unknown function and is subtracted as the adaptive compensating control signal $u_a d$; therefore, the shape of the responses is not affected by the magnitude of the gravity (Figure 4.14 and 4.15). Moreover, the bias current to balance the gravity is not necessary because it is automatically created as part of the adaptive compensating control signal.

4.7 Effect of High Frequency Unmodeled Dynamics

The lowest ω_c achieved by μ-synthesis in Section 4.1 is 2000 rad/s. That means if there is unmodeled dynamics expressed in a multiplicative uncertainty, and if it exceeds $W_3^{-2}(s)$ in Eq.(3.6), the closed-loop system may become unstable. Generally, the rotor levitating with magnetic bearings has elasticity and little damping. For example, for the case of the turbo-pump of Figure 2.1, whose magnetic bearing we
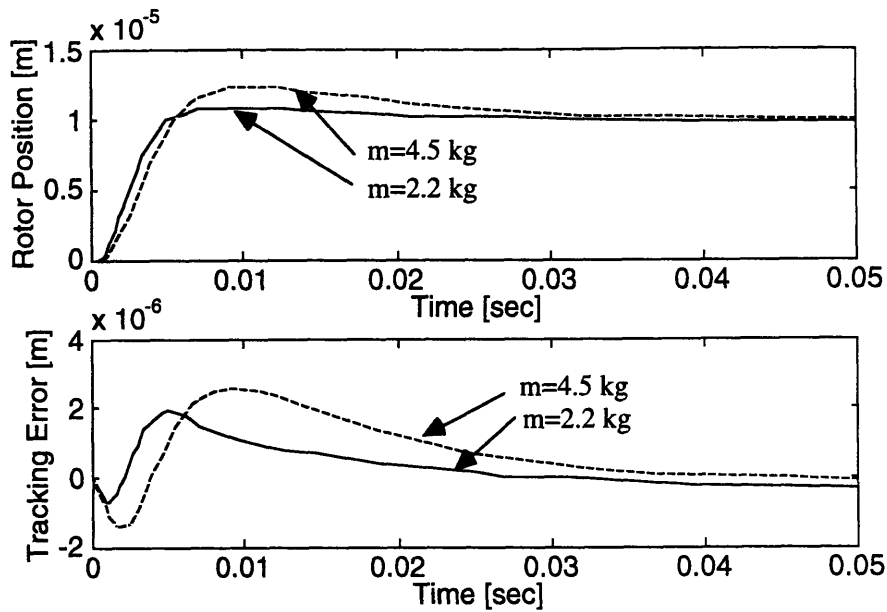
Figure 4.12: 10-μm step responses of the system with the linear controller with m = 2.2 and 4.5 kg (g = 4.9 m/s^2).
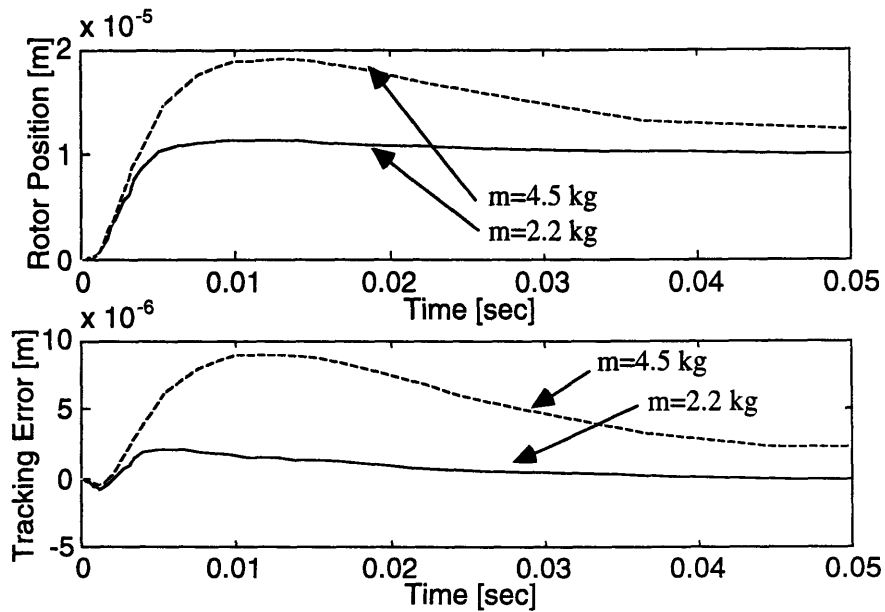
Figure 4.13: 10-μm step responses of the system with the linear controller with m = 2.2 and 4.5 kg (g = 9.8 m/s^2).
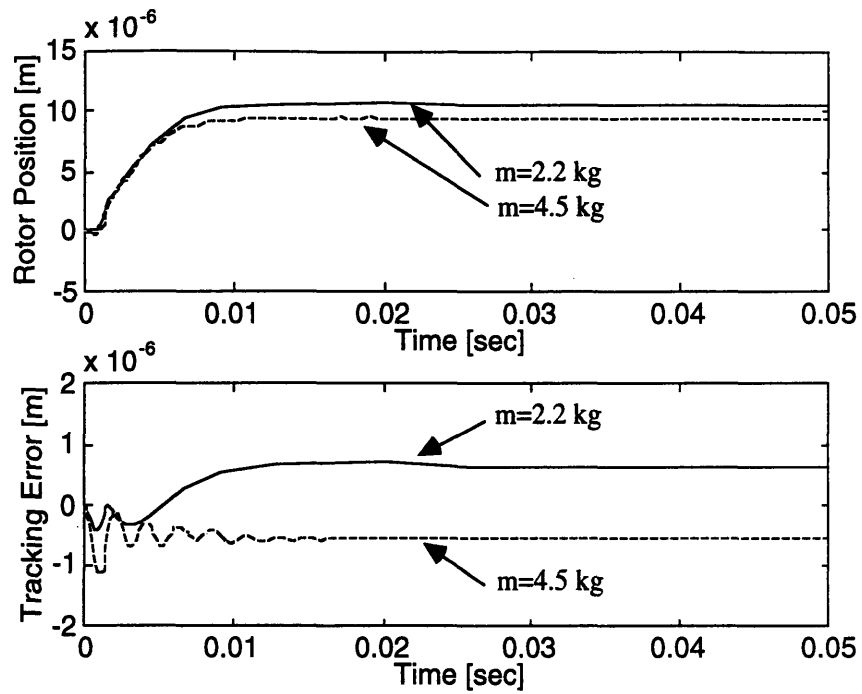
Figure 4.14: 10-μm step responses of the system with the adaptive controller with $m = 2.2$ and 4.5 kg ($g = 4.9$ m/s^2).
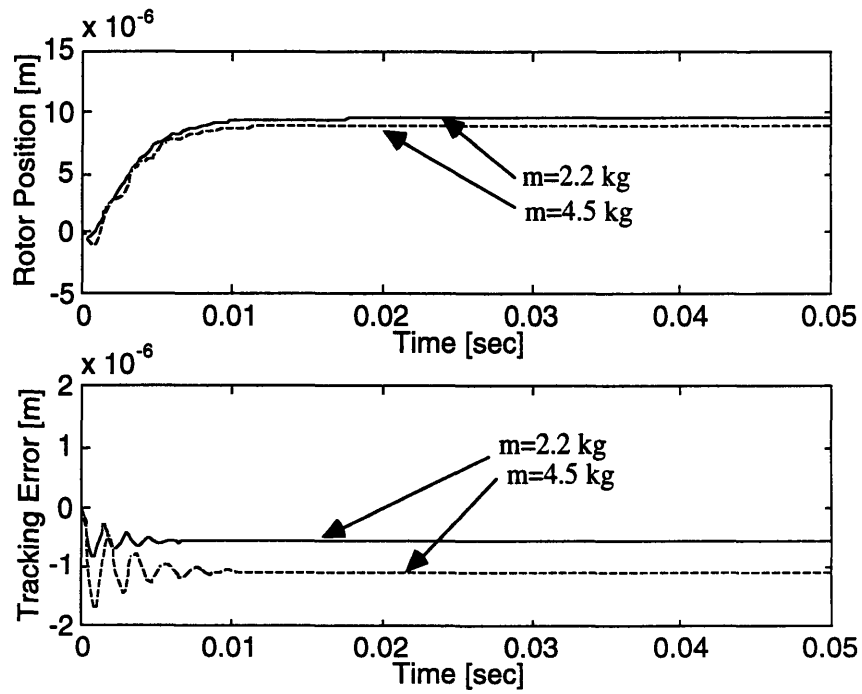
Figure 4.15: 10-μm step responses of the system with the adaptive controller with $m = 2.2$ and 4.5 kg ($g = 9.8$ m/s^2).

are examining, the rotor has the first bending mode at 875 Hz. Therefore, if this unmodeled dynamics makes the closed-loop system unstable, we have to revise the performance specification.

Figure 4.16 shows the example of the rotor-elasticity model, and the motion equations are

$$
\begin{aligned}
m_1 \ddot{z}_1 &= c_1(\dot{z}_2 - \dot{z}_1) + k_1(z_2 - z_1) + F_m \\
m_2 \ddot{z}_2 &= c_1(\dot{z}_1 - \dot{z}_2) + k_1(z_1 - z_2)
\end{aligned}
\tag{4.19}
$$

where F_m is the magnetic force described in Eq.(4.2). The sensor is located at m_2;
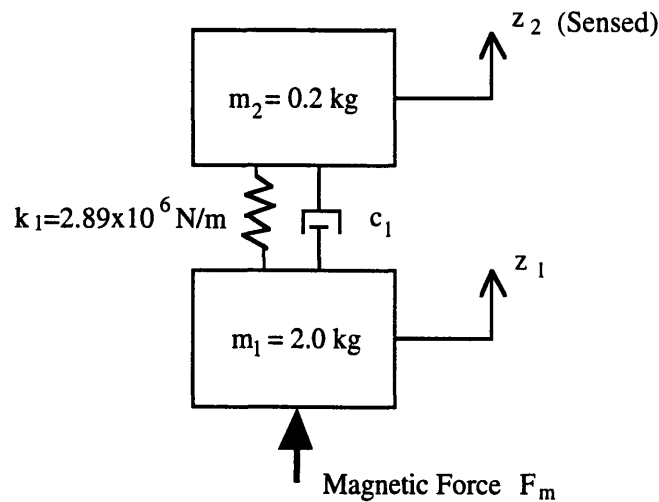
Figure 4.16: Model of the rotor elasticity.

therefore, the transfer function of the actual plant has a resonance at 4000 rad/s (Figure 4.17). If the damping coefficient c_1 is 170 Ns/m, $\Delta(s)$ is lower than $W_3^{-1}(s)$ (Figure 4.18(a)); therefore, the stability is maintained even when this elasticity exists. However, if c_1 is less than 170 Ns/m, $\Delta(s)$ becomes higher than $W_3^{-1}(s)$, and the system is not robustly stable any more. For example, Figure 4.18(b) is the case of $c_1 = 100$ Ns/m; in this case, the closed-loop system has unstable poles at $90 \pm 3666j$. Therefore, the specification must be revised, and the controller must be redesigned to

maintain robust stability. Even though this stability robustness is measured within the linear frame, and it cannot be applied to nonlinear systems, this is obviously one of the important issues for the designer.
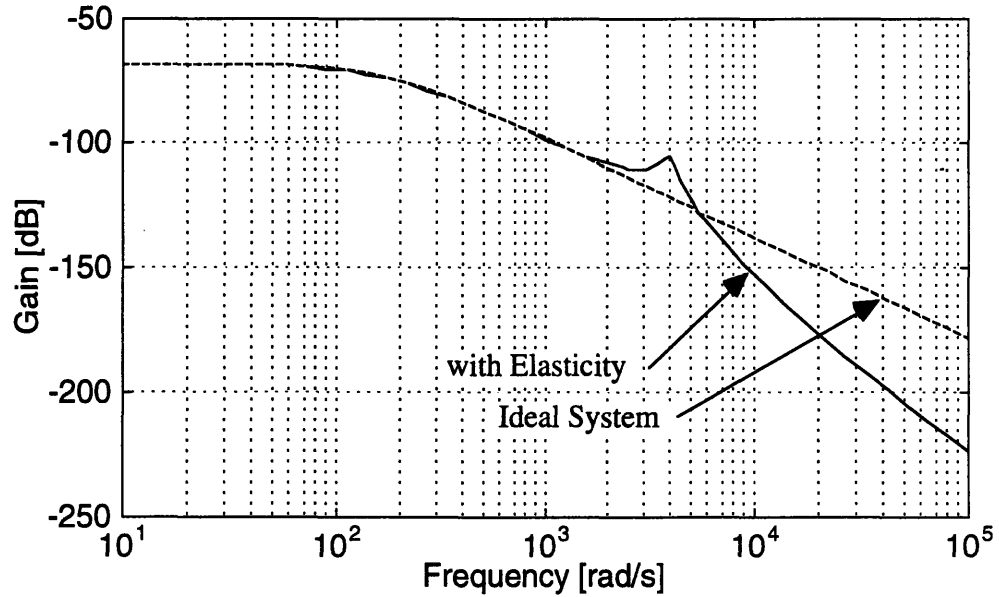
Figure 4.17: Transfer function of the magnetic bearing with the rotor elasticity.

High-frequency unmodeled dynamics also affects the performance of the system controlled by an adaptive controller. Figure 4.19 and 4.20 are the 10-μm step responses of the system controlled by the adaptive controller using local function estimation. The rotor has elasticity described in Figure 4.16 with $c_1 = 100$ Ns/m. We cannot use the adaptive gain $\gamma = 2 \times 10^9$, which is used in the previous section, because the system goes unstable. Even the adaptive gain $\gamma = 1 \times 10^7$ does not make the system stable (Figure 4.19). At $\gamma = 1 \times 10^7$, the system finally becomes stable, but the tracking error of the response becomes unacceptable as shown in Figure 4.20 (The tracking error does not immediately settle within the designed sphere, $\pm 1.5 \mu$m). If $c_1 = 170$ Ns/m, γ can take as large as 5×10^8 without becoming unstable (Figure

(a) $c_1 = 170$ Ns/m. (b) $c_1 = 100$ Ns/m.
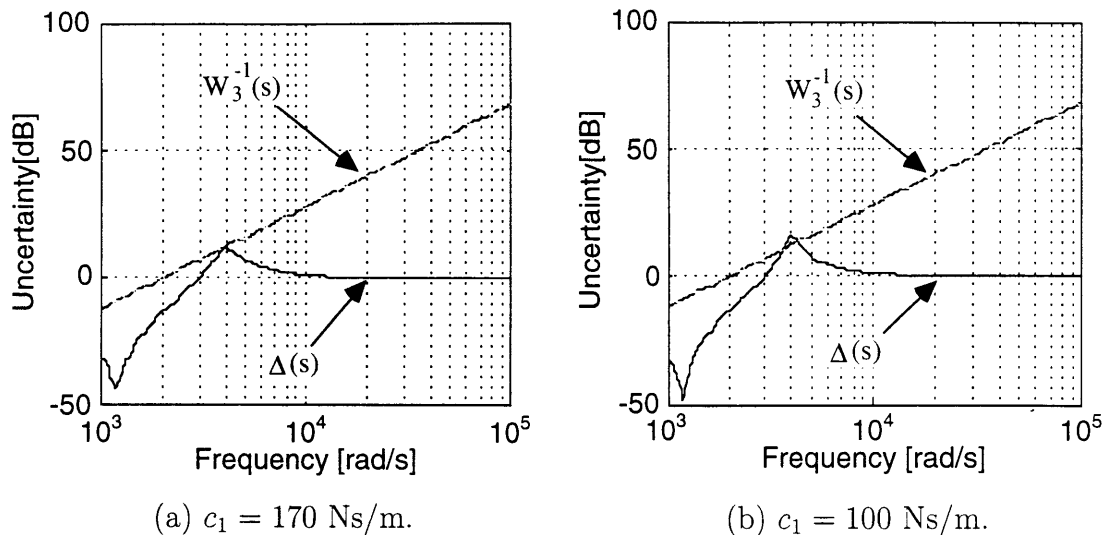
Figure 4.18: Uncertainty by the rotor elasticity and the stability bound.

4.21). In this case, the response follows the reference trajectory. However, γ must be much smaller than the value I designed. At $\gamma = 6.5 \times 10^8$, the system goes unstable as shown in Figure 4.22.

It is difficult to include stability robustness in the adaptive control design because the controller itself is nonlinear. However, this stability robustness issue is important for the control of real mechanical system, and as it was shown in Chapter 2, that is one of the main reasons why the H_∞ design method is developed. In fact, in the real magnetic bearing, $\gamma = 2 \times 10^9$ cannot be achieved when I conducted an experiment.

4.8   Summary

With the advent of μ-synthesis, we can design a controller that achieves performance robustness. However, because of its linear frame, we cannot design a controller that tolerates a wide range of uncertainties. In this chapter, an adaptive control method using local function estimation was presented as an alternative approach for the sys-
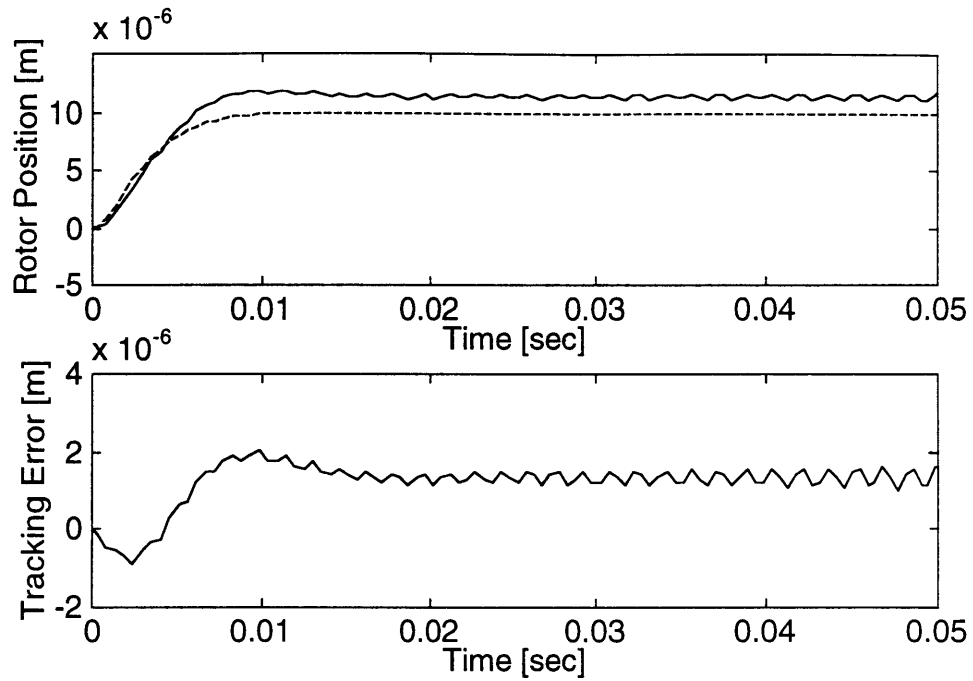
Figure 4.19: Step response of the system with $c_1 = 100$ Ns/m controlled by the adaptive controller ($\gamma = 1 \times 10^7$).
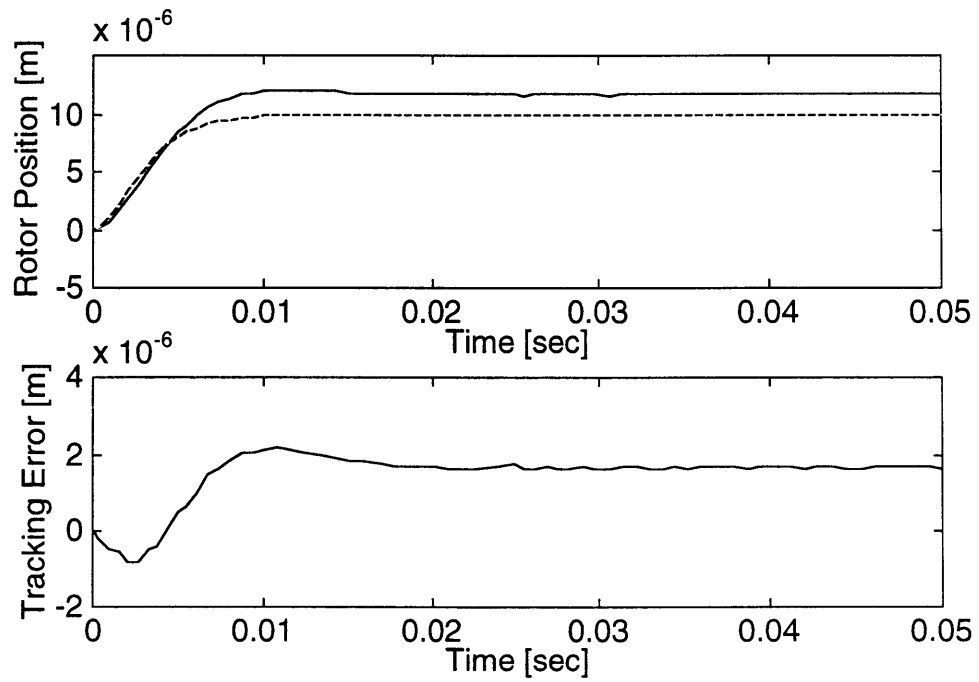
Figure 4.20: Step response of the system with $c_1 = 100$ Ns/m controlled by the adaptive controller ($\gamma = 1 \times 10^6$).
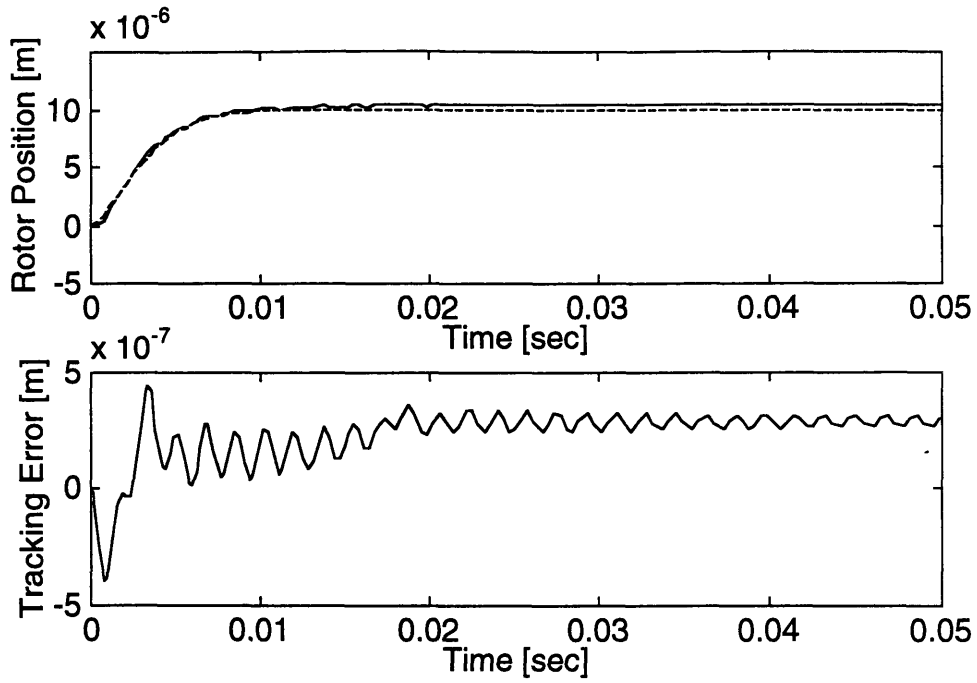
Figure 4.21: Step response of the system with $c_1 = 170$ Ns/m controlled by the adaptive controller ($\gamma = 5 \times 10^8$).
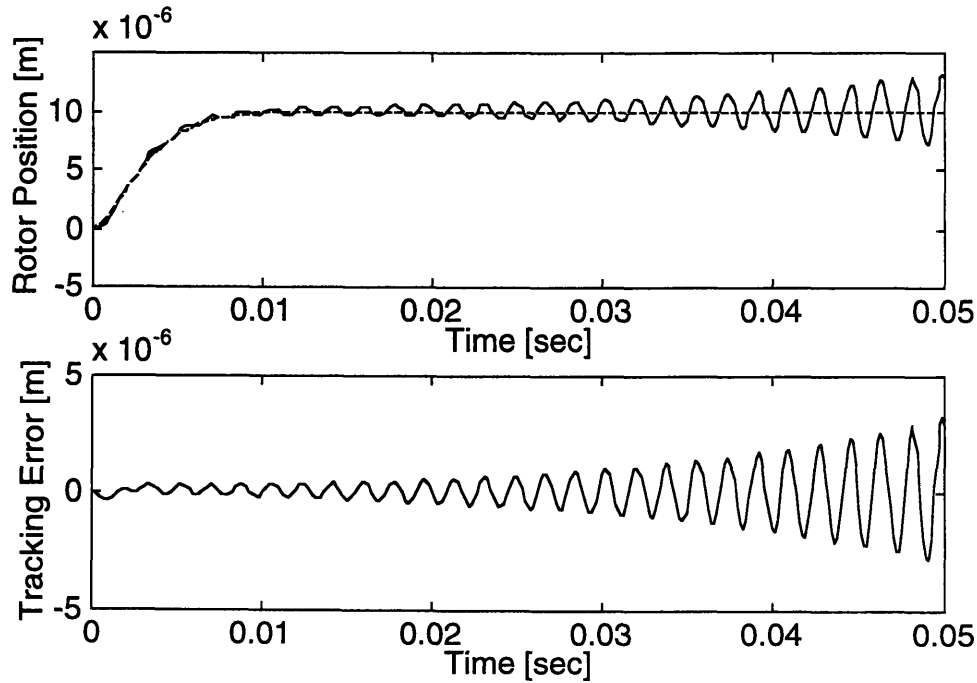
Figure 4.22: Step response of the system with $c_1 = 170$ Ns/m controlled by the adaptive controller ($\gamma = 6.5 \times 10^8$).

tem with uncertainties, and compared two approaches by the nonlinear simulations. This adaptive method has a potential for fast adapting and thus, can achieve precise tracking. The results show that the adaptive approach can achieve high performance with the existence of strong nonlinearity while the system designed by μ-synthesis has difficulty dealing with the equivalent wide uncertainties that nonlinearity impose. However, this adaptive control method still has issues to be solved. It was demonstrated that with high-frequency unmodeled dynamics we have to lower the adaptive gain, and that may make the performance unsatisfactory. Also, this method requires the information of full states that may not be available in real systems. Therefore, the control structure must be chosen by taking all that information into account.

Chapter 5

Conclusions

Total elimination of friction and the active control nature make magnetic bearings attractive. The ability to control the rotor actively especially is essential for some purposes, such as precise positioning control, because this feature cannot be realized by the conventional bearings. However, for this precise use of magnetic bearings, the consideration on performance robustness is required. This thesis focuses on the robustness of performance achieved by the controllers and the relationship between achievable robustness and the existence of the controller.

At first, design examples using an LQG design, H_∞ design, LQG/LTR design, and μ-synthesis to the magnetic bearing are presented for the purpose to show how some of these methods can achieve stability robustness and/or performance robustness. The H_∞ design and LQG/LTR design can achieve robust stability by limiting the gain of the closed-loop transfer function at high frequencies. The H_∞ design method is particularly attractive because it shows the limitation of an achievable sensitivity function; thus, the performance can be maximized. However, neither methods can achieve performance robustness. In contrast, μ-synthesis has the potential to solve an overall robustness problem, and the design example shows that the system designed by μ-synthesis achieves almost the same performance even when the mass of the rotor changes.

In order to choose the structure of the controller at an early stage of a design, the limitation of controllers is of great interest. In Chapter 3, the limitation of the controller designed by H_∞ and μ-synthesis is evaluated. Structured singular value

plots reveal the limitation of linear controllers, and results indicate that if the uncertainty is larger than the certain range, the controller that can achieve the specified performance does not exist. Also, if the system is close to this limitation, the gain of the controller becomes especially high; therefore it should be avoided. However, large control input caused by the high gain of the controller can be avoided by using prefilters. The order reduction method is also applied to reduce the huge order of the controller, but the conventional model reduction method does not effectively reduce the order.

To achieve the performance beyond the limitation of linear controllers, an adaptive control using local function estimation is introduced. In this part, the equivalent linear uncertainties to the nonlinearity are calculated, and it is shown that the range of the uncertainties is much larger than the one that is tolerant to achieve the specified robustness. Next, the simulations with the nonlinear model of the magnetic bearing are conducted, and it is shown that the adaptive controller can achieve similar responses even when the mass of the rotor or operating point changes whereas by the linear controller designed by μ-synthesis, the responses much degrade when the operating point changes. However, according to the simulation, the adaptive gain must be limited if high-frequency unmodeled dynamics exist; thus, the achievable robustness be lowered. In mechanical systems, this problem cannot be avoided. Therefore, further research on maximizing robustness with the existence of high-frequency unmodeled dynamics is inevitable.

Appendix A

Design Programs using MATLAB

A.1 LQG Design

```
%  LQG design for a magnetic bearing
%
%   K : State feedback gain matrix
%   H : Kalman filter gain matix

k0=4.e-6;                          % Plant parameters
z0=400.e-6;
i0=0.5;
m=2.0;

A=[0                    1          % System matrices
   4*k0*i0^2/m/z0^3 0];
B=[0
   4*k0*i0/m/z0^2];
C=[1 0];
D=0;
L=[0
   1/m];

Q=[1 0                             % LQR index
   0 1.0e-5];
R=7.5e-10;
[K,S]=lqr2(A,B,Q,R);

Xi=1;                              % Kalman filter index
Th=1.e-15;
LXL=L*Xi*L';
[Ht,P]=lqr2(A',C',LXL,Th);
H=Ht';
```

A.2 H_∞ Design

```
%  H-infinity design for a magnetic bearing
```

```
%
%    Ac,Bc,Cc,Dc : Controller
%

k0=4.e-6;                         % Plant parameters
z0=400e-6;
i0=0.5;
m=2;

A=[0                  1           % System Matrices
   4*k0*i0^2/m/z0^3 0];
B=[0
   4*k0*i0/m/z0^2];
C=[1 0];
D=0;

kw1=6.1;                          % Weight functions
ww1=200;
ww2_1=1400;
ww2_2=0;

n1=2;
A1=[0        1
    -ww1^2 -2*ww1];
B1=[0
    kw1*ww1^2];
C1=[1 0];
D1=0;
C2=4*k0*i0/m/z0^2/ww2_1^2*[-4*k0*i0^2/m/z0^3 ww2_2];
D2=4*k0*i0/m/z0^2/ww2_1^2;

Aa=[A     zeros(2,n1)             % Augmented plant
    B1*C A1           ];
Ba1=[zeros(2,1)
      B1           ];
Ba2=[B
     zeros(n1,1)];
Ca1=[D1*C C1
     C2    zeros(1,n1)];
Ca2=[C zeros(1,n1)];
Da11=[D1
      0  ];
Da12=[0
      D1];
Da21=1;
```

98

```
Da22=0;

[Ac,Bc,Cc,Dc,Aacl,Bacl,Cacl,Dacl]= ...
        hinf(Aa,Ba1,Ba2,Ca1,Ca2,Da11,Da12,Da21,Da22);
```

A.3 LQG/LTR Design

```
% LQG/LTR design for a magnetic bearing
%
%  Ac,Bc,Cc,Dc : Controller
%

k0=4e-6;                        % Plant parameters
z0=400e-6;
i0=0.5;
m=2;

A=[0                 1          % System matrices
   4*k0*i0^2/m/z0^3 0];
B=[0
   2*k0*i0/m/z0^2];
C=[1 0];
D=0;
L=[0
   1/m];

Sg=[1e-7 0                      % Kalman filter indeces
      0    50];
Th=8e-9;

[Ht,Sf]=lqr2(A',C',Sg,Th);
H=Ht'

As=A-H*C;                       % Sensitivity function
Bs=H;
Cs=-C;
Ds=1;

At=A-H*C;                       % Closed-loop transfer function
Bt=H;
Ct=C;
Dt=0;

sigma(As,Bs,Cs,Ds);            % Singular value plot
```

```
pause
sigma(At,Bt,Ct,Dt);
pause

Q=[1e6 0                        % LQR indeces
   0    1e-3];
R=1e-10;

[K,S]=lqr2(A,B,Q,R);

Ac=A-B*K-H*C;                   % Controller
Bc=H;
Cc=-K;
Dc=0;

nc=length(Ac);

As=[A     B*Cc                  % Sensitivity function
    Bc*C Ac  ];
Bs=[zeros(2,1);Bc];
Cs=[C zeros(1,nc)];
Ds=1;

At=[A     B*Cc                  % Closed-loop transfer function
    Bc*C Ac  ];
Bt=[zeros(2,1);Bc];
Ct=[C zeros(1,nc)];
Dt=0;

sigma(As,Bs,Cs,Ds);            % Singular value plot
pause
sigma(At,Bt,Ct,Dt);
```

A.4 μ-Synthesis

```
% Mu-synthesis for a magnetic bearings
%
%  Ac,Bc,Cc,Dc : Controller
%

w=logspace(1,4);               % Frequency region design procedure
                               % evaluates

k0=4e-6;                       % Plant parameters
```

```
z0=400e-6;
i0=0.5;
m=3.6;                          % Nominal value

A=[0                    1        % System matrices
   4*k0*i0^2/m/z0^3 0];
B=[0
   4*k0*i0/m/z0^2];
C=[1 0];
D=0;

kw1=10;                         % Weight functions
ww1=200.00;
A1=-ww1;
B1=kw1*ww1;
C1=1;
D1=0;

delta=0.055556;                 % Uncertainty
B2=[0
      4*k0*i0^2/z0^3];
C2=[1 0]*delta;
D2=z0/i0*delta;

Aa=[A      zeros(2,1)           % Augmented plant
    B1*C A1           ];
Ba1=[zeros(2,1) B2
     B1         0  ];
Ba2=[B
     0];
Ca1=[D1*C C1
     C2    0 ];
Ca2=[C 0];
Da11=[D1 0
      0  0];
Da12=[0
      D2];
Da21=[1 0];
Da22=0;

[gamopt,Ac,Bc,Cc,Dc,Aacl,Bacl,Cacl,Dacl]= ...
   hinfopt(Aa,Ba1,Ba2,Ca1,Ca2,Da11,Da12,Da21,Da22);
                                % H-infinity optimization

nc=length(Ac);                  % Transfer function from w to z
```

101

```
Aacl=[A+B*Dc*C zeros(2,1) B*Cc
      B1*C     A1            zeros(1,nc)
   Bc*C        zeros(nc,1) Ac         ];
Bacl=[B*Dc B2
      B1   0
   Bc   zeros(nc,1)];
Cacl=[D1*C        C1 zeros(1,nc)
      C2+D2*Dc*C 0  D2*Cc    ];
Dacl=[D1     0
      D2*Dc 0];


[mu,logd]=ssv(Aacl,Bacl,Cacl,Dacl,w);
semilogx(w,20*log10(mu'))
                              % Structured singular values
% and D-scales
pause

[Ad,Bd,Cd,Dd,logdfit]=fitd(logd,w,5);subplot
                              % Fifth order curve fitting

[Aa,Ba1,Ba2,Ca1,Ca2,Da11,Da12,Da21,Da22]= ...
   augd(Aa,Ba1,Ba2,Ca1,Ca2,Da11,Da12,Da21,Da22,Ad,Bd,Cd,Dd);
                              % Augmented plant

[gamopt,Ac,Bc,Cc,Dc,Aacl,Bacl,Cacl,Dacl]= ...
     hinfopt(Aa,Ba1,Ba2,Ca1,Ca2,Da11,Da12,Da21,Da22);
                         % H-infinity optimization

nc=length(Ac);              % Transfer function from w to z
Aacl=[A+B*Dc*C zeros(2,1) B*Cc
      B1*C     A1            zeros(1,nc)
   Bc*C        zeros(nc,1) Ac         ];
Bacl=[B*Dc B2
      B1   0
   Bc   zeros(nc,1)];
Cacl=[D1*C        C1 zeros(1,nc)
      C2+D2*Dc*C 0  D2*Cc    ];
Dacl=[D1     0
      D2*Dc 0];


[mu,logd]=ssv(Aacl,Bacl,Cacl,Dacl,w);
semilogx(w,20*log10(mu'))        % Structured singular values
```

A.5 μ-Synthesis (with bandwidth limit)

```
% Mu-synthesis for a magnetic bearings with bandwidth limit
%
%  Ac,Bc,Cc,Dc : Controller
%

w=logspace(1,4);               % Frequency region design procedure
                               % evaluates


k0=4e-6;                        % Plant parameters
z0=400e-6;
i0=0.5;
m=3.6;                          % Nominal value


A=[0                  1        % System matrices
   4*k0*i0^2/m/z0^3 0];
B=[0
   4*k0*i0/m/z0^2];
C=[1 0];
D=0;

kw1=10;                         % Weight functions
ww1=200.00;
A1=-ww1;
B1=kw1*ww1;
C1=1;
D1=0;

delta=0.055556;                 % Uncertainty
B2=[0
      4*k0*i0^2/z0^3];
C2=[1 0]*delta;
D2=z0/i0*delta;

wc=20000;
B3=4*k0*i0/m/z0^2/wc^2*[-4*k0*i0^2/m/z0^3 0];
D3=4*k0*i0/m/z0^2/wc^2;

Aa=[A     zeros(2,1)           % Augmented plant
    B1*C A1          ];
Ba1=[zeros(2,1) zeros(2,1) B2
     B1           B1          0 ];
Ba2=[B
```

```
      0];
Ca1=[D1*C C1
      B3    0
  C2    0 ];
Ca2=[C 0];
Da11=[D1 D1 0
       0  0  0
   0  0  0];
Da12=[0
       D3
   D2];
Da21=[1 1 0];
Da22=0;


[gamopt,Ac,Bc,Cc,Dc,Aacl,Bacl,Cacl,Dacl]= ...
    hinfopt(Aa,Ba1,Ba2,Ca1,Ca2,Da11,Da12,Da21,Da22);
                                 % H-infinity optimization


nc=length(Ac);               % Transfer function from w to z
Aacl=[A+B*Dc*C zeros(2,1)  B*Cc
       B1*C       A1        zeros(1,nc)
   Bc*C      zeros(nc,1) Ac           ];
Bacl=[B*Dc B*Dc B2
       B1   B1   0
   Bc   Bc   zeros(nc,1)];
Cacl=[D1*C        C1 zeros(1,nc)
       B3+D3*Dc*C 0  D3*Cc
   C2+D2*Dc*C 0  D2*Cc        ];
Dacl=[D1     D1    0
       D3*Dc D3*Dc 0
   D2*Dc D2*Dc 0];


[mu,logd]=ssv(Aacl,Bacl,Cacl,Dacl,w);
semilogx(w,20*log10(mu'))
                                 % Structured singular values
% and D-scales
pause


[Ad,Bd,Cd,Dd,logdfit]=fitd(logd,w,5);subplot
                                 % Fifth order curve fitting


[Aa,Ba1,Ba2,Ca1,Ca2,Da11,Da12,Da21,Da22]= ...
    augd(Aa,Ba1,Ba2,Ca1,Ca2,Da11,Da12,Da21,Da22,Ad,Bd,Cd,Dd);
                                 % Augmented plant
```

```
[gamopt,Ac,Bc,Cc,Dc,Aacl,Bacl,Cacl,Dacl]= ...
     hinfopt(Aa,Ba1,Ba2,Ca1,Ca2,Da11,Da12,Da21,Da22);
                              % H-infinity optimization

nc=length(Ac);                   % Transfer function from w to z
Aacl=[A+B*Dc*C zeros(2,1)  B*Cc
     B1*C      A1          zeros(1,nc)
  Bc*C       zeros(nc,1) Ac         ];
Bacl=[B*Dc B*Dc B2
     B1    B1   0
  Bc    Bc    zeros(nc,1)];
Cacl=[D1*C        C1 zeros(1,nc)
     B3+D3*Dc*C 0 D3*Cc
  C2+D2*Dc*C 0 D2*Cc      ];
Dacl=[D1     D1    0
     D3*Dc D3*Dc 0
  D2*Dc D2*Dc 0];

[mu,logd]=ssv(Aacl,Bacl,Cacl,Dacl,w);
semilogx(w,20*log10(mu'))       % Structured singular values
```

Bibliography

[1] R.Y.Chiang and M.G.Safonov, *Robust Control Toolbox for Use with MATLAB*, The Mathworks Inc., 1992.

[2] G.Balas, J.Doyle, K.Glover, A.Packard and R.Smith, *μ Analysis and Synthesis Toolbox User's Guide*, The Mathworks Inc., 1991

[3] K.Nonami and T.Ito, "μ-Synthesis of Flexible Rotor-Magnetic Bearing Systems," *IEEE Trans.on Control Systems and Technology*, Vol.4, pp.503-512, 1996.

[4] S.Sinha, K.L.Meese, and K.W.Wang, "Sliding Mode Control of a Rigid Rotor via Magnetic Bearings," *ASME Biennial Conference on Mechanical Vibration and Noise*, Florida, September 1991.

[5] T.-J Yeh, "Modeling, Analysis and Control of Magnetically Levitated Rotating Machines," Ph.D. thesis, Department of Mechanical Engineering, Massachusetts Institute of Technology, January 1996.

[6] K.J.Åström and B.Wittenmark, *Adaptive Control*, Addison-Welsely, 1989.

[7] K.Youcef-Toumi and S.Reddy,"Dynamic Analysis and Control of High Speed and High Precision Active Magnetic Bearings," *ASME J.of Dynamic Systems, Measurement, and Control*, Vol.114, pp.623-633, 1992.

[8] J.M.Maciejowski, *Multivariable Feedback Design*, Addison-Welsely, 1989.

[9] J.C.Doyle, J.E.Wall and G.Stein, "Performance and Robustness Analysis for Structured Uncertainty," *Proc. IEEE Conf.on Decision and Control*, Florida, 1982.